DEPDC5 is a metabolic checkpoint regulator in the B cell AA-mTORC1 pathway

Jasmine Joy Wilson, B.Sc (Adv)

Department of Molecular & Biomedical Science

School of Biological Sciences

The University of Adelaide

A thesis submitted to the University of Adelaide in fulfillment of the requirements for the degree of Doctor of Philosophy

2020

Declaration

I certify that this work contains no material which has been accepted for the award of any other degree or diploma in my name, in any university or other tertiary institution and, to the best of my knowledge and belief, contains no material previously published or written by another person, except where due reference has been made in the text. In addition, I certify that no part of this work will, in the future, be used in a submission in my name, for any other degree or diploma in any university or other tertiary institution without the prior approval of the University of Adelaide and where applicable, any partner institution responsible for the joint-award of this degree.

I give permission for the digital version of my thesis to be made available on the web, via the University's digital research repository, the Library Search and also through web search engines, unless permission has been granted by the University to restrict access for a period of time. I acknowledge the support I have received for my research through the provision of an Australian Government Research Training Program Scholarship.

Signed,

Jasmine Wilson, B.Sc.
2020

Acknowledgements

I would like to thank my supervisors, Dr Iain Comerford and Prof. Shaun McColl, for the guidance, encouragement and advice you both gave me throughout my time here. I appreciate the opportunity you both gave me to experience the world of science during my undergraduate years, which fostered my interest in pursuing science and ultimately brought me here today. And, to Adriana the "Wizard of Western Blot" for helping my westerns go smoothly and effortlessly.

To my lab family. We've all had our highs, lows, challenges and setbacks. But we've always made it through, and I know that you all will do many great and wonderful things in your lives with whatever you set your minds to.

Caity, thanks for the sass and the teas. Aaron, always cheerful and our first ever 'bioinformatician'. Maddie, for inviting us 'old' people to your parties. Dylan, for letting me impart my weaning and colony maintenance to you. Timmy – it was pretty fun exploring Europe and Cyprus with you. Maleika – always had the trendiest food places to try. Cam, thanks for the coffees and chats during my transition into a working lab. Duncan and Ervin, for the life and lab advice. Jade, who would have thought science speed dating on our first day of university would lead us here? Thank you for the all the memories and support throughout our friendship. And Paris, who knew your influence would uncover the gamer inside. Kerrie, I love your spontaneous yoga poses in the lab and keeping Todd in check. Todd, for the banter, the bets, the memes that were all too real. Shannon, for enabling each other with house plants and escaping from everything with our movie nights. But for the gang who have been there since the beginning of time: Jade, Kerrie, Shannon and Todd –the last 5 years have been wild and aside from the laughs, we've been through all the ups and downs life could throw at us. I couldn't imagine doing this with anyone else.

Thank you to Prof. Sarah Robertson and Lachie Moldenhauer for welcoming me to their lab. It was intimidating entering the research world outside of my PhD studies, and you both have showed nothing but encouragement and support. Holly, Bridget, Dexter, Ricky, Allie, Sharkey, Cam, Loretta– thank you for adopting me, for the *Thirsty Thursdays,* chai lattes and laughs.

And dearest Lynn Rogers, my dear friend and mentor, thank you for the support and friendship you have given me throughout these many years. I don't know how I would have survived without your wisdom, your cheer, the chats and the coffees. Thank you for everything.

My Family.

Mum and Dad (Wilma and Peter), thank you for your unfailing support and love. You both have always encouraged, supported and believed in me no matter what. When things got tough, you were always there to help me up. Not to mention the much appreciated pick-me up yoga & tai chi sessions, rom-coms, movie nights and the home cooked meals. And thank you to my brothers and sister, Brian, Raoul and Vanessa. Brian, thanks for always keeping me on my toes!

And Kim, the fact that we survived while the both of us were writing up our theses is amazing – and now I know we can get through anything! Thank you for being kind, understanding and loving throughout everything.

And of course, all my family in Australia and the Philippines, who have always believed I could do anything and only ever showed me support.

Publications arising from this work

Manuscripts

Wilson, J., Norton, T., Foyle, K., Abbot, C., Tyllis, T., Dawson, R., Hughes, J., Good-Jacobsen, K., Thomas, P., McColl, S. and Comerford, I. DEPDC5 is a metabolic checkpoint regulator of B cells, Manuscript in preparation.

Conference presentations

Wilson, J., Norton, T., Foyle, K., Abbot, C., Tyllis, T., Dawson, R., Hughes, J., Good-Jacobsen, K., Thomas, P., McColl, S. and Comerford, I. DEPDC5 is a metabolic checkpoint regulator of B cells, Oral presentation at the 48th Annual Scientific Meeting of The Australian & New Zealand Society for Immunology, *Adelaide, December 2019*.

Table of contents

List of Figures

List of Tables

Abbreviations

AA	Amino acid
Ab	Antibody
APC	Antigen presenting cell
ASC	Antibody secreting cells
ATP	Adenosine triphosphate
BLP	B cell biased lymphoid progenitors
BM	Bone marrow
CLP	Common lymphoid progenitors
CSR	Class switch recombination
DLN	Draining lymph node
DZ	Dark zone
EF	Extrafollicular
EFPB	Extrafollicular plasmablast
ELISA	Enzyme-linked immunosorbent assay
ELP	Early lymphoid progenitors
FACS	Fluorescence activated cell sorter
FDC	Follicular Dendritic Cell
FoB	Follicular B cell
GALT	Gut associated lymphoid tissues
GATOR1	GTPase-activating proteins toward Rags 1
GATOR2	GTPase-activating proteins toward Rags 2
GC	Germinal Center
GCB	GC B cells
GIT	Gastrointestinal tract
GLT	Germ line transcript
gMFI	Geometric fluorescence intensity

GSK3	Glycogen synthase kinase 3
HSC	Hematopoietic stem cells
IAV	Influenza A virus
Ig	Immunoglobulin
iLN	Inguinal LN
LN	Lymph node
LP	Lamina propria
LMP	Lympho-myeloid progenitor
LZ	Light zone
MALT	Mucosal associated lymphoid tissues
MBCs	Memory B cells
mesLN	Mesenteric lymph node
medLN	Mediastinal lymph node
MPP	Multipotent progenitors
MRCLB	Mouse red cell lysis buffer
mTOR	Mechanistic target of rapamycin
mTORC1	mammalian target of rapamycin complex 1
MZB	Marginal Zone B cell
mγg	Mouse γ-globulin
PAMPs	Pathogen-associated molecular pattern
PB	Plasmablast
PBS	Phosphate-buffered saline
PCR	Polymerase chain reaction
PCs	Plasma cells
PP	Peyers Patches
PRR	Pattern recognition receptor
qPCR	Quantitative polymerase chain reaction
RT	Room temperature
SHM	Somatic hypermutation
SLO	Secondary lymphoid organ

SP	Spleen
T1	Transitional type 1
T2	Transitional type 2
T3	Transitional type 3
TD	Thymus dependent
TFH	T follicular helper cells
TH	T helper cell
TI	Thymus independent
TLR	Toll like receptor
Treg	T regulatory cell
TSC	Tuberous sclerosis complex

Abstract

Immunometabolism is a rapidly developing field that is central to understanding the homeostatic maintenance and induction of immune responses. Naïve B cells rest in quiescent states until antigen (Ag) is encountered, which simultaneously triggers a metabolic switch enabling enhanced growth, proliferation and differentiation in activated B cells. Central to this metabolic activation is the mechanistic target of rapamycin (mTOR) complex 1 (mTORC1) pathway, which is required for multiple inputs to determine if sufficient nutrients are available to drive these metabolic programs. In recent years amino acid (AA) sensing and availability have been shown to be important for the control of mTORC1 in various cell types, however their importance in B cell metabolism was largely unknown. DEPDC5 is a metabolic checkpoint protein that mediates crosstalk between AA availability and the mTORC1 pathway, but it's role in B cells has not been explored.

The results in this thesis showed that *Depdc5* is expressed in B cells and most abundantly in germinal center (GC) B cells (GCB). A novel line of conditional knock-out mice was generated that lack DEPDC5 in mature B cells (*Depdc5*$^{flox/flox}$ x *Cd23*^{Cre}). This deletion led to constitutive mTORC1 activation in mature B cells. Analysis of *Depdc5*$^{flox/flox}$ x *Cd23*^{Cre} mice showed no impairment of B cell development and at homeostasis, mature B cell frequencies were unchanged from controls. Despite this, mature B cells in resting mice that lacked B cell expression of DEPDC5 exhibited a hyperactive phenotype with increased mTOR signalling, increased biomass and higher levels of expression of B cell activation markers. The effects of DEPDC5 deletion in B cells became more apparent in challenged animals. Fewer GC B cells were present in draining LNs following viral infection than in littermate controls. Furthermore, the absence of *Depdc5* in B cells led to reduced generation of anti-viral IgM Ab, but not anti-viral IgG, and impaired affinity maturation in a protein immunisation model. Mechanistically it was shown that DEPDC5 was required to protect GC B cells from late-stage apoptosis and restrain B cell proliferation following viral infection. Thus, *Depdc5* was required to ensure the sustained expansion of GC B cells in humoral immune responses, likely by restraining their metabolic activity in response to the limited nutrient microenvironment in the GC. However, in contrast, an increase GC B cells frequency and number was also observed in the lung of *Depdc5*-deficient mice following IAV infection. Furthermore, DEPDC5 was observed to be dispensable in B cell activation within GALT-associated chronic GCs. These results broaden

understanding of AA responsive metabolic checkpoint regulators and have implications for nutritional control of optimal humoral responses. Thus, this study contributed to broadening the understanding of how metabolic pathways shape immunity in health and disease.

CHAPTER 1

Introduction

Chapter 1

Chapter 1

Introduction

B cells are engaged in numerous aspects of immunity by contributing to both health and disease. B cells are vital for the generation of antibody (Ab) responses and immunological memory but can also contribute to various disease states including autoimmunity, allergy and cancer. Importantly, understanding B cell biology is vitally important for the rational design of vaccines and cancer immunotherapies (reviewed (Sharonov et al. 2020; Wennhold, Shimabukuro-Vornhagen, and von Bergwelt-Baildon 2019; Palm and Henry 2019)). When Ag-specific naive B cells first encounter Ag they undergo proliferation, clonal expansion and differentiation into GC B cells (GCBs), memory B cells (MBCs) and Ab-secreting cells (ASCs) (Boothby, Hodges, and Thomas 2019). Metabolic adaptation is important as B cells occupy a wide range of microenvironmental niches during the process of clonal selection, proliferation and differentiation (Raybuck et al. 2018; Chiu et al. 2019; Buck et al. 2017; Keating et al. 2013; Benhamron and Tirosh 2011). Nutrient composition and availability differ within these microenvironments and during the progression of infection, these directly influence metabolic programming in B cells through the metabolic master regulator mTOR. mTORC1 integrates the nutrient and energy sensing machinery of the cell and controls protein synthesis in response to nutrient availability. Accordingly, disruption of mTORC1 signalling in B cells after development leads to disruptions in B cell proliferation, growth and Ab responses (Raybuck et al. 2018; Ersching et al. 2017). Metabolic regulation is essential for activated B cells to adapt to the availability of nutrients and generate effective humoral responses. However, details of the molecular mechanisms driving these processes require more understanding.

1.1 Humoral Immunity

Early B cell development begins with the commitment of hematopoietic stem cell (HSC) precursors within the bone marrow (BM) to the B cell lineage and continues in the spleen (SP) for maturation through a series of distinct stepwise stages that occur continually throughout life. During these process, rearrangement and expression of immunoglobulin (Ig) genes occurs, leading to development of a diverse repertoire of mature B cells comprising various subsets, including naive follicular B cells (FoB) and marginal zone B cells (MZB) cells. Naive B cells are capable of recognising a broad range of Ag, facilitating a broad Ab-mediated response against pathogens and the formation of protective memory. Activated B cells can contribute to early memory and ASC responses independent of the GC. In addition, Ag-driven B cell responses can lead to formation of the GC, in which GCB cells partake in development of high affinity B cell responses, long-lived memory and ASC formation. The development and activation of the humoral response will now be described in further detail.

1.1.1 B cell ontology

Mature B cells derive and are replenished from HSCs in the fetal liver and postnatally in the BM. HSCs give rise to all mature B cell subsets through a series of developmental stages stringently controlled by distinct transcription factors (TFs) and receptor signalling. HSCs at the earliest stage of differentiation become multipotent progenitors (MPP) which subsequently obtain lymphoid and myeloid differentiation potential (Adolfsson et al. 2001). Within the lympho-myeloid progenitor (LMP) population, lymphoid restriction gives rise to early lymphoid progenitors (ELP) that can differentiate into common lymphoid progenitors (CLP) which give rise to lymphoid lineages; B cells, T cells, dendritic cells and natural killer cells. CLPs commit to the B cell lineage through expression of the TFs, E box binding protein 2A (E2A) and Early B cell Factor-1 (EBF1) (as reviewed here (Ramirez, Lukin, and Hagman 2010)). The B cell-biased lymphoid progenitors (BLP) within the CLP population further differentiate and progress through pre-pro and pro-B cell stages signified by expression of the surface markers B220 and CD19 (Nutt and Kee 2007). Multiple TFs are involved in B cell lineage commitment, including Paired box 5 (PAX5), PU.1, Ikaros family zinc finger protein 1

(IKAROS), E2A and EBF1 (Yoshida et al. 2006; DeKoter and Singh 2000). PU.1 and IKAROS direct commitment to the CLP lineage within the BM (Yoshida et al. 2006; DeKoter and Singh 2000). CLP progenitors express E2A, which regulates EBF1 and Forkhead box protein O1 (FOXO1) expression and these in turn induce expression of PAX-5 and promote heavy/light chain rearrangements in pro/pre B cells in concert with other TFs (Welinder et al. 2011; Lin et al. 2010; Kee and Murre 1998; Decker et al. 2009). PAX-5 is an essential regulator and promoter of B cell lineage commitment (Decker et al. 2009). Early descriptions of B cell lineage commitment used a combination of four markers (B220, CD43, CD24 and BP-1) to identify early B cell populations within the BM (Hardy et al. 1991). Pre-Pro-B cells were defined as $B220^{+}CD43^{+}$ $CD24^{-}$ $BP\text{-}1^{-}$ and had low levels of RAG-1/RAG-2 mRNA expression and limited Ig rearrangement. This population was later determined to be largely heterogenous and the addition of the marker AA4.1 (CD93) was able to identify B lineage cells ($AA4.1^{+}$) and non-B lineage cells ($AA4.1^{-}$) within this subset (Li et al. 1996). B cells then lose expression of CD43 as they differentiate further through the stages termed Pro-B cells ($B220^{+}CD43^{lo}$ $CD24^{+}$ $BP\text{-}1^{-}$), Late Pro-B cells ($B220^{+}CD43^{lo}$ $CD24^{+}$ $BP\text{-}1^{+}$), and Pre-B cells ($B220^{+}CD43^{-}$ $CD24^{+}BP\text{-}1^{+}$) and B cells ($B220^{+}CD43^{-}$ $CD24^{+}$ $BP\text{-}1^{-}$) (Hardy et al. 1991). D-J Heavy chain rearrangements begin within the early pro-B cell subset and continue over the course of this developmental scheme, whereas V-D-J heavy and V-J kappa chain rearrangement began in the pre-B cell faction.

In 2016, Jensen and colleagues performed a 176 protein screen to identify new stage-specific markers and reaffirm the use of known stage-specific markers during B cell development (Jensen et al. 2016). Using these new strategies, Jensen et al. described successful Ig heavy chain rearrangement within the pro-B cell ($B220^{+}$ $CD2^{-}$ IgM^{-}) (Jensen et al. 2016) compartment leads to development of pre-B cells ($B220^{+}$ $CD2^{+}$ IgM^{-}) (Jensen et al. 2016). Igκ light-chain rearrangement occurs in pre-B cells, leading to the expression of surface Ig and a potentially functional B cell receptor (BCR) in immature B cells ($B220^{+}$ $CD2^{+}$ IgM^{+}). Finally, expression of IgD demarcates differentiation of immature B cells into mature B lymphocytes ($B220^{+}$ $CD2^{+}$ IgD^{+} IgM^{+}) (Jensen et al. 2016). Negative selection during the B cell development process removes B cells expressing BCRs that recognise host Ag and occurs both during BM development and the splenic transitional stages. Hence, this stage of B cell development leads to the generation of a diverse repertoire of B cell clones and removal of the most self-reactive clones.

Immature B lymphocytes emigrate from the BM and enter the SP (Tze et al. 2005). Following positive selection via tonic signalling, a fraction of immature B cells enter the transitional stages of development: transitional type 1 (T1), transitional type 2 (T2) and transitional type 3 (T3) (Tze et al. 2005) (Allman et al. 2001). T1 cells are predisposed to apoptosis, leading to deletion of self-reactive clones that react against peripheral Ag not seen in the BM. T1 cells in the follicles that are rescued from selection give rise to T2 cells which are responsive to positive selection (Petro et al. 2002). From this point, T2 cells in the SP differentiate into FoB or MZB cells, or alternatively give rise to T3 cells (Vossenkamper and Spencer 2011; Martin et al. 2016). Teague *et al*. indicates that the T3 cell population do not contribute to the formation of mature B cell subsets, and instead are likely to be a reservoir for autoreactive and anergic B cells (Teague et al. 2007). MZBs are a self-renewing population which provide rapid innate-like protective IgM responses against conserved protein and carbohydrate Ags, which are important in protection against blood-borne Ag and are characterised by high expression of CD21 and low expression of CD23. MZBs shuttle between the follicles and marginal zone within the SP, depositing Ag to follicular dendritic cells (FDCs), which FDCs then take up and present to FoB cells in order to initiate more diverse, high-affinity and isotype-switched ASC responses (Cinamon et al. 2008). As discussed earlier, FoB cells are naive precursors for Ag-specific GCBs, ASCs and MBCs. FoB cells within secondary lymphoid organ (SLO) follicles can participate in the thymus-dependent (TD) or independent (TI) immune responses. Exposure of naive B cells to Ag promotes differentiation of these cells into different fates; GCB cells, ASCs or MBCs. The formation of ASC and MBC compartments can occur in both GC-dependent and -independent manners. Entry into the GC relies on the presence of both cognate Ag and co-stimulatory signals from T cells which have specificity to peptide/major histocompatibility class II (MHC-II) complexes presented by activated B cells. Class switch recombination (CSR) occurs before SHM and differentiation of activated B cells into GCBs or plasmablasts (Roco et al. 2019). The GC is a specialised micro-structure within SLOs in which Ag-activated B cells diversify their BCRs through AID-driven SHM.

1.1.2 B cell activation and the GC response

The body is armed with a repertoire of naive B cells theoretically capable of recognising any potential Ag. Induction of effective Ag-specific B cell responses against the diverse range of pathogens encountered by the immune system relies on the presence of an equally diverse range

of BCR specificities. The development and initiation of the humoral response relies upon activation and triggering of the BCR by Ag and/or stimulation of Toll-like receptors (TLRs) which enable broad recognition of microbial molecules, such as pathogen-associated molecular pattern (PAMP) molecules and are also associated with innate-like B cell responses (Douagi et al. 2009). Co-stimulatory signals can be provided through TI and TD means. Pathogens expressing repetitive epitopes such as viral capsids or TLR ligands such as lipopolysaccharide (LPS) can elicit polyclonal TI B cell responses through combinatorial stimulation of the BCR and TLRs. TI Ag elicit strong BCR and co-receptor signalling are generally mitogenic and generate humoral responses to a diverse range of natural pathogens (Rawlings et al. 2012; Bachmann and Zinkernagel 1997). By contrast, TD Ag include epitopes from complex soluble proteins which stimulate BCRs in a highly Ag-specific manner and elicits a BCR signal strength insufficient to fully activate naïve B cells without T cell help. Subsequent Ag internalisation, processing and then MHC-II-mediated presentation of peptides derived from the Ag to T cells leads to the co-operative interaction of cognate B and T cells which facilitates the generation of high affinity and Ag-specific B cell responses.

SLOs are the main tissue microenvironment which facilitate Ag-driven activation of lymphocytes. Naive B cells are organised in primary follicles adjacent to the T cell zone of SLOs. A heterogenous network of stromal cells in the B cell follicle include both FDCs and marginal reticular cells (MRCs) (Katakai et al. 2008). This stromal network expresses the chemokine CXCL13 which attracts naive B cells expressing the cognate receptor CXCR5, which is critical for Ag-scanning and activation of naive B cells (Forster et al. 1996). Small soluble Ag entering LNs via afferent lymph can gain direct access to the follicle and be recognised by FoB cells (Pape et al. 2007). Larger Ags are captured in the subcapsular sinus (SCS) region by specialised Ag-presenting cells (APCs) including $CD169^{+}$ SCS macrophages. Ag captured by SCS macrophages is relayed to FDCs via B cells to promote affinity maturation (Phan et al. 2009). In addition, FDCs capture and present Ag as immune complexes to both FoB cells in primary follicles and to GCB cells during affinity maturation within the GC (Suzuki et al. 2009; Phan et al. 2009). After naive B cells encounter cognate Ag, early activated B cells increase expression of Epstein-Barr virus induced gene 2 (EBI2) to migrate to the outer follicle (Kelly et al. 2011). Expression of EBI2 and migration to extrafollicular sites is important for early extrafollicular (EF) Ab responses (Gatto et al. 2009).

T independent (TI) Ag can stimulate Ab responses in B cells in the absence of T cell help. TI Ags do not associate with APCs MHCII molecules, thus do not participate in the activation of Ag-specific T cells which participate in T cell dependent B cell responses (as reviewed here (Mond, Lees, and Snapper 1995; Mond et al. 1995). TI type I Ags such as LPS, CpG and poly:IC are mitogens which stimulate B cell activation through TLR. Type II TI Ags include large polysaccharides with repeating epitopes which simulate B cells via the BCR (Obukhanych and Nussenzweig 2006). TI type II Ags promote isotype switching to IgG3 in mice and IgG2 in humans (Perlmutter et al. 1978; Garcia de Vinuesa et al. 1999). Induction of TI Type II responses induce the formation of Ag specific B cells and differentiation into plasmablasts in the extrafollicular regions and lead to long lived responses (Garcia de Vinuesa et al. 1999).

T dependent (TD) Ag are soluble proteins or hapten conjugated to proteins which bind BCR and in turn can be internalized and processed for presentation on MHCII. Ag activated B cells upregulate CCR7 and EBI2 which facilitates their migration to T cell rich zones for interaction with Ag-specific T helper cells (Kelly et al. 2011). Ag-activated B cells present peptide:MHC-II complexes to cognate $CD4^+$ T helper cells. At the T:B border, T helper (Th) cells provide multiple co-stimulatory signals for B cell activation (Okada et al. 2005). This is mediated by CD40L/CD40 interactions, wherein activated T cells transiently express CD40L under inflammatory conditions and stimulate CD40 signalling by B cells; leading to NF-κB activation, B cell proliferation, Ab affinity maturation and CSR (Lee et al. 2003; van Zelm et al. 2014; Miyashita et al. 1997). Further, interactions between Intercellular Adhesion Molecule 1 (ICAM-1) on activated Th cells and Lymphocyte function-associated antigen 1 (LFA-1) on B cells is essential for B cells is essential for B cell proliferation and differentiation while promoting interleukin-2 (IL-2) production by Th cells (Tohma, Hirohata, and Lipsky 1991). In the absence of T cells, a second co-stimulatory signal can be delivered through Toll Like Receptors (TLRs) (Ruprecht and Lanzavecchia 2006). Without this second co-stimulator signal within an appropriate window of time, activated B cells progressively experience metabolic dysfunction; with reduced glycolytic capacity and mitochondrial function, leading to apoptosis (Akkaya et al. 2018) or can revert to a naïve-like state (Turner, Benet, and Grigorova 2017).

B cells undergo CSR prior to their commitment to a GC fate. Recent studies have shown that isotype switching occurs prior to GC-driven B cell selection due to early up-regulation of

the germline transcript (GLT) in B cells following T cell interactions (Roco et al. 2019). Initiation of CSR relies upon the activation of activation-induced cytidine deaminase (AID), uracil-DNA glycosylase (UNG), and Apurinic/apyrimidinic endonuclease 1 (APE1) to target switch regions in the GLT. Following CSR, the GLT is down-regulated and B cells undergo further fate commitment (Roco et al. 2019). B-cell lymphoma 6 (Bcl-6) and PR domain zinc finger protein 1 (Blimp-1) are TFs that elicit mutually exclusive gene expression programs involved in the differentiation of both B and T cells. In B cells, Bcl-6 commits B cells to a GCB cell fate (Huang et al. 2014; Fukuda et al. 1997; Dent et al. 1997) while Blimp-1 is important for formation of ASCs (Shapiro-Shelef et al. 2003). Bcl-6 is also important for T cell commitment to a follicular Th lineage (TFH) following T:B cell interactions, to provide support for generation of GC, MBC and ASC responses (Lee et al. 2011; Schaerli et al. 2000; Breitfeld et al. 2000). TFH cells express markers of activation including CD69, low levels of CCR7 and CD62L, and high levels of CXCR5, PD1 and IL-21 (Schaerli et al. 2000; Breitfeld et al. 2000; Vogelzang et al. 2008; Shi et al. 2018), a detailed review of TFH cells can be found here (Vinuesa et al. 2016). CXCR5 mediates migration of TFH cells from the interfollicular region to within the B cell follicles where CXCL13 is produced by FDCs located within the follicular region (Schaerli et al. 2000; Breitfeld et al. 2000). TFH cells play an important role in affinity-based selection of pre-GCB cells at the T:B border. Pre-GCB cells with the highest affinity BCRs consequently present the highest amounts of peptide:MHC-II to TFH cells. This creates an affinity threshold, in which TFH cell help is restricted to B cells with the highest Ag-binding capacity (Schwickert et al. 2011). The mechanism underlying TFH mediated pre-GCB cell selection lies in stabilisation of pro-survival proteins. Higher affinity B cells receive signals to express higher levels of receptors for B-cell activating factor (BAFF), a pro-survival protein, and consequently BAFF stimulates increased phosphatidylinositol-3 kinase (PI3K) signalling. This feed-forward loop leads to increased stabilisation of pro-survival molecules Myeloid cell leukemia 1 (Mcl-1) and B-cell lymphoma-extra large (Bcl-XL), which improve the survival of high affinity B cells compared to those of lower affinity (Pape et al. 2007; Wensveen et al. 2016; Vikstrom et al. 2010). Following this selection process, pre-GCB cells and TFH cells migrate to the B cell follicle in a CXCR5-dependent fashion and participate in development and maintenance of the GC response. Alternatively, GC-independent MBCs can form from the developmentally plastic pre-GCB cells (Taylor, Pape, and Jenkins 2012; Inamine et al. 2005).

The rapid development and expansion of the GC leads to GC maturation and is observed with the formation of polarised light zone (LZ) and dark zone (DZ), through which GCB cells re-cycle using timed programs (Bannard et al. 2013; MacLennan 1994). GCB cells migrate toward CXCL12 within the DZ via expression of CXCR4 (Allen et al. 2004) wherein activity of AID leads to diversification of the Ig variable (V) region genes during the process of SHM (Muramatsu et al. 2000). B cells within the DZ proliferate extensively as identified by comparing cell cycle analysis of GCB cells within the DZ and LZ. GCB cells within the G2/M phase of the cell cycle were localised to the DZ only (Victora et al. 2010). This leads to a pool of GCB cells expressing mutated BCRs of varying Ag affinities within the DZ. Downregulation of CXCR4 during proliferation and upregulation of CXCR5 directs mutated GCB cells towards the LZ, wherein CXCL13 is produced by FDCs (Allen et al. 2004; Bannard et al. 2013). The LZ is defined by the presence of TFH cells and FDCs which partake in the process of LZ clonal selection (Mesin, Ersching, and Victora 2016). FDCs present native Ag to B cells in the form of immune complexes on their surface to drive competition for Ag binding amongst GCB cells with varying BCR affinities. Those GCB cells with higher BCR affinities more efficiently sequester Ag than their lower affinity competitors and process it for presentation on the surface via a peptide:MHC-II complex to gain activating signals from TFH cells within the LZ. Thus, GCB cells with high affinity BCRs capture greater amounts of Ag, leading to a high density of peptide:MHC-II on their surface which is presented to TFH cells for positive selection signals. These GCB:TFH interactions engage in a feedforward loop, in which GCB cell expression of inducible costimulator ligand (ICOSL) promotes the upregulation of CD40L on TFH cells, that in turn further stimulates ICOSL upregulation in B cells to generate an intimate interaction between TFH cells and high affinity GCB cells. High affinity GCB cell variants were enriched for the expression of ICOSL, and in the absence of ICOSL in GCB cells the selection of high affinity is impaired (Liu et al. 2015). This interaction stimulates the release of helper and survival cytokines for B cells by TFH cells, including IL-4, IL-21 and BAFF (Shulman et al. 2014; Goenka et al. 2014). Iterative rounds of cycling through the DZ and LZ lead to the progressive increase in BCR affinity, known as affinity maturation (Victora et al. 2010; Allen et al. 2007). GCB cells subsequently commit to PC or MBC fates to establish long-lived humoral immunity. An overview of the events in the GC is shown in **Figure 1.1**.

1.1.3 Ab responses and memory

The formation of memory and PCs occurs in a temporal manner, in which MBCs are formed prior to PC generation due to a temporal switch in GC output (Weisel et al. 2016). Using a series of BrdU pulse-labeling studies, V region sequencing and GCB cell ablation techniques, Weisel *et al*. found that early responses led to the appearance of unswitched MBCs, followed by isotype-switched MBCs prior to the peak GC response and finally the generation of isotype-switched long-lived PCs significantly later in the GC response. A GC-independent pathway for MBC generation is also observed in Bcl-6-deficient mice which are unable to form GCB cells in response to TD Ag (Toyama et al. 2002). An early wave of MBCs which are long-lived, unmutated and switched can thus be formed in the absence of GC formation (Toyama et al. 2002; Kaji et al. 2012). The GC-independent MBCs comprise an equivalent fraction of the total MBC, signifying their equal importance to the GC-derived MBCs, perhaps in the generation of rapid responses to insult by the Ag as supposed by Kaji and colleagues. The unmutated BCR carried by the early wave of MBCs is indicative of a developmental pathway which precedes the occurrence of GC-dependent somatic hypermutation (Taylor, Pape, and Jenkins 2012; Weisel et al. 2016). During the progression of a TD humoral response, GCs give rise to the development of long-lived, isotype-switched MBCs with affinity matured BCRs. In the absence of GCs, somatically hypermutated MBCs are unable to form and this compromises humoral recall responses (Good-Jacobson and Shlomchik 2010; Weisel et al. 2016). The scarcity of SHM observed within the IgV genes of long-lived MBCs is consistent with the early commitment of GCB cells to this fate as it precedes the development of high affinity clones through affinity maturation. The possession of low-affinity BCRs have been shown to be a beneficial strategy for protection against multiple strains of virus (Keating et al. 2013). During secondary responses, MBCs have the capacity to differentiate into PCs or GCB cells. $CD80^{hi}$ MBCs were observed to preferentially commit to a PC fate, whilst $CD80^{lo}$ MBCs preferentially commit to a GC pathway in response to re-infection. The amount of CD40 stimulation the cell receives from TFH cells is the critical step in determining the committed fate. The development of these MBC subsets is found to be differentially controlled by the signalling strength provided by CD40:CD40L interactions with TFH cells within the GC (Koike et al. 2019). Following generation, MBCs enter circulation to patrol or take up tissue residency to proliferate and differentiate into ASCs and GCs to efficiently protect the host against reinfection (Onodera et al. 2012; Joo, He, and Sangster 2008).

Three distinct pathways have been elucidated for formation of ASCs and a general overview will be discussed. As discussed previously, Ag-specific activation of naive B cells can directly produce unmutated Ab-secreting EFPB cells early during the immune response even in the absence of T cell help. Second, T:B interactions can lead to the commitment of high affinity B cells to form extrafollicular ASCs, whilst lower affinity B cells enter the GC reaction to undergo affinity maturation where the formation of high affinity GCB cells leads to the generation of long-lived PCs (Paus et al. 2006; Phan et al. 2006). Expression of the BLIMP-1 TF is essential for commitment of GC-derived PCs, and studies have demonstrated that high-affinity GCB cells predominantly commit to the PC fate (Phan et al. 2006; Kallies et al. 2004; Smith et al. 1996). High affinity B cells express lower levels of Basic Leucine Zipper Transcription Factor 2 (BACH2), promoting re-entry into the GC cycle or upregulation of PC transcriptional programs. Further, prolonged T:B interactions mediated by the expression of high affinity BCRs enable GCB cells to gain IL-21 stimulation from TFHs, which promote PC differentiation (Zotos et al. 2010). Conversely, low affinity B cells express high levels of BACH2 and maintain quite weak TFH interactions in the LZ, which favours a MBC fate (Shinnakasu et al. 2016). Thus, generation of PCs at later time points coincides with the selection of the highest affinity clones from the GC reaction. Each PC secretes clonally specific, class-switched Ab. While this is a brief summation of this process, it is important to note a more complex developmental pathway exists in the formation of ASCs. Ab isotype influences the effector function and category of immune protection that PCs elicit (Higgins, McHeyzer-Williams, and McHeyzer-Williams 2019). Following egress from the GC, long-lived PCs migrate and take up residency within the tissues, such as the BM, intestines and thymus to provide long-term and systemic Ab-mediated protection to the host (Landsverk et al. 2017; Halliley et al. 2015; Glatman Zaretsky et al. 2017; Nunez et al. 2016; Manz et al. 2002), which may aid in the development of tissue specific functional Ab-mediated protection. Further, the nature of stimulation and transcriptional programming can influence PC isotype and thus influence their effector function. The IgG isotype and subclasses (e.g. IgG1, IgG2, IgG3, and IgG4 in humans, and IgG1, IgG2a, IgG2b, IgG2c, IgG3 in mice) are commonly associated with protection against intracellular pathogens such as viruses and some bacteria (Huber et al. 2006), while IgE promotes clearance of helminth and parasite infections (Gurish et al. 2004). IgM and IgA isotypes are associated with maintenance of type III mucosal immunity associated with the

microbiota and fungal challenge (Lopez et al. 2016; Bioley et al. 2017). IgM responses also play a role in ongoing homeostasis and maintenance of tolerance (Ouchida et al. 2012).

1.2 B cell metabolism

A complex relationship exists between nutrition, infection and immunity. Limited access to nutrients can lead to malnutrition, which increases the risk of infection (Fock et al. 2010; Nohr et al. 1986; McMurray, Watson, and Reyes 1981). One form of malnutrition originates from insufficiency in dietary protein or AA intake (Carlomagno et al. 1982; Ibrahim et al. 2017; Fock et al. 2010; Nohr et al. 1986; McMurray, Watson, and Reyes 1981). Protein or AA malnutrition increases susceptibility to infections such as influenza A virus (IAV) (Ritz et al. 2008), due to effects on both humoral immunity and cell-mediated immune responses (Carlomagno et al. 1982; Ibrahim et al. 2017; Fock et al. 2010; Nohr et al. 1986; McMurray, Watson, and Reyes 1981). Dietary supplementation with protein is shown to restore optimal immunity in response to IAV infection (Taylor et al. 2013). Further, poor induction of vaccine-induced Ab responses to IAV vaccination is associated with malnutrition in the elderly (Bellei et al. 2006). However, few studies have examined the mechanistic basis of these phenomena or which nutrient sensors mediate nutritional control of humoral immunity. However, it is clear that B cells require sufficient nutrients to drive their changing metabolic processes as they develop, differentiate and perform effector functions.

1.2.1 Cellular metabolism

Naive B cells rest in a quiescent state until Ag-induced activation, which induces a bioenergetic response to provide energy in the form of adenosine triphosphate (ATP) and anabolic precursors to support growth and expansion of activated B cells (Jellusova et al. 2017; Waters et al. 2018). B cell activation is accompanied by an increase in metabolic glycolysis and glutaminolysis (Caro-Maldonado et al. 2014b; Dufort et al. 2007). Sufficient levels of anabolic precursors are required for generation of biomass, including protein, lipid and nucleotides during growth and proliferation (Waters et al. 2018). Glucose is required to fuel glycolysis, *de novo* lipogenesis, generate mitochondrial mass and intracellular membranes required for the

proliferation and growth of B cells (Caro-Maldonado et al. 2014a). Further, synthesis of fatty acids essential for expansion and differentiation of splenic B cells into PCs also requires glucose (Dufort et al. 2014). Glucose and glutamine have been shown to be important carbon sources for biomass production and contribute to ATP production (Doughty et al. 2006; Cho et al. 2011; Caro-Maldonado et al. 2014b; Jellusova et al. 2017; Waters et al. 2018; Yang et al. 2014). Activation of B cells *in vitro* with TLR4 stimulation using LPS or crosslinking the BCR with anti-IgM Ab, has been shown in multiple studies to increase glucose uptake and enhance oxygen consumption rate (OCR), which is used as a surrogate marker of mitochondrial function (Doughty et al. 2006; Cho et al. 2011; Caro-Maldonado et al. 2014b; Jellusova et al. 2017). Ag-driven stimulation of the BCR signals through the phosphatidylinositol 3-kinase (PI3-K) pathway, which leads to increases in glucose metabolism and precedes cellular growth and proliferation, and B cell growth requires this enhanced glycolytic flux (Doughty et al. 2006). Glucose is processed through the pentose phosphate pathway (PPP), the tricarboxylic acid (TCA) cycle, and nucleotide biosynthesis pathways (Waters et al. 2018). In addition, ribonucleotides and lactate are generated, whilst reactive oxygen species (ROS) and nicotinamide adenine dinucleotide (NAD) and NAD phosphate (NADPH) are reduced. Glutamine contributes to the accumulation of B cell biomass, protein synthesis, DNA replication and ATP production (Waters et al. 2018). Uptake of glutamine provides an additional carbon source for anabolism of other AAs and nucleic acid precursors and is processed for oxidative metabolism through the mitochondria and Krebs cycle following conversion into glutamate (Yang et al. 2014). Following activation, proliferation of lymphocytes requires sufficient uptake of the essential molecules such as nitrogen, phosphate and sulphur to increase biomass. AAs are required for mTORC1 activation and contribute to the magnitude of signalling in combination with growth factors (Carroll et al. 2017). AAs are essential for protein synthesis to fuel B cell growth, proliferation and are a source of metabolites for metabolic programs, such as the TCA cycle (Cobbold et al. 2009). AAs are processed into keto acids which undergo oxidative decarboxylation, to generate derivatives which enter the TCA cycle and be converted to usable forms of energy (Owen, Kalhan, and Hanson 2002). Activation of B cells promotes uptake of leucine and nutrient transport expression (Cho et al. 2016). Further, leucine is sufficient to promote metabolic activity though activation of mTORC1 (Abbott et al. 2016) and is required for upregulating transcriptional programs for activated B cells (Peng, Golub, and Sabatini 2002; Cho et al. 2016). Increased uptake of leucine is observed in T lymphocytes post

activation to support protein synthesis (Hayashi et al. 2013; Nakaya et al. 2014). A general overview of the metabolic pathways used by lymphocytes is depicted in **Figure 1.2.**

1.2.2 The role of nutrient- mTORC1 signalling axes in B cells

The mTORC1 complex integrates nutrient and mitogen signals which govern the size and proliferation of cells and is implicated in a range of human diseases such as cancer, autoimmunity, heart disease and diabetes (Yuskaitis et al. 2019; Nascimento et al. 2015). mTOR is an evolutionarily conserved serine-threonine kinase that acts as a sensor of intracellular nutrient availability (Dennis et al. 2001; Ekim et al. 2011). It is central for adapting cellular metabolism to a range of environmental inputs such as presence of hormones and growth factors (e.g. insulin and epidermal growth factor) (Vander Haar et al. 2007; Galbaugh et al. 2006), oxygen levels (Cho et al. 2016) and availability of nutrients (e.g. AAs and glucose) (Wolfson et al. 2016; Saxton et al. 2016; Kim et al. 2015; Hu et al. 2018). mTOR is a multi-protein complex which includes mTORC1 and mTORC2 (Martin et al. 2015). mTORC1 is an integral part of this evolutionarily conserved pathway, and complete loss of mTORC1 function in mice leads to embryonic loss (Murakami et al. 2004). Activated mTORC1 phosphorylates downstream targets p70 S6 kinase and 4E-EBP1, which leads to the control of anabolic programs which regulate cell growth, ribosomal biogenesis, protein synthesis, lipid synthesis and cell cycle progression to promote cellular proliferation (Magnuson, Ekim, and Fingar 2012; Jastrzebski et al. 2007; Iadevaia, Liu, and Proud 2014; Beirowski et al. 2017; Han and Wang 2018).

Within the cell, AAs stimulate the recruitment of inactive mTORC1 to the lysosomal membrane through Rag GTPases. Translocation of mTORC1 to the surface of this organelle enables interaction and activation by Ras homolog enriched in brain (RHEB), a small GTPase which activates mTORC1 when in its GTP-bound form. Positive and negative regulatory pathways control activation of mTORC1, which enable cells to adapt to environmental stimuli (Wong et al. 2016; Hay and Sonenberg 2004). For example, insulin and glucose activate mTORC1 activity via the inactivation of the tuberous sclerosis complex (TSC) and signalling through the PI3K-Akt pathway in order to activate RHEB and subsequently mTORC1 (Menon et al. 2014). Glucose can also signal to mTORC1 through the glycogen synthase kinase 3 (GSK3) pathway (Ma et al. 2011). Independent of this pathway, AA sufficiency is shown to be important regulating the magnitude of mTORC1 activity in the context of growth factors

through a range of signalling pathways (Wolfson et al. 2016; Chantranupong et al. 2016; Carroll et al. 2017). Arginine and leucine availability dynamically regulate mTORC1 activation through the Sestrin2 and CASTOR/ GATOR2/ GATOR1/ RagGTPase pathway which recruits and activates mTORC1 at the lysosome in conditions of AA sufficiency. An overview of this pathway is shown in **Figure 1.3**.

Conversely, insufficient AAs inactivates mTORC1, and subsequently decreases PS6-kinase activity which leads to reduced translation and protein synthesis. Compounding this effect, the mTORC1 target 4E-EBP1 also experiences increased activity as a translational inhibitor in the absence of sufficient AAs (Guertin et al. 2006). Cellular energy status is alternatively sensed by adenosine monophosphate-activated protein (AMP) kinase (AMPK), which is activated in response to elevated AMP:ATP and ADP:ATP during periods of energy stress (Zhang, Guo, et al. 2013). AMPK complexes with liver kinase B1 (LKB1) and Axis inhibitor protein (AXIN) (Zhang, Guo, et al. 2013) in order to localise to the lysosome and interact with LAMTOR1, a lysosomal protein a part of the RAGULATOR complex cooperates with RAG-GTPases to recruit and enable activation of mTORC1 (Zhang et al. 2014). The existence of multiple independent pathways allows for the spatial recruitment and activation of mTORC1 to the lysosome in response to a diverse range of activation and growth signals.

Importantly, mTORC1 signalling is important for immunity via regulation of production of cytokines, Ag presentation, cell activation, differentiation, migration, polarisation, maturation and growth (Zhang et al. 2011; Bi, Liu, and Yang 2011; Saric et al. 2016; Kim et al. 2008). The various ways in which the mTORC1 signalling pathway is shown to play an important role for maintenance and generation of B cell responses is summarised in **Table 1.1**. In brief, murine models have been used extensively to explore the role of mTORC1 signalling *in vivo* through the conditional deletion of mTORC1 regulators in the B cell compartment or through the use of rapamycin treatment to suppress mTORC1 signalling. Partial loss of mTORC1 signalling in a non-lethal mouse model showed widespread defects across organ and cellular systems, in particular a pronounced defect in the B cell compartment is noted including, altered cell size, development and Ab production (Zhang et al. 2011). In murine B cells, mTORC1 is shown to be essential for fuelling growth and enhancing proliferation following Ag exposure (Raybuck et al. 2018; Ersching et al. 2017). In addition, during development in the BM, mTORC1 signalling is essential at the pre-B cell stage and formation of downstream

immature B and mature peripheral B cells. The subsequent loss of an adequate pool of mature B cells in mice with impaired mTORC1 signalling in B cells limited ASC formation and Ab production (Iwata et al. 2016). Following generation of the mature B cell repertoire, energy requirements of resting naive B cells are relatively low. Compared with transitional B cells, FoB cells have significantly reduced expression levels of mTORC1 and reduced activity of growth pathways including ribosomal biogenesis and aerobic respiration (Farmer et al. 2019). In activated B cells, mTORC1 is vital for induction of the major GC transcriptional regulator Bcl6, and is required for optimal GCB cell development, AID expression, CSR and control of viral infection (Raybuck et al. 2018; Jones, Chernova, and Allman 2014; Li et al. 2017). Defective mTORC1 signalling impaired B cell differentiation into GCB cells, as the initiation of metabolic reprogramming in activated B cells is required to support the energetically demanding GC response (Mendoza et al. 2018). Conversely, chronic mTORC1 signalling in the absence of adaptor protein CARD11 in GCB cells, led to rapid contraction of the GC response, promoted DZ polarisation, increased cell cycling and cell size, and elevated the expression of AID and subsequent CSR (Wray-Dutra et al. 2018). However, in recent years studies have examined how essential nutritional regulators of mTORC1 are for B cell biology.

Nutrient availability and regulation of mTORC1 activation is shown to be important within the B cell compartment (Bar-Peled et al. 2013). However, there is a limited breadth in knowledge of the impact of nutrient regulation of GCB cell metabolism. The GC is a site of high metabolic activity and demand, and therefore highly influenced by availability of nutrients (Caro-Maldonado et al. 2014a; Dufort et al. 2014). Productive humoral responses rely on the ability of activated B cells to respond to a variety of nutrient availabilities throughout the occupation of distinct microenvironmental niches that differ significantly in their composition of nutrients (Jellusova et al. 2017). Activation of B cells enhances the uptake of glucose, AAs and oxygen consumption which consequently promote mTORC1 activity (Caro-Maldonado et al. 2014a; Cho et al. 2016; Doughty et al. 2006; Jellusova et al. 2017). Limitation of nutrient availability in murine studies that utilise starvation and re-feeding protocols reported that nutritional signals regulate B cell maturation and GCB apoptosis within the Peyer's patches (PP) (Okada et al. 2017; Rangan et al. 2019; Nagai et al. 2019). The growth, proliferation and survival of GCB cells hinge upon stringently controlled nutrient-mTORC1 axes (Ersching et al. 2017;

Raybuck et al. 2018). Studies which have disrupted mTORC1 and glucose and/or insulin PI3K-mTORC1 signalling pathways have reported reductions in GCB cell frequencies and impaired GCB cell glucose metabolism, maturation, proliferation, growth and SHM (Mendoza et al. 2018; Ersching et al. 2017; Benhamron and Tirosh 2011; Kunisawa et al. 2015; Jellusova et al. 2017). This affected both TD responses and chronic spontaneous GCs in the PPs, leading to diminished high affinity Ab responses and reduced serum IgM and IgG levels (Baracho et al. 2014; Benhamron and Tirosh 2011; Ersching et al. 2017). Contrary to these studies, another group reported that disrupting mTORC1 activation by deleting TSC1 in B cells has no effect on chronic or TD Ag-induced GC responses (Ci et al. 2015).

Hypoxia also controls mTORC1 activity in GCB cells. GCBs experience hypoxia within the GC and dynamically regulate their responses to oxygen availability through the binding of Von Hippel-Lindau protein to the hypoxia induced factor (HIF). HIF regulates expression of proteins involved in lipid metabolism, including the cyclooxygenase (COX)-2 enzymes (Kaidi et al. 2006). COX-2 expression is likewise required for induction of arginase-1 (Rodriguez et al. 2005; Rodriguez et al. 2009), which is essential for processing of arginine in B cells (de Jonge et al. 2002). Exposure of B cells to hypoxia or forced hypoxic programs inhibits mTORC1 activity in B cells, GCB cell clonal expansion, and consequently impairs high affinity IgG Ab responses (Cho et al. 2016).

In recent years, regulators of AA-mTORC1 signalling pathways have also emerged as important in the control of metabolism in health and disease. Using arginine-deficient transgenic mice, arginine deficiency is shown to be detrimental to the maturation of B cells in PP and SP (de Jonge et al. 2002). Loss of RagGTPase activity within the AA-mTORC1 pathway significantly reduced high affinity Ab production, GC polarisation and promoted growth programs during B cell activation for clonal expansion (Ersching et al. 2017). The clinical implications of aberrant AA-mTORC1 signalling pathways have been associated diffuse large B cell lymphomas (DLBCL) from GCB cells and activated B cell-DLBCL, whilst pre-clinical treatments have targeted AAs for cancer therapies (reviewed in (Ricci and Chiche 2018)). Together, these studies show that the generation and maintenance of GCB cells requires dynamic regulation of metabolism in response to nutrient availability.

1.2.3 Metabolic regulation of GALT-associated GCB cell responses

Humoral responses at mucosal sites are important for the maintenance of local intestinal and systemic homeostasis through selection and maintenance healthy microbiota populations (Fagarasan et al. 2010; Bergqvist et al. 2013). Gut-associated lymphoid tissue (GALT) is a component of the mucosal immune system and is comprised of the PPs, mesenteric lymph nodes (mesLN) and cells dispersed throughout the lamina propria (LP). The PP and mesLN are GALT-associated SLOs in close proximity to the gut microbiome and nutrients (Reboldi and Cyster 2016). The PPs are aggregations of lymphoid cells that form in the subepithelial space along the lumen of the intestines. B cell follicles, T cell interfollicular zones and a $CD11c^+$ DC-enriched subepithelial dome are organised within the PP lymphoid structure (Reboldi and Cyster 2016). Nutrients and microbial Ags derived from the gut are continually delivered to these sites through specialised epithelial cells and induce a state of chronic GC activity (Casola and Rajewsky 2006; Reboldi and Cyster 2016). In addition, responses in mesLNs have been described to partake in the generation of mucosal IgA (Lee et al. 2008). The generation of IgA secreting ASCs residing within the gut LP is essential for the regulation of gut microbes, and limit the penetration of microbial metabolites and promote defence against pathogens (Nagai et al. 2019; Uchimura et al. 2018). Ag within the lumen is delivered to the GALT, where CSR to IgA occurs and secretory IgA responses are induced.

Studies into the role of metabolic signalling in B cells within GALT-associated GCs have produced variable results in the literature. Examination of mTORC1 signalling in the regulation of chronic GC in the PP were examined in the context of TSC1 loss in B cells (Ci et al. 2015; Benhamron and Tirosh 2011). Ci and colleagues reported that constitutive mTORC1 signalling in the absence of TSC1-mediated regulation of insulin and glucose availability has no effect on GCB cells in the PP, while GC formation is intact (Ci et al. 2015). However, the study by Benhamron and colleagues showed that while TSC1 deletion did not affect B cell numbers, GCB cells in the PPs were significantly reduced and showed that constitutive mTORC1 signalling led to defects in TD immune responses (Benhamron and Tirosh 2011). Treatment of WT mice with rapamycin, a selective inhibitor of mTORC1, significantly reduced GCB cells in the PPs (Zeng et al. 2016). Further, the loss of Ras-related guanosine triphosphate hydrolase (GTPase) R-Ras2 which is intertwined with both the BCR and CD40 signalling pathway and the PI3K-Akt-mTORC1 pathway led to impaired glucose metabolism and GC

responses in the PP of non-immunised mice (Mendoza et al. 2018). Therefore, studies thus far indicated that mTORC1 signalling influences GCB responses in the GALT-associated GCs. Interestingly, these studies indicated that nutrient-mTORC1 signalling axes are important for GCB cell regulation within GALT-associated PPs.

The gastrointestinal tract (GIT) is the main site for nutrient absorption and AA metabolism in the body (Ruth and Field 2013). Reduced protein intake or single AA deficiencies leads to defects in intestinal integrity and gut-associated immune responses (Ziegler et al. 2003). Early studies indicated that arginine deficiency affected the maturation of B cells, and the development of PP in arginine-deficient transgenic mice (de Jonge et al. 2002). Arginine deficiency affected B cell maturation in the BM and led to a reduction of B cells in the PP and SP. However, arginine-deficiency was global and led to widespread defects from birth and thus the specific effect on B cells was not isolated. Further, starvation and re-feeding studies reported nutritional signals regulate B cell maturation and GCB cell apoptosis within the PP (Nagai et al. 2019; de Jonge et al. 2002). However, given how important AAs are for B cell activation in PPs, little is known about the regulation of mTORC1 by AAs in GALT-associated GCB cells.

1.2.4 Metabolic regulation of virus-induced GCB cell responses

Viral infection is widely used to understand the factors which govern the development of effective humoral immunity due to the importance of vaccine development and anti-viral therapies in modern medicine. A low frequency of Ag-specific lymphocytes to any given Ag persists at steady state until Ag exposure. Following infectious challenge or vaccination, Ag-specific cells are activated and undergo clonal expansion to drive adaptive humoral immunity. Studies have shown that mTOR is important for the regulation of anti-viral humoral immune responses. Disruption of mTORC1 signalling through Raptor deletion (Raybuck et al. 2018) in GCB cells impaired GC responses, Ag-specific Ab and control of viral infection. Combinatorial treatment of mice infected with lymphocytic choriomeningitis virus (LCMV) with rapamycin and RNA-interference of mTORC1 revealed that mTORC1 signalling differentially affects $CD4^+$ T cell and B cell responses during anti-viral immunity. B cells in particular required mTORC1 signalling to drive humoral responses and support the generation of TFH cells required for antiviral immunity (Ye et al. 2017). Further, the suppression of mTORC1 with rapamycin in mice infected with the IAV H3N2 subtype actually led to generation of beneficial

cross-protective Ab which provided immunity to otherwise lethal doses of heterosubtypic strains of IAV (Keating et al. 2013). Together these studies establish a requirement for mTORC1 signalling for GC responses and class switching in response to viral infection. However, the role of nutrient sensing in anti-viral B cell responses is not yet understood, despite studies indicating that viral infection induces metabolic changes in local and systemic immune responses.

1.2.5 DEPDC5

Nutrient-sensing systems, composed of sensors, transporters and signalling proteins, are utilised by cells to monitor and respond to fluctuations in environmental nutrient levels. As described above, AA sufficiency is required for mTORC1 signalling. In recent years the major checkpoint regulator of AA sensing, DEPDC5, was discovered and shown to suppress mTORC1 activity during AA deprivation conditions (Mizuno et al. 2018; Dawson et al. 2019). DEPDC5 is an evolutionarily conserved AA-sensitive negative regulator of mTORC1 and is complexed NPRL2 and NPRL3 within the GATOR1 complex, enabling mTORC1 signalling to be controlled under AA-limited conditions (Chen, Ou, et al. 2018). Two upstream proteins that sense AAs and signal to the GTPase-activating proteins toward Rags 1 (GATOR1) and Rag GTPases were recently identified as CASTOR and Sestrin2, which sense leucine and arginine respectively (Chantranupong et al. 2016). These proteins interact with the GATOR2 complex in the absence of AA, which releases negative regulation of the GATOR1 complex by GATOR2. GATOR1 activates Rag GTPases and recruits mTORC1 to the lysosomal surface for activation. DEPDC5 is essential for the GTPase-activating protein activity of the GATOR1 protein complex, as it directly interacts and facilitates regulation of Rag GTPases (Shen et al. 2018). In the presence of sufficient AAs, a ubiquitin ligase KLHL22 targets DEPDC5 for proteasome-mediated degradation through polyubiquitination, leading to mTORC1 activation in the cell (Chen, Ou, et al. 2018). Loss of DEPDC5 renders mTORC1 signalling insensitive to deprivation of nutrients and is associated with mTORC1 hyperactivation and disease (Bar-Peled et al. 2013). DEPDC5 is essential for sensing AA availability in order to negatively regulate mTORC1 signalling during periods of AA limitation and loss of DEPDC5 activity leads to mTORC1 hyperactive signalling that is insensitive to AA starvation (Dawson et al. 2019; Hughes et al. 2017). The AA sensing pathway involving DEPDC5 that controls mTORC1 is depicted in **Figure 1.3**.

Mutations in DEPDC5 have been associated with focal epilepsy, cancer, focal cortical dysplasia, hepatocellular carcinoma and metabolic dysfunction (Mizuno et al. 2018; Swaminathan et al. 2018; Ribierre et al. 2018; Nascimento et al. 2015; Anderson 2018). Global homozygous knock-out of DEPDC5 is known to be embryonically lethal in rodents. Rats homozygous for *Depdc5* deletion had delayed growth and died at day 14.5 (D14.5) post-gestation during embryogenesis (Marsan *et al*. 2016). This has been similarly observed in mice with global loss of *Depdc5,* where embryonic death is attributed to a range of defects experienced over the course of mid-gestation, including those affecting the cardiovascular system, or acquisition of hypoplasia and cranial dysplasia (Hughes *et al*. 2017). Conditional knock out of DEPDC5 in neurons led to enhanced metabolic signalling in neurons and functional neuronal defects (Yuskaitis *et al*. 2018)(Dawson et al. 2019). Further, DEPDC5 expression was shown to suppress tumour growth in breast cancer and slow ageing (Swaminathan et al. 2018; Ribierre et al. 2018; Nascimento et al. 2015; Anderson 2018).

Nutrient checkpoints, such as the GS3K-glucose checkpoint, can affect naïve B cells by regulating growth, size and quiescence (Jellusova et al. 2017). Leucine (an AA that DEPDC5 is responsive to upstream of mTORC1) is shown to affect B cell activity and metabolic gene expression (Li et al. 2018; Ersching et al. 2017). Together these findings show that AA availability shapes the metabolic programming of B cells. However, the role of AA metabolic checkpoints, such as DEPDC5, in B cells remains unexplored. Therefore, the hypothesis that DEPDC5 is required in B cells for effective humoral immune responses is to be tested in this project.

1.3 Summary of the project

At the outset of this PhD study, virtually nothing was known about the regulation of mTORC1 by AAs in B cells. However, during the period of this research, a study emerged that did lend support to the idea that AA sensing is important in B cell biology. Ersching *et al.*, showed that deletion of *Rraga*, which influences the AA-mTORC1 axis, led to increased mTORC1 activity in GCB cells, favoured DZ polarisation and resulted in defective SHM (Ersching et al. 2017). However, the contribution of the AA-mTORC1 axis to naïve B cells, GCB generation and maintenance, and Ab responses to complex Ag remain to be explored. Furthermore, the specific contribution of DEPDC5 to B cell biology is completely unknown.

To address these issues, *Depdc5* was deleted in mature B cells to disrupt the AA-mTORC1 axis and the effect on the humoral response was studied in response to IAV infection and GALT associated responses to Ag drained from the gut.

Therefore, the broad aims of this project are

1. To develop a mouse model to investigate the role of DEPDC5 in B cells.

2. To investigate the functional consequences of loss of DEPDC5 in the B cell compartment at homeostasis.

3. To investigate whether DEPDC5 influences B cell activation and the GCB cell response.

Table 1.1: The role of mTORC1 in B cell development and activation

mTOR manipulation	Model	mTOR activity	Outcome	References
Global mTORC1 hypomorphic mouse	Homeostasis	↓ mTORC1	↓ $CD138^+$ B cells ↓ B cells ↓ B cell size ↓ Transitional, FoB, MZB ↓ Migration to SDF-1/SIP	(Zhang et al. 2011)
CD19 ^{Cre} $mTOR^{f/f}$	*Streptococcus pneumoniae* NP-CGG immunisation	↓ mTORC1	Impaired GC formation ↓ IgG ↓ affinity maturation	(Zhang, Pruitt, et al. 2013)
Global mTORC1 hypomorphic mouse	Homeostasis	↓ mTORC1	Increased mouse lethality	(Zhang, Pruitt, et al. 2013)
CD20 $^{Tam\text{-}Cre}$ *Raptor* $^{f/f}$	NP-CγG immunisation	↓ mTORC1	↓ NP-specific GCBs ↓ NP-specific IgG1 Ab responses ↓ NP-specific IgM Ab responses No effect on naive B cells [Transitional, FoB, MZB] or NP-specific MBC	(Jones et al. 2016)
mTOR inhibitor Torin 1	Homeostasis	↓ mTORC1	↓ splenic MZ ↓ transitional B cells ↓ immature BM B cells	(Jones et al. 2016)
mTOR inhibitor Rapamycin	Mouse model of systemic lupus erythematosus (NZB/W mice)	↓ mTORC1	↓ autoAb production	(Lui et al. 2008)
mTOR inhibitor Rapamycin	*In vitro* LPS stimulation	↓ mTORC1	↓ GCBs ↓ anti-DNA serum Ab titres ↓frequencies of dsDNA-specific plasma	(Jones et al. 2016)
mTOR inhibitor Rapamycin	NP-CγG immunisation	↓ mTORC1	↓ phospho-S6 ↓ 70% Protein synthesis	(Benhamron and Tirosh 2011)
mTOR inhibitor Rapamycin	NP-CγG immunisation	↓ mTORC1	↓ NP-specific IgG1 Ab responses No effect on naive B cells [Transitional, FoB, MZB] or NP-specific MBC ↓ NP-specific GCBs ↑LZ:DZ ratio ↓ Expression of genes for protein translation and intracellular transport in LLPCs ↑Autophagy	(Jones et al. 2016)
mTOR inhibitor Rapamycin	NP-OVA immunisation	↓ mTORC1	↓ phospho-S6 ↓ cell growth ↓ accumulation in DZ	(Ersching et al. 2017)
Antagonist Ab to CD40L (MR-1)	NP-OVA immunisation	Prevent induction of mTORC1	↓ PHOSPHO-S6	(Ersching et al. 2017)

hu*CD20*^{CreERT2} *Raptor* $^{f/f}$	Inhibit mTOR activity	↓ mTORC1	↓ Ag-specific MBCs, PCs and GCBs ↓ AICDA ↓ SHM ↓ high affinity IgG1	(Raybuck et al. 2018)
Mb1 ^{Cre} *Raptor*$^{f/f}$	KLH	↓ mTORC1	↓ Pre-B cells, immature B, mature peripheral B cells Developmental block at pre-B cell stage ↓ mTOR, p-S6K1, ↓ Proliferation and survival ↓ Ag-specific Ab production due to lack of generation of ASCs	(Iwata et al. 2016)
mTOR inhibitor Rapamycin	Homeostasis	↓ mTORC1	↓ Pre-B cells, peripheral B cells	(Iwata et al. 2016)
CD19 ^{Cre} Tsc1$^{f/f}$	Homeostasis	Constitutive mTORC1	↑T1 / T2 transition states = partial block in maturation ↓ MZB	(Zhang, Pruitt, et al. 2013)
CD19 ^{Cre} Tsc1$^{f/f}$	Homeostasis	Constitutive mTORC1	↓ MZB No change FoB	(Meena et al. 2018)
Vav ^{Cre} *Rictor* $^{f/f}$	Homeostasis	Constitutive mTORC1	↓ MZB ↓ FoB ↑ Transitional	(Lee et al. 2013)
CD19 ^{Cre} Tsc1$^{f/f}$	T-independent type II (NP-ficoll) T-dependent (NP-CGG)	Constitutive mTORC1	↓ anti-NP IgM, IgG1 and IgG3 *in vivo* NP Ficoll no response Reduced titres NP CGG ↓ IgM *in vitro* LPS stimulation Dispersed GCs in NP-CGG D17	(Zhang, Pruitt, et al. 2013)
RERT $^{mt/mt}$ *TSC1*$^{f/f}$	*In vitro* LPS stimulation	Constitutive mTORC1	↑ phospho-S6 ↑ 30% Late apoptotic cells	(Benhamron and Tirosh 2011)
Agonist (FKG4.5) of CD40	KLH	Induce mTORC1	Induce ↑ phospho-S6 in GCBs	(Ersching et al. 2017)
Track positively selected GCBs (Ly75/Dec-OVA model)	Deliver Dec-OVA *in vivo* to positively select for Ly75+/+ GCBs	↑ mTORC1 activity	↑ phospho-S6 in GCBs (c-myc+ LZ GCBs) ↑ Glucose uptake ↑ dsRNA content ↑ cell size ↑ DZ:LZ ratio and LZ to DZ migration	(Ersching et al. 2017)
Aicda$^{cre/+}$ *Tsc1* $^{f/f}$ B1-8h	Transferred a 1:1 mixture of 1. *Aicda*$^{cre/+}$ *Tsc1* $^{fl/fl}$ B1-8h 2. *Aicda*$^{cre/+}$ *Tsc1* $^{+/+}$ B1-8h B cells into WT hosts, and immunized with NP-OVA	Constitutive mTORC1 in GCBs	↑ PHOSPHO-S6 in Tsc1 $^{f/f}$ GCBs and enriched DZ Proportion of Tsc1$^{f/f}$ GCBs ↓ overtime mTORC1 hyperactivation is competitive disadvantage	(Ersching et al. 2017)
Cd79a $^{cre/+}$ *Tsc1* $^{f/f}$	Homeostasis	Constitutive mTORC1 in B cells	↓ affinity maturation	(Ersching et al. 2017)

Rraga$^{GTP/GTP}$ or *Rraga*$^{+/+}$	Haematopoietic chimeras made from fetal livers and NP immunisation Adoptive transfer of B1-8i Rraga$^{GTP/GTP}$ or B1-8i Rraga$^{+/+}$ B cells from fetal liver chimeras into WT mice NP immunisation	Constitutive mTORC1	↓ affinity maturation Single cell sequencing of GCBs of Igh Equal accumulation of somatic mutations. ↓ Rraga$^{GTP/GTP}$ GC B cells affinity-enhancing	(Ersching et al. 2017)

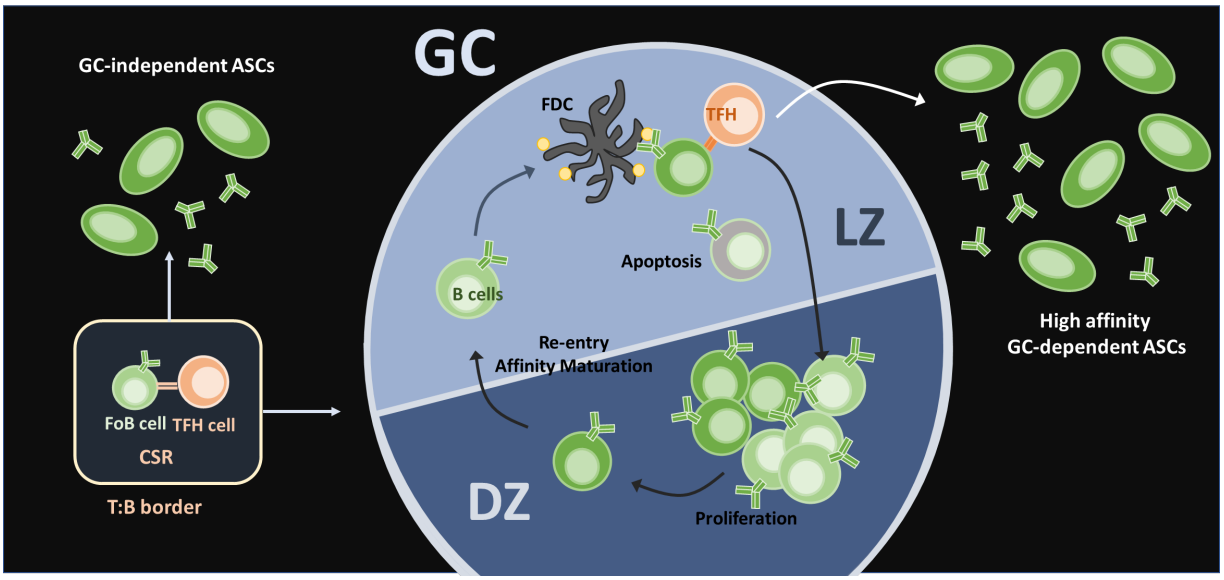

Figure 1.1: General overview of GCB and ASC formation

In TD B cell responses, naïve FoB cells are activated via Ag-driven BCR stimulation and migrate to the T-B border to present T cell Ags and receive costimulatory signals and cytokines from cognate TFH cells. CSR occurs prior to formation of the GC. Activated B cells may differentiate into short-lived ASCs independent of the GC or contribute to the formation of the GC. The GC response promotes selection of high affinity GCB cells through iterative rounds of DZ:LZ cycling, affinity based selection, proliferation and apoptosis. GCB cells may exit the GC reaction to form long-lived and high affinity ASCs.

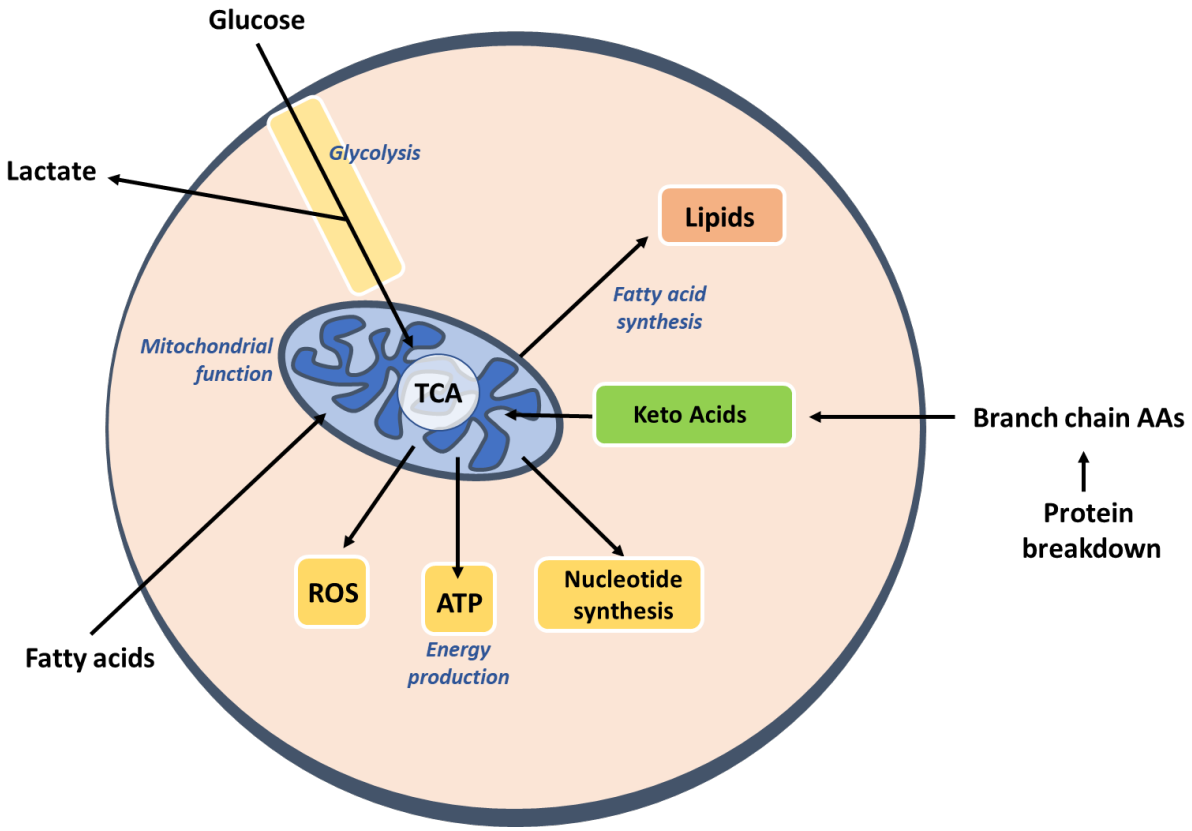

Figure 1.2: Overview of nutrients and metabolism

Glucose, fatty acids and branch chain AAs enter the cell to fuel OXPHOS and participate in the TCA cycle which occurs within the mitochondria. Branch chain AAs are converted to keto used as carbon sources for the TCA cycle. Fatty acids are broken down within the mitochondria and in turn, lipids are synthesised from precursors from the TCA cycle. The TCA cycle also promotes generation of ROS, ATP and contributes to synthesis of nucleotides. Glucose is also metabolised into pyruvate and then converted lactate through glycolysis, independent of reactions within the mitochondria. Figure adapted from (O'Sullivan and Pearce 2015).

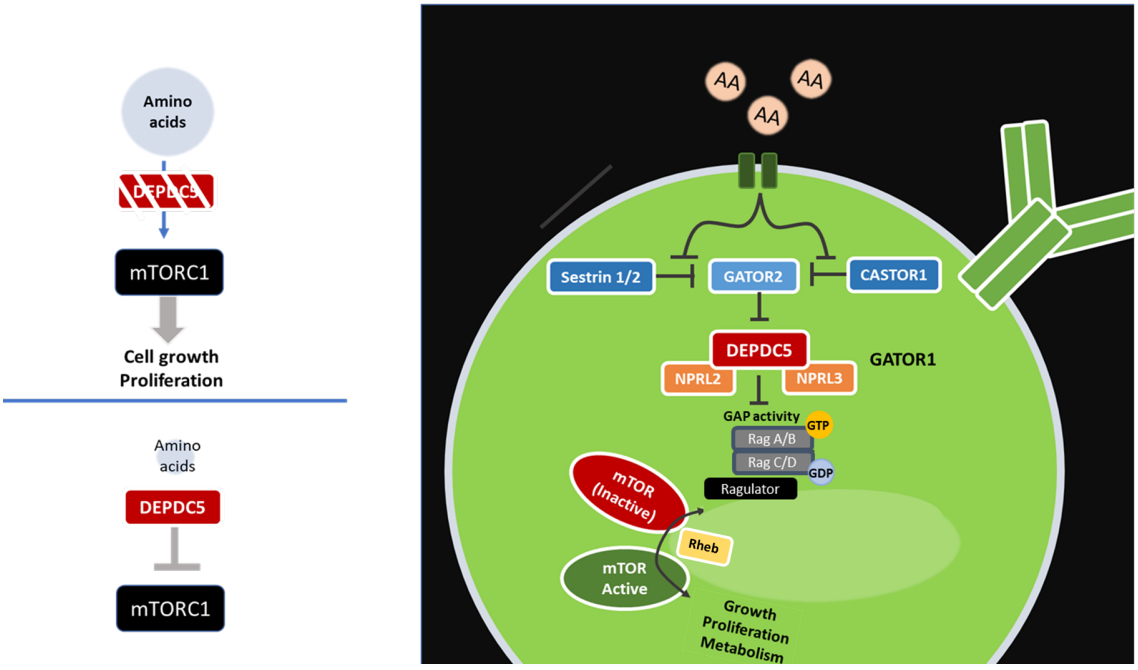

Figure 1.3: Overview of DEPDC5 mediated control of the AA-mTORC1 axis

The mTORC1 pathway promotes cell growth, proliferation and metabolism. DEPDC5 is part of the GATOR1 complex, together with proteins NPRL2 and NPRL3. GATOR1 has GTPase-activating protein activity for RagA and RagB. During AA withdrawal, Sestrin 1/2 and CASTOR1 inhibit GATOR2, a negative regulator of GATOR1. Therefore, when AAs are restricted, RagA and RagB become guanosine diphosphate (GDP)–bound causing mTORC1 to leave the surface of the lysosome and renders it inactive. When AA levels are sufficient, Setrin 1/2 and CASTOR1 release their inhibition of GATOR2, leading to the negative regulation of GATOR1. Consequently, Rag A and Rag B are loaded with guanosine triphosphate (GTP) and cooperate with the RAGULATOR complex to recruit mTORC1 on the lysosomal surface where it is activated by Rheb.

CHAPTER 2

Materials & Methods

Chapter 2

Chapter 2

Materials & methods

2.1 Mice

All mice were housed in IVC caging in specific pathogen-free conditions at the University of Adelaide central animal house. C57Bl/6J (B6) were obtained from Animal Resource Centre (Western Australia). *Depdc5*$^{fl/fl}$ mice (Dawson et al. 2019)(generated on a C57Bl/6J background) were obtained from Prof. Paul Thomas (The University of Adelaide) and were crossed with *Cd23*$^{Cre/+}$ mice (Kwon et al. 2008) obtained from Dr Kim Good-Jacobson (Monash University) to generate *Cd23*$^{Cre/+}$ *Depdc5*$^{fl/+}$ breeders for the F_1 cross. Experimental mice were generated by crossing *Depdc5*$^{fl/fl}$ with *Cd23*$^{Cre/+}$*Depdc5*$^{fl/+}$ mice. Male and female mice were used at 8 to 14 weeks old. At endpoints, mice were humanely euthanised with CO_2. The University of Adelaide Animal Ethics Committee approved all experimental procedures (dealing numbers S-2016-142, S-2017-040).

2.2 Infections and immunisations

2.2.1 Influenza challenge

Mice were anaesthetised with pentobarbital sodium (Nembutal; Ilium; 66 mg / g body weight) via the intraperitoneal route (IP). Twenty minutes (min) following anaesthesia, mice were challenged intranasally (IN) with 32µl of a preparation of A/HKx31 (X31) IAV containing 1×10^2 $TCID_{50}$ / mouse. X31 virus (Rangel-Moreno et al. 2008) was prepared by Dr Mohammed Alsharifi (University of Adelaide) and stocks provided at 2.87 x 10^6 $TCID_{50}$ / mL. Stock virus was diluted 1 in 900 in phosphate-buffered saline (PBS) to arrive at 1×10^2 $TCID_{50}$ / 32 µl. Challenged mice were monitored daily for body weight and for other clinical signs of IAV infection and were humanely euthanised if body weight loss exceeded 20% of their starting body weight (as per animal welfare guidelines).

2.2.2 NP-OVA immunisation

For ELISA experiments: To generate NP-specific Ab responses, mice were immunised IP with 100 μg / mouse of NP-OVA (BioSearch technologies) absorbed in alum in a 100 μL volume. Serum was assayed at D7, D14 and D21 post-immunisation.

For flow cytometry experiments: Mice were immunised subcutaneously with 10 μg/footpad of NP-OVA absorbed in alum in a 12 μL volume. Draining LNs were assessed at D14 post-immunisation for NP-specific GCB cells.

2.2.2 Transfers and SRCB- HEL^{2X} immunisation

Hen Egg Lysozyme (HEL)-specific B cells from transgenic B cells from MD4 x *Ptprca* (CD45.1) mice were isolated from the SP and transferred IV into WT C57Bl/6 hosts (CD45.2). The day after transfer, TD B cell responses were induced with 2×10^9 HEL^{2X} -conjugated SRBCs. Conjugation of HEL proteins to SRBCs was performed as described in (Brink et al. 2015). Immunised mice were euthanised at D6 for isolation of 'GCB MD4' cells: HEL-specific MD4 GCBs [$HyHEL9^+B220^+CD45.1^+GL\text{-}7^+CD138^-$] and 'd6 endo GCB': endogenous GCBs [$B220^+CD45.2^+GL\text{-}7^+CD138^-$]. In addition, FoB cells [$B220^+$ $CD93^-CD23^+$] and MZB cells [$B220^+$ $CD93^-CD21^+$] were sorted also from SP of naive mice. Tissue processing and flow cytometry protocols were used as described in **(2.3.1)** and **(2.4.1)**, respectively. RNA was prepared for transcriptional analysis by qPCR as described in **(2.7.2)**.

2.3 Tissue processing

2.3.1 Lymphoid tissues

SPs were dissected from recently euthanised mice, macerated into PBS and the cell suspension filtered through 70 μm nylon filters, spun at 300 x *g* for 5 minutes and then resuspended in sterile mouse red cell lysis buffer (mRCLB; **Table 2.1**) for 5 min at 37°C. The resulting single cell suspensions were washed twice in PBS and counted using a haemocytometer. Lymphoid tissues, such as PP and LNs were macerated and passed through 70 μm filters into complete B cell media (**Table 2.1**) and washed into PBS. All centrifugation steps for cells were performed at 300 x *g* for 5-20 min.

2.3.2 Lung

Following humane euthanasia, mice were perfused with 10 ml of PBS through the right ventricle to remove circulating cells. Lungs were then excised and minced within digestion medium (**Table 2.1**) in which the minced lungs were incubated for 45 min at 37°C with mixing every 15 min. Cells were then filtered through a 70 μm filter, washed with PBS and incubated with mRCLB for 5 min at 37°C before 2 X washes in PBS.

2.3.3 Peripheral blood

For end-point analysis of peripheral blood, the chest cavity of euthanised mice was opened to expose the heart. An insulin syringe was then used to extract 500 μl of blood from the heart. For time-course experiments, mice were cheek-bled. For ELISAs, blood was harvested into Eppendorf tubes and incubated at room temperature (RT) for a minimum of 60 min, prior to centrifugation at 3,000 rpm for 10-15 min. The supernatant was transferred to a fresh Eppendorf tube and stored at -20°C. For flow cytometry experiments, blood was harvested and immediately diluted in 10 mL of cold PBS, centrifuged and treated with mRCLB for 20 min at 37°C. Cells were washed twice with PBS.

2.3.4 Isolation of BM

Femurs were removed and the ends cut off. The long bones were then flushed twice with 3mL of PBS using a 23-gauge needle and syringe inserted into the end of each femur. Cells were rinsed in PBS and treated with 5 mL of mRCLB, followed by a second wash with PBS.

2.4 Protein analysis

2.4.1 Flow cytometry

To assess surface marker expression, single cell suspensions were plated at 2 x 10^6 lymphocytes per well in a round-bottom 96-well plates. Cells were stained using the Ab and reagents detailed in **Table 2.1** and **Table 2.2.** Single cell suspensions were incubated in a 1:1000 dilution of live/dead fixable dye (Life Technologies) for 10 min at RT. Cells were washed in PBS and blocked with 200 μg / mL of mouse gamma globulin (mγg) in FACS buffer (**Table 2.1**) for 5 min at RT. Cells were then stained for 20 min in FACS buffer (**Table 2.1**) using directly conjugated or biotinylated Abs detailed in **Table 2.2**. For biotinylated Ab stains, cells were

washed in FACS buffer and incubated with streptavidin conjugates in FACS buffer (see **Table 2.1**) for 15 min. Cells were always maintained on ice unless otherwise specified.

For intracellular staining, cells were fixed and permeabilised in Cytofix/Cytoperm (BD) for 30 min RT and washed in Permwash buffer (BD). The cells were then stained with intracellular Abs for 30 min. For phosphor-S6 staining, cells were stained for 2 hours (hrs). After staining, cells were washed once in Permwash buffer and then given a final rinse in PBS.

For nuclear stains, cells were fixed and permeabilised with the Perm buffer from the eBioscience Foxp3 staining kit for 30 min at RT and then washed with the Permwash bufferfrom the eBioscience Foxp3 staining kit. The cells were incubated with Abs against intracellular Ags for 30 min. For BrdU staining, cells were treated with 50 U / mL of DNase I (Sigma) in PBS for 45 min at 37°C. Cells were then washed in Permwash buffer from the eBioscience Foxp3 staining kit and stained with a fluorochrome conjugated Ab against BrdU for 30 min at RT. All stains were washed in Permwash buffer (eBioscience) and then in PBS. Stained cells were acquired on the same day using a Fortessa X20 flow cytometer (BD Biosciences) or FACSAriaIII (BD Biosciences).

2.4.2 ELISA

Serum samples or supernatants were collected from homogenized tissues or cell cultures. Samples were stored at -80°C. All incubations were performed at RT and after each step, 3X washes with PBS/0.05% Tween solution (**Table 2.1**) were performed Capture Ab or Ag were diluted in ELISA coating buffer (**Table 2.1**) and plated onto 96-well high-binding plates (Corning) overnight. The next morning, plates were washed and blocked with 200 µl of 3% bovine serum albumin (BSA) in PBS for 2 hrs and washed. Samples were diluted in 1% BSA/PBS and 50 µl / well was plated and incubated for 1.5 hrs. Plates were washed and an HRP-conjugated detection Ab was diluted in 1% BSA/PBS and 50 µl / well was added. Following a 45 min incubation, plates were washed and 80 µl of 3,3′,5,5′-Tetramethylbenzidine (TMB) solution (BioRad) was added. After the colour change had developed (approx. 2 minutes), the reaction was stopped with 50 µl of 1M orthophosphoric acid per well. Optical density of the plates was then immediately read at 450 nm using a Biotrak II spectrophotometer.

2.4.3 Western Blot (WB)

1 x 10^6 B cells were lysed in in 20 µl of lysis buffer (1 x Laemmli buffer containing 10% Dithiothreitol) and boiled for 5 min at 95°C. Samples were then loaded into the wells of a Bolt® Bis-Tris Plus pre-cast gel submerged in 1X Bolt MOPS sodium dodecyl sulphate (SDS) running buffer (Thermo Fisher). The gel was subjected to electrophoresis at 165V for 30 min at RT. The gel was then electro transferred onto a PVDF pure nitrocellulose membrane, which had been previously incubated for 10 seconds in 100% methanol and washed in MQ H_2O. The electro transfer occurred at 100V for 1 hr, with magnetic stirring at 4°C. The membrane was then incubated in blocking buffer (**Table 2.1**) for 30 min at RT before incubating with the primary anti-phospho-S6 Ab (**Table 2.2**) overnight at 4°C on a shaker and washing 3X in Tris-buffered saline (TBST) (**Table 2.1**) for 30 min. The membrane was then incubated with the primary anti-phospho-S6 Ab (**Table 2.2**) overnight at 4°C on a shaker and washed 3X in TBST for 30 min. The membrane was then incubated with anti-rabbit horseradish peroxidase (HRP) (**Table 2.2**) for 30 min at RT in blocking buffer. The membrane was washed 3X in TBST for 30 min before treating with ECL substrate (Bio-Rad) for 5 min. The membrane was then analysed using a Bio-Rad ChemiDoc imaging system. To perform subsequent stains, the membrane was washed in stripping solution for 30 min on an orbital shaker at RT (**Table 2.1**). The membrane was then incubated in blocking buffer (**Table 2.1**) for 30 min at RT, before incubation with the primary anti-β-actin Ab (**Table 2.2**) in blocking buffer for 1 hr at RT on an orbital shaker. Following 3X TBST washes, the membrane was incubated with a secondary anti-mouse-HRP (**Table 2.3**) for 30 min at RT in blocking buffer with shaking. A final round of TBST washes and ECL substrate (Bio-Rad) treatment was performed prior to chemiluminescence detection using the ChemiDoc imaging system (Bio-Rad). Band densitometry analysis of WBs was performed using ImageJ software (NIH, MD, USA).

2.6 B Cell culture

2.6.1 B cell culture

B cells were isolated from mouse spleens by negative selection using anti-CD43 beads (StemCell) followed by magnetic cell separation (MACS; Miltenyi Biotech) as per the manufacturer's instructions. Purity of the B cells was confirmed by flow cytometry using cells

sampled pre- and post-isolation and the purity was >90%. 2.5 x 10^6 B cells were rested in complete B cell media (**Table 2.1**) for 30 min at 37°C in Eppendorf tubes. Rapamycin (20 μM) (Selleck Chem) was added to inhibit mTORC1 activity. Following culture, B cells were spun down in 1.5 ml Eppendorf tubes at 300 x *g* for 6 min at 4°C. Supernatants were aspirated and cell pellets were processed for WB (**Section 2.4.3**).

2.7 Gene expression analysis

2.7.1 DNA isolation and polymerase chain reaction (PCR)

DNA isolated from B cells: Isolated B cells were processed using the QIAamp DNA kit (Qiagen). Lysates were prepared in buffer RLT (Qiagen) and DNA was isolated according to the manufacturer's instructions.

DNA isolated from tissue samples: Genomic DNA was isolated from mouse tail tips or ear notches by lysing overnight at 55°C in 100 μl of tail tip lysis buffer (**Table 2.1**) and 0.1 mg/mL of Proteinase K (Bioline). Samples were heat-shocked at 95°C for 10 min and resuspended in 400 μl UltraPure Distilled water (Thermofisher). Samples were centrifuged at 12,000 g for 15 min and stored at 4°C short-term or -20°C long-term. PCR was performed using the conditions and primers listed in the **Table 2.3**.

2.7.2 mRNA isolation and quantitative PCR (qPCR)

Cells were stained as above and sorted using a FACSAriaIII. RNA was prepared with the RNeasy Micro kit (Qiagen) and was treated with DNase I (Sigma) according to manufacturer's instructions. cDNA was prepared using the Transcriptor First Strand cDNA Synthesis Kit (Roche). qPCR was performed using the LightCycler-480 SYBR Green I Master Mix and read with a LightCycler-480 instrument (Roche). Relative gene expression of targets was calculated using the equation $2^{-(\text{CT target} - \text{CT reference})}$ where the reference gene was *Rplp0*. All primer sequences used are listed in **Table 2.3**.

2.8 Statistical analysis

GraphPad Prism v6 (San Diego, CA, USA) was used to perform statistical analysis. Data were analysed using Mann-Whitney U-tests, Chi squared analysis or a one-way ANOVA test was used for statistical analysis (each test was used as appropriate). Mann-Whitney U-tests were used for comparisons of data sets from two separate groups where a normal distribution of data could not be determined, One-way ANOVA tests were used for comparisons of data sets from 3 or more groups with a single variable, and Chi squared analysis was used to analyse statistical significance between expected and observed results for grouped data. Quantitative results are as presented as mean ± SEM. In all figure legends, $p \geq 0.05$, *; $p = 0.01$ to 0.05, **; $p = 0.001$ to 0.01, ***; $p = 0.0001$ to 0.001; ns = not significant.

Table 2.1: Solutions and reagents

SOLUTIONS	COMPOSITION	REAGENT SOURCE
PBS	1 X PBS was used for all experiments.	The University of Adelaide technical services unit (TSU)
MRCLB	- 9 parts 155 mM NH_4Cl solution - 1 part 170 mM TRIS solution - Adjusted to pH 7.2 with 1M HCL	NH_4Cl (AnalaR) TRIS (Biochemicals)
LUNG DIGEST MEDIA	-Dulbecco's modified Eagle medium (DMEM) -10% FCS -10 mM HEPES -1X penicillin/streptomycin (P/S) -2.5 mM $MgCl_2$ -30 U/ml DNase 1 -1 mg/ml collagenase from Clostridium histolyticum	DMEM (Gibco) FCS (Sigma) HEPES (ThermoFisher) P/S (Gibco) $CalCl_2$ (BDH Chemicals) DNase 1 (Sigma) Collagenase (Sigma)
FACS BUFFER	-1X PBS -1% bovine serum albumin (BSA) - 0.04% sodium azide	 BSA (Sigma) Sodium azide (Ajax Finechem)

Table 2.1 (continued)

SOLUTIONS	COMPOSITION	REAGENT SOURCE
TAIL TIP LYSIS BUFFER	-100 mM Tris buffered with HCL (pH 8.5) - 5 mM ethylenediaminetetraacetic acid (EDTA) - 0.2% SDS - 200 nM NaCL - 0.1 mg / mL Proteinase K (Stock @ 20 mg / ml in MQ) was added 1:200 as required fresh on the day of lysis.	Tris-HCL (Biochemicals) EDTA (TSU) SDS (TSU) NaCl (AnalaR) Proteinase K (Roche)
SORTING BUFFER	- PBS - 2% FCS - 1mM EDTA	 FCS (Sigma) EDTA (TSU)
4% PFA	- 1L PBS - 400 mg paraformaldehyde (PFA)	 PFA (Sigma)
1% PFA	1:4 dilution of 4% PFA in PBS	
PENTOBARBITONE	1:10 dilution in sterile PBS	
ELISA COATING BUFFER	0.1M $NaHCO_3$ in MQ, pH 9.6	$NaHCO_3$
ELISA STOP SOLUTION	1M Orthophosphoric acid	
ELISA WASH BUFFER	PBS 0.05% Tween-20	Tween-20 (Bio-Rad)
ELISA 1% BLOCKING SOLUTION	1% BSA in PBS	BSA (Sigma)

TABLE 2.1 (CONTINUED)

SOLUTIONS	COMPOSITION	REAGENT SOURCE
ELISA 3% BLOCKING SOLUTION	3% BSA in PBS	BSA (Sigma)
ELISA DEVELOPING SOLUTION	1 X TMB	eBioscience
X31 COATING AG	Used 1:200 in ELISA coating buffer	Prepared in-house by Mohammad Alsharifi lab and Timona Tyllis
NP-BSA_2 COATING AG	1:50 in ELISA coating buffer	Biosearch Technologies
NP-BSA_{21} COATING AG	1:50 in ELISA coating buffer	Biosearch Technologies
COMPLETE B CELL CULTURE MEDIA	-Dulbecco's modified Eagle medium (DMEM) -10 mM HEPES -1X Penecillin/Streptomycin - 54 μM β-mercaptoethanol	DMEM (Gibco) HEPES (ThermoFisher) Penecillin/Streptomycin (Gibco) β-mercaptoethanol (Sigma)
RAPAMYCIN	Used at 20 nM (prepared in PBS)	Merck 553210-1MG

Table 2.1 (continued)

SOLUTIONS	COMPOSITION	REAGENT SOURCE
NP-OVA/ALUM	**For I.P injections:** 100µg/mouse $NP_{(16)}$-OVA was adsorbed in alum.	$NP_{(16)}$-OVA (Biosearch Technologies) Alum (Imject Alum, Thermo Scientific)
WB LYSIS BUFFER	- 2 x Laemmli Sample buffer + 10% DTT	Laemmli buffer (Sigma) DTT (ThermoFisher)
MOPS RUNNING BUFFER	-1 Part XBolt MOPS SDS Running - Buffer -9 Parts MQ	XBolt MOPS SDS (ThermoFisher)
WB BLOCKING BUFFER	-2% BSA -0.1% Tween-20 -1 x PBS	BSA (Sigma) Tween-20 (Sigma)
WB WASHING BUFFER	-0.1% Tween-20 -1 x TBS	TBS (TSU)
WB STRIPPING SOLUTION	-25 mM glycine-HCl -1% SDS -MQ water -Adjust pH to 2	Glycine-HCl (TSU) SDS (TSU)
DEPDC5 PCR mix	- 10µl Failsafe PCR 2X PreMix J Buffer - 1µl F1 primer [20 nM] - 1µl R1 primer [20 nM] - 6.75 µl PCR Water - 0.25 µl Polymerase	BufferJ (Astral scientific) Primers (Sigma) Pol (Roche)
$CD23^{cre}$ PCR mix	- 10 µl MyTaq buffer - 1 µl F1 primer [1:5 200 nM] - 1 µl R1 primer [1:5 200 nM] - 6.75 µl PCR Water - 0.25 µl MyTaq Polymerase	MyTaqbuffer (Bioline) MyTaq Pol (Bioline)

Table 2.2: Antibodies used in this study

Specificity	Conjugate	Reactivity	Species	Clone	Stock conc [mg/ml]	Final Dilution	Source	Cat
				Application: flow cytometry				
B220	UV395	Anti-mouse	Rat	RA3-6B2	0.2	0.25	BD	563793
B220	BV510	Anti-mouse	Rat	RA3-6B2	0.2	0.25	BD	563103
B220	FITC	Anti-mouse	Rat	RA3-6b2	0.5	0.25	BD	533088
B220	BV450	Anti-mouse	Rat	RA3-6B2	0.2	0.25	eBioscience	48-0452-82
B220	PerCP-Cy5.5	Anti-mouse	Rat	RA3-6B2	0.2	0.25	BD	552771
B220	BUV496	Anti-mouse	Rat	RA3-6B2	0.2	0.25	BD	612950
BrdU	FITC	Anti-mouse	Rat	B44	20ul /test	0.25	BD	347583
CD2	PE	Anti-mouse	Rat	RM2-5	0.2	0.25	Biolegend	100107
CD5	PE	Anti-mouse	Rat	53-7.3	0.2	0.25	Biolegend	100607
CD11b	PE-Cy7	Anti-mouse	Rat	M1/70	0.2	0.25	BD	561098
CD19	PE-Cy7	Anti-mouse	Rat	eBio1D3	0.2	0.25	eBioscienc	25-0193-82
CD21	BV421	Anti-mouse	Rat	7.00E+09	0.7	0.25	Biolegend	123421
CD23	APC/AF647	Anti-Mouse	Rat	B3B4	0.2	0.25	BD	562826
CD23	Biotin	Anti-mouse	Rat	B3B4	0.5	0.25	eBioscience	13-0232-82
CD38	BV421	Anti-mouse	Rat	90/CD38	0.2	0.25	BD	562768

CD38	A647	Anti-mouse	Rat	90/CD38	0.2	0.25	BD	562769
CD38	BUV395	Anti-mouse	Rat	90/CD38	0.2	0.25	BD	740245
CD69	PE-Cy7	Anti-mouse	Hamster	H1.2F3	0.2	0.25	BD	552879
CD86	BV711	Anti-mouse	Rat	GL1	0.2	0.20	BD	740688
CD86	BV786	Anti-mouse	Rat	GL-1	0.2	0.25	Biolegend	105043
CD93	PE	Anti-mouse	Rat	Aa4.1	0.2	0.25	Biolegend	136503
CD95	PE-Cy7	Anti-mouse	Hamster	Jo2	0.2	0.25	BD	557653
CD138	510	Anti-mouse	Rat	281-2	0.2	0.25	BD	563192
CXCR4	Biotin	Anti-mouse	Rat	2B11	0.5	0.25	BD	551968
CXCR4	BV510	Anti-mouse	Rat	2B11	0.2	0.20	BD	563468
CXCR4	BV421	Anti-mouse	Rat	2B11	0.2	0.16	BD	562738
GL7	FITC	Anti-mouse	Rat	GL7	0.5	0.25	BD	561529
GL7	APC	Anti-mouse	Rat	GL7	0.2	0.25	BD	561529
IgA	PE	Anti-mouse	Goat	N/A	0.5	0.16	Southern Biotech	1040-09
IgD	PerCP-Cy5.5	Anti-mouse	Rat	11-26c.2a	0.2	0.25	BD	564273
IgG	eFlour 710	Anti-mouse	Rat	IA6-2	0.2	0.25	BD	555778
IgG1	PE	Anti-mouse	Mouse	RMG1-1	0.5	0.25	Biolegend	406607
IgG1	A647	Anti-mouse	Mouse	RMG1-1	0.5	0.25	BD	406617
IgM	BV450	Anti-mouse	Rat	R6-60.2	0.5	0.16	BD	560575
IgM	FITC	Anti-mouse	Rat	eB121-15F9	0.5	0.16	eBiosciences	11-5890-85
Ki67	eFlour 660	Anti-mouse	Rat	SolA15	0.2	0.16	Invitrogen	50-5698-82

Ki67	FITC	Anti-mouse	Rat	35/Ki-67	0.2	0.16	BD	556026
Ki67	PE-Cy7	Anti-mouse	Rat	16A8	0.2	0.16	Biolegend	652426
MHCII	FITC	Anti-mouse	Rat	2G9	0.5	0.25	BD	553623
MHCII	BB515	Anti-mouse	Rat	2G9	0.2	0.25	BD	565254
PhosphoS6 (Ser235/236)	AF647	Anti-mouse	Rat	D57.2.2E	(10mM)	0.16	Cell Signalling	4851
Probes and Dyes								
Probe/dye name								
Annexin V	FITC		-	-	(2.5ul/test)	-	BD	556547
Propidium iodide	PE		-	-	(5ul/test)	-	BD	556547
Streptavidin	BV510			-	0.1	0.21	BD	563261
Streptavidin	BUV395			-	0.1	0.21	BD	564176
Streptavidin	PE			-	0.2	0.21	BD	554062

Application: Cell culture								
IgM, μ chain specific	Purified	Anti-mouse	Goat	Polyclonal	1	1:130	Abacus	115-006-020
CD40 1mg/mL	Purified	Anti-mouse	Rat	FGK45	0.7	1:100	BioXCell	BE0016-2
Application: Western Blot								
β-actin	Purified	Anti-mouse	Rat	-	1	1:10000	Cell Signalling	4967
Mouse	HRP	Anti-mouse	Horse	-	1	1:10000	Cell Signalling	7076
phospho-S6	Purified	Anti-mouse	Rabbit	-	1	1:1000	Cell Signalling	2211
Rabbit	HRP	Anti-mouse	Rabbit	-	1	1:10000	Cell Signalling	7074
Application: ELISA								
IgG	HRP	Anti-mouse	Goat	-	1	1:10000	Southern Biotech	1021-05
IgM	HRP	Anti-mouse	Goat	-	1	1:4000	Southern Biotech	1030-05

Table 2.3: Primer Sequences

Gene	***Sequence (5'→3')***	***Dilution (Stock at 200mM)***	*Band size*	*Buffer type*	*Cycling conditions (Tm)*
LoxP PCR					
These primers amplify across the 5' loxP site of the *Depdc5^{flox} allele*					
F1	AGAGCTTCAGCCCAACTCTG	1:10	634 bp	Epicentre	95°C 1min,
R1	CTGCACTCACATGCACAGG	1:10		Buffer J	(95°C 15 sec, 60°C 15 sec, 72°C 10 sec) x35; 72°C 10 min
CD23-cre PCR					
These primers amplify the WT *Cd23* allele and the *Cd23^{Cre}* transgene					
F2	GCACGAGTAACAGCAGACATG	1:5	Cre: 1.2 kb	MyTaq Buffer	95°C 1min,
R2	CTGGGAATCTTCCTACCTGAGTATTC	1:10	WT: 403 bp		(95°C 15 sec, 55°C 15 sec, 72°C 10 sec) x35; 72°C 10 min
R3	ATCAGCCACACCAGACACAGAGATC	1:10			

Table 2.3: Primer Sequences **(continued)**

PCR to identify excision of *Depdc5* exon 3					
PCR amplifies across the recombined Depdc5 allelle (*does not amplify the WT/unrecombined Depdc5 allele due to a short extension time)*					
F3	CATGCCTACCTACCTTGAATTTTT	1:10	503 bp	KAPA Taq	95°C 1min,
R4	AACAGCCAGTGCTCTTACCAG	1:10		Buffer A	(95°C 15 sec, 62°C 15 sec, 72°C 10 sec) x35; 72°C 10 min
PCR to identify WT/non-recombined *Depdc5* exon 3					
PCR amplifies the WT allele/unrecombined Depdc5 allele (no amplification occurs following recombination)					
F4	GGCTGATCCGTGTGGAGTAT	1:10	647 bp	Epicentre	95°C 1min,
R5	AGGGCCACAACAGTAAATGG	1:10		FailSafe 2× PreMix Buffer D	(95°C 15 sec, 60°C 15 sec, 72°C 10 sec) x35; 72°C 10 min
qPCR primers					
mRPLP0 F	AGATGCAGCAGATCCGCAT				
mRPLP0 R	GGATGGCCTTGCGCA				
DEPDC5 F	TGGGGACAAACCCCGTGCAG				
DEPDC5 R	CATGCGGTCTGAGCGGTGGC				

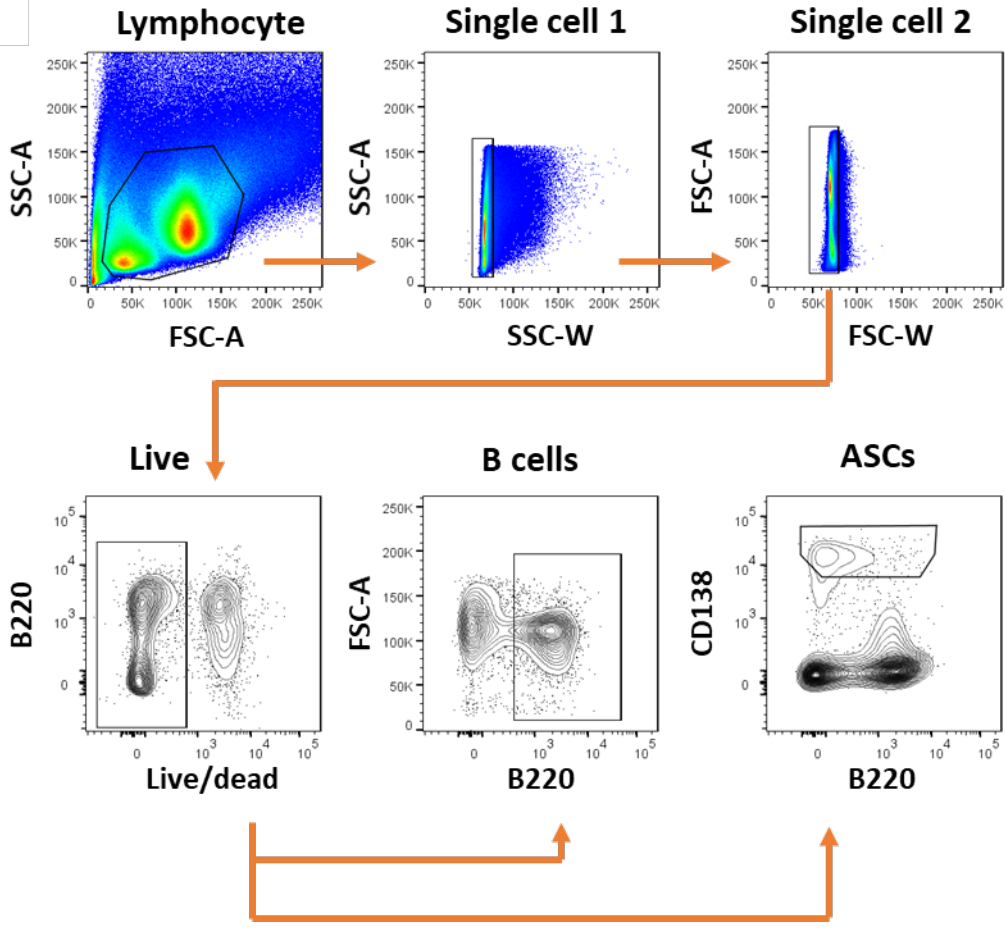

Figure 2.1: Pre-gating strategy for flow cytometric analysis

Representative flow cytometry of the pre-gating strategy used to analyse B cell populations: Lymphocyte populations (SSC-A/FSC-A), Single cell 1 (SSC-A/SSC-W), Single cell 2 (FSC-A/FSC-W), Live (Live/Dead^{-}), B cells (B220^{+}) and ASCs (CD138^{+}).

CHAPTER 3

Role of *Depdc5* in B cell homeostasis

Chapter 3

Chapter 3

Role of *Depdc5* in B cell homeostasis

3.1 Introduction

Naïve B cells are in a relatively quiescent state until Ag was encountered. Activated B cells switch to metabolic programs which support rapid growth, proliferation and differentiation. As discussed in Chapter 1, nutritional regulators were important for enabling B cells to respond and shift their metabolism in response to the availability of nutrients in different microenvironmental niches. Impaired mTORC1 signalling in B cell has been assessed using a range of knock-out and drug-based systems (summarised in **Table 1.1**), which has led to contrasting observations. Previous work has provided evidence that a global reduction in mTORC1 signalling impaired the development of mature B cells and/or B cell haematopoiesis (Zhang et al. 2011) (Jones et al. 2016). However, modification of mTORC1 signalling specifically in mature B cells has had variable impact (Zhang, Pruitt, et al. 2013) (Jones et al. 2016). Overall these reports indicated that mTORC1 signalling had a potential role in naïve B cell development and quiescence. However, it remains to be understood how the different regulatory or suppressive factors exert different effects have upon the B cell compartment. At the outset of this study, the role of AA regulators had not been examined in B cells. Furthermore, the role of AA regulators in naïve B cells has not been determined. Therefore, this study began with an investigation of the role of DEPDC5 in mature B cell development and metabolic quiescence.

3.2 DEPDC5 expression in B cells

The expression of *Depdc5* in B cell compartment was examined first by qPCR of sorted B cell subsets (B cell cDNA samples previously prepared by Dr Iain Comerford). Ag-specific and total GCBs in addition to FoB cells and MZ B cells had been purified *ex vivo* and subjected to RNA isolation and cDNA synthesis. The Ag-specific B cells were from transgenic B cells from MD4 x *Ptprca* (CD45.1) mice, which have a BCR specific for Hen Egg Lysozyme (HEL), that had been isolated from SPs and transferred IV into WT C57Bl/6J hosts. These mice had then been immunised with SRBC conjugated to HEL^{2X} peptide IP the following day. On day 6 (D6), HEL-specific MD4 GCB cells and endogenous WT GCB cells had been isolated from the SPs of the immunised mice and RNA prepared. In addition, FoB cells and MZB cells had also been sorted from naïve mice. Therefore, cDNA from all of these samples was analysed by qPCR to assess the levels of *Depdc5* transcript. A 2-fold increase in *Depdc5* transcript was observed in FoB cells compared to MZB cells (**Figure 3.1**). A significant increase in relative level of *Depdc5* transcripts was also observed in GCB cells compared to naïve FoB and MZB cells (**Figure 3.1**). Further, *Depdc5* was enriched in the high affinity Ag-specific GCB cells compared to endogenous GCB cells. Therefore, these results indicated that *Depdc5* was differentially expressed across naïve B cell and GCB compartments.

3.3 DEPDC5 was conditionally inactivated in *CD23-cre*$^{+}$ B cells

To directly address DEPDC5 function in B cell homeostasis, mice harbouring *loxP*-flanked (floxed) *Depdc5* (*Depdc5*$^{fl/f}$) alleles (Dawson et al. 2019) were inter-crossed with *Cd23*$^{cre/+}$ mice (Kwon et al. 2008), which expressed Cre recombinase under the control of the B cell-specific CD23 promoter. A schematic of the floxed *Depdc5* allele was illustrated in (**Figure 3.2**). To yield experimental mice, *Cd23*$^{cre/+}$ *Depdc5*$^{+/f}$ mice from the F2 generation were crossed to *Depdc5*$^{fl/fl}$ mice. From this cross, the experimental control mice inherited a WT and floxed *Depdc5* allele (*Cd23*$^{cre/+}$ *Depdc5*$^{+/f}$), whilst *Depdc5* experimental mice harbored both floxed *Depdc5* alleles (*Cd23*$^{cre/+}$ *Depdc5*$^{f/f}$) which facilitated Cre-mediated deletion in cells with transcriptionally active *Cd23*. *Cd23*$^{cre/+}$ *Depdc5*$^{+/f}$ and *Cd23*$^{cre/+}$ *Depdc5*$^{f/f}$

(henceforth referred to as *Depdc5*$^{+/-}$ and *Depdc5*$^{-/-}$ mice) controls were used for all experiments. Both male and female mice were used, as no sex-specific effects from DEPDC5 regulation has been previously reported (Yuskaitis et al. 2018). The inheritance of *Cd23*^{cre} and WT or floxed *Depdc5* allele(s) was assessed throughout this process (**Figure 3.3**). Previously described genotyping PCRs were employed to detect the floxed *Depdc5* allele (illustrated in **Figure 3.4a**) (Dawson et al. 2019) and the presence of the *Cd23*^{cre} transgene (illustrated in **Figure 3.4c**) (Kara et al. 2018). These assays confirmed the inheritance of floxed *Depdc5* alleles and the *Cd23*^{cre} transgene required for deletion of *Depdc5* in B cells (**Figure 3.3b** and **3.3d**).

B cells were then screened to validate efficient cell type specific deletion of *Depdc5* in these mice. FACS sorted splenic B cells from naive *Depdc5*$^{+/-}$, *Depdc5*$^{-/-}$ and WT B6 mice were prepared and genomic DNA extracted. This was subjected to PCR to screen for the recombination event that deletes *Depdc5*. As controls, DNA was also prepared from each donor's tail tip as cells in this site do not express *Cd23* and thus no recombination of the floxed *Depdc5* allele should occur regardless of genotype. The PCR to detect the deletion of *Depdc5* was as previously described (Dawson et al. 2019) (illustrated in **Figure 3.5a**). *Depdc5*$^{+/-}$ and *Depdc5*$^{-/-}$ B cells were positive for recombination of the floxed *Depdc5* allele, while tail tip DNA isolated from both strains of mice were negative (**Figure 3.5b**). The WT *Depdc5* exon 3 was amplified from *Depdc5*$^{+/-}$ B cells, *Depdc5*$^{-/-}$ tail tips and *Depdc5*$^{+/-}$ tail tips but was completely absent in *Depdc5*$^{-/-}$ B cells (**Figure 3.5b**). Together this indicates that exon 3 of *Depdc5* was efficiently deleted in *Depdc5*$^{-/-}$ B cells. *Depdc5*$^{+/-}$ B cells were positive for both the intact exon 3 and for the PCR product produced when the *Depdc5* allele was excised, consistent with their inheritance of a WT and floxed *Depdc5* allele. Therefore, these two strains of mice were deemed suitable for examining essential roles of *Depdc5* in B cell biology.

Global homozygous deletions of *Depdc5* result embryonic lethality in mice (Ricos et al. 2016; Swaminathan et al. 2018) . To test the effect of loss of DEPDC5 in B cells on the viability of mice, the frequency of each genotype from *Cd23*$^{cre/+}$ *Depdc5*$^{+/f}$ x *Depdc5*$^{f/f}$ crosses was calculated and compared to the expected Mendelian ratios if there was no impact of loss of *Depdc5* in B cells on viability. In total, 100 pups were sampled from the litters, and a 1:1:1:1 Mendelian ratio (25 mice/genotype) for the F3 offspring would be expected for all

four genotypes: *Cd23*$^{cre/+}$*Depdc5*$^{+/f}$, *Cd23*$^{cre/+}$ *Depdc5*$^{f/f}$, *Cd23*$^{+/+}$*Depdc5*$^{+/f}$ and *Cd23*$^{+/+}$*Depdc5*$^{f/f}$ (**Figure 3.6a**). There was no significant difference between the frequencies of these genotypes observed in the offspring as assessed by Chi squared analysis (**Figure 3.6b** p=0.8863). Therefore, unlike global *Depdc5* deletion, loss of *Depdc5* in mature B cells was not embryonically lethal and does not impact on mouse viability.

3.4 Effect of *Depdc5* deletion on mTORC1 signalling in B cells

DEPDC5 has been established to restrain mTORC1 signalling in various cell types (Swaminathan et al. 2018; Ricos et al. 2016; Dawson et al. 2019; Hughes et al. 2017; Yuskaitis et al. 2019; de Calbiac et al. 2018; Yuskaitis et al. 2018). Therefore, to verify if *Depdc5* deletion in B cells also had a functional impact on mTORC1 signalling, an mTORC1 activity assay was employed. Phosphorylation of the ribosomal protein S6 (240/244) (phospho-S6) by PS6-K, a downstream effector of mTORC1, was used to assess mTORC1 activity (Swaminathan et al. 2018; de Calbiac et al. 2018). B cells were isolated from *Depdc5*$^{+/-}$, and *Depdc5*$^{-/-}$ mice and incubated in B cell medium in the absence of serum. Rapamycin treated cells were also included to assess the dependency on mTORC1 activation for any observed changes in phospho-S6 levels. Thus, B cells were rested for 1 hour at 37°C in the presence or absence of rapamycin. Lysates were prepared from these B cell preparations and western blot (WB) was performed using an Ab specific for the phosphorylation of ribosomal protein S6 (Ser240/244). A β-actin WB was sequentially performed on the membrane as a loading control. In resting untreated B cells, phospho-S6 levels were increased significantly in *Depdc5*$^{-/-}$ B cells compared to *Depdc5*$^{+/-}$ B cells (**Figure 3.7a** and **b**). Treatment of B cells with rapamycin reduced phospho-S6 levels in *Depdc5*$^{-/-}$ B cells significantly compared to untreated *Depdc5*$^{-/-}$ B cells. The level of phospho-S6 in both B cell groups were equivalent following rapamycin treatment. Thus, DEPDC5 restrains basal mTORC1 activity in resting mature B cells.

3.5 Effect of loss of DEPDC5 in B cells on their development

The consequence of *Depdc5*-deletion in the B cell compartment in the context of the B cell

development and maturation *in vivo* was investigated next. B cell haematopoiesis has been reported to be unaffected by deletions driven by *Cd23*^{cre} activity as CD23 expression was restricted to transitional and mature B cells (Kwon et al. 2008). Therefore, no changes in B cell development were expected in the *Depdc5*$^{-/-}$ mice. To verify this, developmental B cell populations in the BM of each group were assessed by flow cytometry. Equivalent frequencies and numbers of pre-B [B220^{+}CD2^{-}IgM^{-}], mature B cells [B220^{+}CD2^{+}IgD^{+}], pro-B cells [B220^{+}CD2^{+}IgD^{-} IgM^{-}] and immature B cells [B220^{+}CD2^{+}IgD^{-}IgM^{+}] were observed in the BM of *Depdc5*$^{+/-}$ and *Depdc5*$^{-/-}$ mice (**Figure 3.8**). Therefore, *Depdc5*$^{-/-}$ mice exhibited no defect in B cell ontogeny that would lead to downstream effects that could confound interpretation of phenotypes in peripheral mature B cells.

Following exit from the BM, B cells migrate to the SP to undergo development through three transitional stages of development and lead to maturation of the B cell compartment (discussed in Chapter 1). The overall B cell compartment was assessed in the SLOs of *Depdc5*$^{+/-}$ and *Depdc5*$^{+/-}$ mice at homeostasis. B cells were unchanged in both frequency and number in both SP and skin-draining LNs between these genotypes (**Figure 3.9**). As discussed previously, the role of mTORC1 signalling on the transitional B cell and mature B cell compartment was still poorly understood. Variable outcomes have been observed in B cell development following manipulation of mTORC1 signalling (discussed in Chapter 1), however drawing conclusions from a limited range of broad-inactivation systems and cellular-restricted systems may not be sufficiently robust. Firstly, knock-on effects from defective developmental B cell populations following global mTORC1 suppression or inactivation could manifest in the defects observed in transitional or mature compartments. Second, mTORC1 integrates signals from a wide range of environmental stimuli using regulatory factors, and the contribution of each environmental-regulatory protein axis may be different for each cell type assessed. Third, inconsistencies in the mode of selective deletion of mTORC1 regulators may lead to further variability. Therefore, the role of DEPDC5 in the development of transitional and mature B cells was examined to contribute to this growing field. Transitional B cells in the spleen were gated according to a published strategy as T1: B220^{+}CD93^{+}CD23^{-}IgM^{+}, T2: B220^{+}CD93^{+}CD23^{+}IgM^{+}, T3: B220^{+}CD93^{+}CD23^{-}IgM^{-} (Teague et al. 2007) (**Figure 3.10a**). The frequency and number of T1 and T2 B cells were assessed by flow cytometry as they were a part of the maturation process that generates mature FoB and MZB cells. Results indicated that both T1 and T2 B

cell frequencies were unaltered between *Depdc5*$^{+/-}$ and *Depdc5*$^{-/-}$ mice (**Figure 3.10b** and **c**). This indicated that the T1→T2→mature B cell pathway appeared to be intact in the absence of DEPDC5 in B cells. T3 B cells were shown to be anergic and following disruption in this population, a defect in tolerance was observed (Teague et al. 2007). Assessment of T3 B cell populations also revealed no difference between the *Depdc5*$^{+/-}$ and *Depdc5*$^{-/-}$ mice. Together, analysis of these subsets revealed no apparent block in the early B cell maturation or in anergic dysfunction in the absence of *Depdc5* in B cells.

The mature B cell compartment was examined in the SLOs to assess the impact of *Depdc5* deletion. As discussed previously, FoB cells were the central focus of the mature B cell compartment due to the impact of nutrient and metabolic regulation on their quiescence (Farmer et al. 2019). However, the impact of mTORC1 on MZB populations has not been robustly explored. Recent studies which have noted that disruptions in MZB cells following manipulation of mTORC1 was in the context of upstream affects in the B cell developmental pathway (Sintes et al. 2017). Thus, FoB and MZB cells were both analysed by flow cytometry according to widely used gating strategies (FoB: B220^{+}CD93^{-}CD23^{+}CD21$^{lo/mid}$, MZB: B220^{+}CD23^{lo}CD93^{-}CD21^{hi}) (Kwon et al. 2008; Vilagos et al. 2012). Splenic MZB cell frequencies and numbers were unchanged between *Depdc5*$^{+/-}$ and *Depdc5*$^{-/-}$ mice (**Figure 3.11**). In both the SP and iLNs, FoB cells were examined and were observed to be indistinguishable in terms of frequency and number between *Depdc5*$^{+/-}$ and *Depdc5*$^{-/-}$ mice (**Figure 3.12**). Overall, no defects in B cell development were apparent between *Depdc5*$^{-/-}$ mice compared with *Depdc5*$^{+/-}$ littermate controls. Collectively, these data showed that loss of *Depdc5* in B cells does not affect mature B cell generation.

3.6 DEPDC5 regulates basal activity of FoB cells

At homeostasis, FoB cells are quiescent until encounter with cognate Ag which signals growth, proliferation and differentiation. Metabolic checkpoint sensors, such as GSK3, have been reported to enhance naive B cell survival by preventing unchecked cell growth when glucose was limiting (Jellusova et al. 2017). Following activation, FoB cells switch to anabolic metabolism to support proliferation, growth and differentiation. To determine whether increased levels of mTORC1 signalling in B cells resulting from *Depdc5* loss (**Figure 3.7**) led to perturbations in B cell activation; cellular growth and activation

parameters were assessed at homeostasis analysed by flow cytometry. In freshly isolated B cells, the mean forward scatter (FSC-A) values were used as a measure of cell size, which was known to be under the control of the mTORC1 pathway (Ersching et al. 2017). FoB cells showed signs of unrestrained cellular growth in the absence of *Depdc5*, as evidenced by an increase in FoB cell size (**Figure 3.13a**). B cell activation has not previously been assessed in prior studies examining the role of nutrient signalling and/or mTORC1 signalling in naive FoB cells. MHC-II and CD86 were upregulated following B cell activation (Adler et al. 2017) and were measured in naive *Depdc5*$^{+/-}$ and *Depdc5*$^{-/-}$ mice to assess basal activity of FoB cells. The frequency, but not number, of CD86^{+} MHCII^{+} FoB cells was increased in *Depdc5*$^{-/-}$ mice compared to *Depdc5*$^{+/-}$ mice (**Figure 3.13b(i)**). This was accompanied with an increase in expression levels of CD86 and MHCII in *Depdc5*$^{-/-}$ FoB cells compared to *Depdc5*$^{+/-}$ as measured by geometric mean fluorescent intensity (gMFI) (**Figure 3.13b (ii)**). These data showed that *Depdc5* deletion in B cells increased basal activity and growth in FoB cells.

Increased cell growth and basal activity typically precede cellular division or lead to cell death (Ersching et al. 2017). Therefore, proliferation and apoptosis in FoB cells was assessed in naive *Depdc5*$^{+/-}$ and *Depdc5*$^{-/-}$ mice. Homeostatic proliferation has been reported to contribute to maintaining naive B cell populations in the periphery (van Zelm et al. 2007). Ki67 expression increases as cells transition through mitosis. A low frequency and number of Ki67^{+} FoB cells were present in both *Depdc5*$^{+/-}$ and *Depdc5*$^{-/-}$ mice at homeostasis, and these did not differ significantly between these genotypes (**Figure 3.14a**). Therefore, these data indicated that DEPDC5 did not affect homeostatic proliferation of FoB cells. Apoptosis was regulated by metabolic signalling and activation (Liu, Xu, and An 2017; Kakiuchi et al. 2019) and was assessed by annexin V (AV) and propidium iodide (PI) staining. AV/PI staining was used to identify live, early apoptotic or late apoptotic cells (as indicated in **Figure 3.14b**). Briefly, AV binds to phosphatidylserine located within the inner surface of the cell membrane in live cells but which flips to the extracellular side during apoptosis. PI was a DNA-binding dye that stains late stage apoptotic or necrotic cells due to rupturing of the plasma and nuclear membranes. Therefore, cells can be categorised based on their expression of AV and PI as follows: AV^{-}PI^{-} (live), AV^{+}PI^{-} (early apoptotic) and AV^{+}PI^{+} (late apoptotic). No perturbations were observed in FoB cell survival or death in *Depdc5*$^{-/-}$ mice compared to *Depdc5*$^{+/-}$ controls (**Figure 3.14b**).

Together, these data indicated that, despite the increased cell size and activation status measured when DEPDC5 was deleted in B cells, DEPDC5 did not affect homeostatic proliferation or survival of FoB cells. However, the results indicated that AA-mTORC1 signalling regulated metabolic quiescence in naïve B cells.

3.7 Conclusions

The data in this chapter established the following:

- *Depdc5* was expressed by FoB and MZ B cells but was more abundant in FoB cells. It appeared to be expressed at even higher levels in GCB cells.
- A transgenic mouse with conditional deletion of *Depdc5* in B cells was generated and led to efficient B cell-specific gene-knock out of *Depdc5*.
- Deletion of *Depdc5* in mature B cells had no detriment to overall mouse viability.
- There were no apparent alteration in the generation of B cells in the absence of DEPDC5 in B cells.
- Loss of DEPDC5 in B cells increased levels of phospho-S6 in resting mature B cells, a key indicator of increased mTORC1 activity.
- In mice lacking DEPDC5 in B cells, FoB cells exhibited increased basal activation and growth signatures; an indicator of elevated metabolic rate.
- No changes in homeostatic B cell proliferation or apoptosis were apparent in resting animals when DEPDC5 was deleted.

Together, these data revealed a novel role for the AA-mTORC1 checkpoint, DEPDC5 and constitutive mTORC1 signalling for the regulation of the FoB basal activation state at homeostasis. These data was discussed in more detail in Chapter 5.

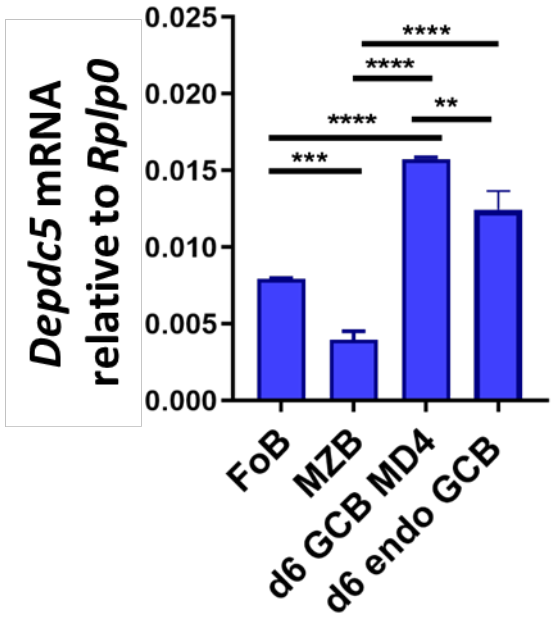

Figure 3.1: *Depdc5* expression in B cells

cDNA from MD4 x *Ptprca* B cells (CD45.1) that had been transferred into C57Bl/6 (CD45.2) recipient mice immunized with SRBC:HEL^{2X} was analysed by qPCR. This cDNA was prepared from cells sorted on D6 post-immunisation, ('D6 GCB MD4' were: HEL-specific MD4 GCBs [HyHEL9^{+}B220^{+}CD45.1^{+}GL-7^{+}CD138^{-}] and 'D6 endo GCB' were endogenous GCBs [B220^{+}CD45.2^{+}GL-7^{+}CD138^{-}]. In addition, FoB cells [B220^{+}CD93^{-}CD23^{+}] and MZB cells [B220^{+}CD93^{-}CD21^{+}] were sorted also from SP of naive mice. All samples were analysed by qPCR for *Depdc5* expression. *Depdc5* expression was calculated relative to the level of *Rplp0*. Each column represents the mean ± SD, N= 3 mice. P values were generated using a one-way ANOVA test.

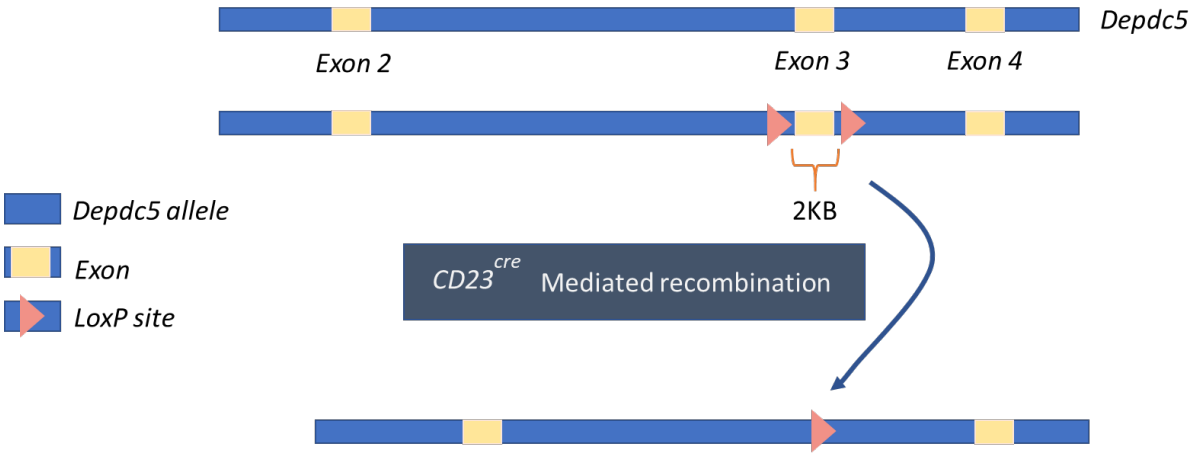

Figure 3.2: Schematic of conditional CD23^{cre} mediated deletion of *Depdc5* Exon 3

Illustration of the exon-intron structure of the *mus musculus Depdc5* gene based on NCBI Genomic Sequence: NC_000071.6 Chromosome 5 (Ref. GRCm38.p6 C57BL/6J). Magnified schematic of the *Depdc5* exon 3 region. In the floxed *Depdc5* allele, LoxP sites flank exon 3 of the *Depdc5* allele over a 2kb region. *CD23*-Cre recombinase mediated recombination of the floxed sites leads to excision of exon 3.

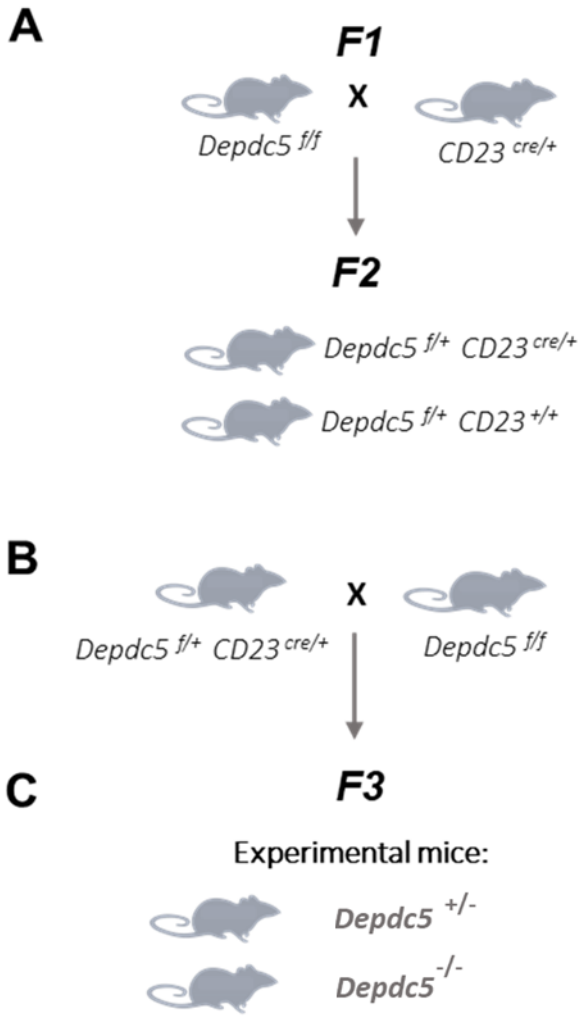

Figure 3.3: Breeding strategy to generate *Cd23*$^{cre/+}$ *Depdc5*$^{+/f}$ and *Cd23*$^{cre/+}$ *Depdc5*$^{f/f}$ littermate controls

(A) F1 cross: A homozygous *Depdc5* floxed mouse (*Depdc5*$^{f/f}$) and *Cd23*$^{cre/+}$ mouse were crossed**. (B)** F2 cross: *Cd23*$^{cre/+}$ *Depdc5*$^{+/f}$ offspring from the F1 cross were mated with *Depdc5*$^{f/f}$ mice. **(C)** F3 generation: *Cd23*$^{cre/+}$ *Depdc5*$^{+/f}$ and *Cd23*$^{cre/+}$ *Depdc5*$^{f/f}$, referred to in the text as *Depdc5*$^{+/-}$ and *Depdc5*$^{-/-}$ mice respectively, were used experimentally.

Figure 3.4: Inheritance of the floxed *Depdc5* allele

(A) Schematic representation validating the insertion of loxP sites using primers (red) flanking the 5' and 3' regions of exon 3. **(B)** Representative PCR using DNA from tail tips from *Depdc5*$^{+/-}$ and *Depdc5*$^{+/+}$ mice. **(C)** Schematic representation for the amplification of wild type *Cd23* [403bp] (primers: 5' purple, 3' blue) and *Cd23*^{cre} [1.2kb] (primers: 5' purple, 3' purple). **(D)** Representative PCR and amplification of a wild-type allele and/or Cre transgene from tail tip DNA from *Cd23*$^{+/+}$ and *CD23*$^{cre/+}$ mice.

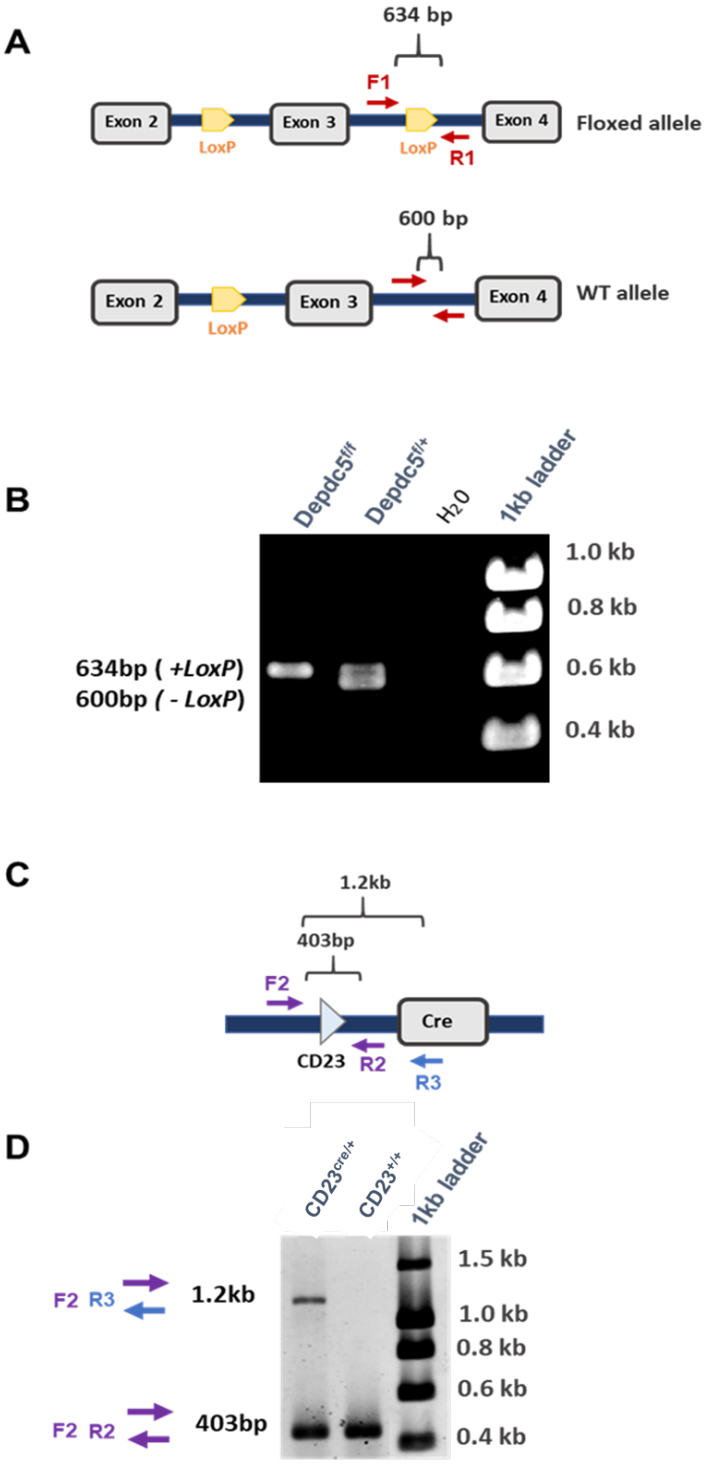
A
634 bp
F1
Exon 2
LoxP
Exon 3
LoxP
Exon 4
R1
Floxed allele
600 bp
Exon 2
LoxP
Exon 3
Exon 4
WT allele
B
Depdc5f/f
Depdc5f/+
H20
1kb ladder
634bp (+LoxP)
600bp (- LoxP)
1.0 kb
0.8 kb
0.6 kb
0.4 kb
C
1.2kb
403bp
F2
Cre
CD23
R2
R3
D
CD23cre/+
CD23+/+
1kb ladder
F2 R3
1.2kb
F2 R2
403bp
1.5 kb
1.0 kb
0.8 kb
0.6 kb
0.4 kb

Figure 3.5: The floxed *Depdc5* allele was deleted in B cells

(A) Schematic representation for amplification of exon 3 regions of *Depdc5* that were excised following Cre-mediated recombination of LoxP sites. Primers F4 and R5 (in orange) were located outside of the region flanked by LoxP sites. Primers F3 and R4 (in green) were within the region flanked by LoxP sites. PCR was performed on DNA isolated from the tail tips (as a control) and B cells from both *Depdc5*$^{+/-}$ and *Depdc5*$^{+/+}$ mice. **(B)** PCR amplification of the site following exon 3 excision [504bp band] using primers F4 and R5 (LHS of the gel). PCR amplification of exon 3 in the non-recombined *Depdc5* allele [647bp band] using Primers F4 and R5 (right hand side of the gel).

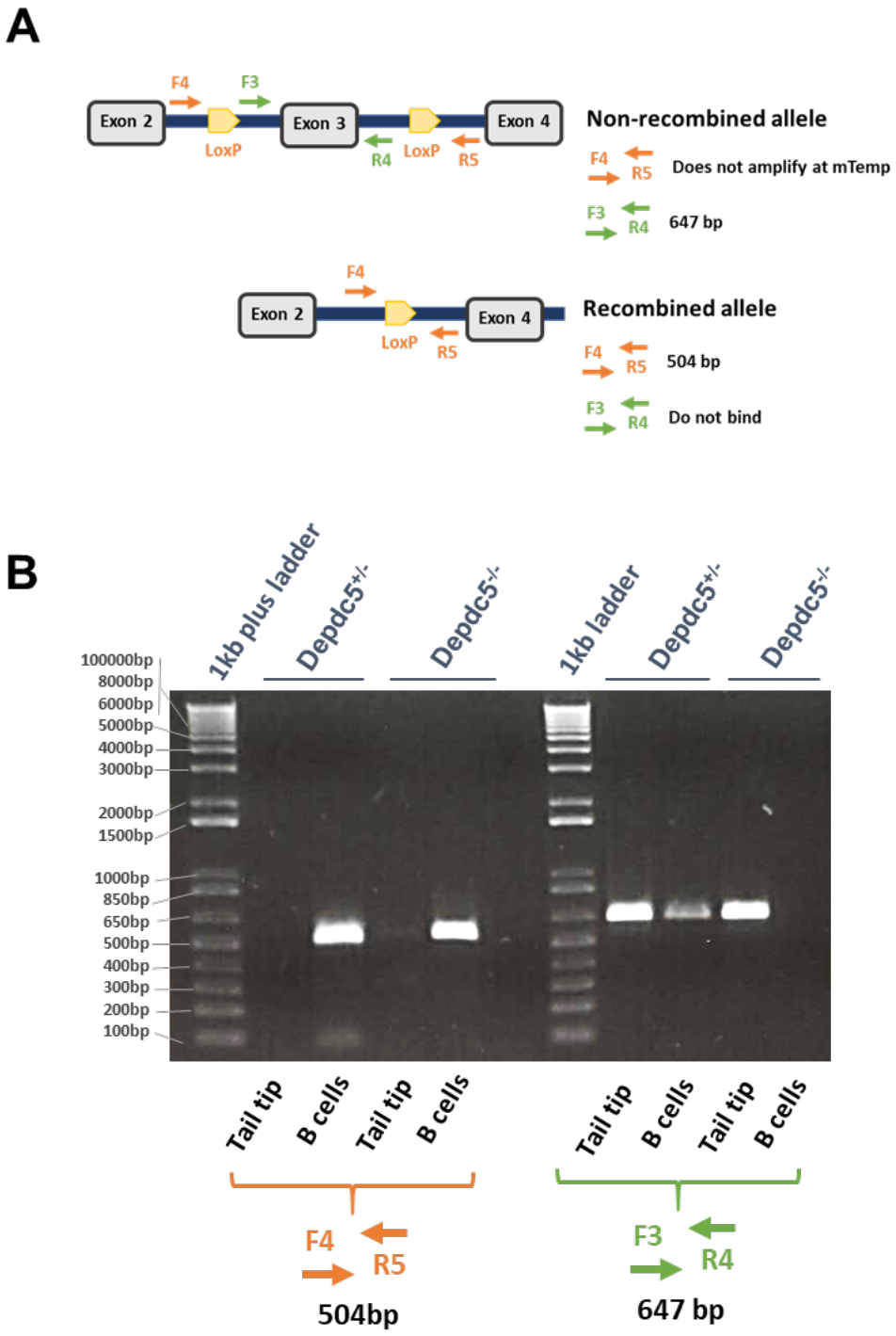
A
F4
F3
Exon 2
Exon 3
Exon 4
LoxP
LoxP
R4
R5
Non-recombined allele
F4
R5
Does not amplify at mTemp
F3
R4
647 bp
F4
Exon 2
Exon 4
LoxP
R5
Recombined allele
F4
R5
504 bp
F3
R4
Do not bind
B
1kb plus ladder
Depdc5+/-
Depdc5-/-
1kb ladder
Depdc5+/-
Depdc5-/-
100000bp
8000bp
6000bp
5000bp
4000bp
3000bp
2000bp
1500bp
1000bp
850bp
650bp
500bp
400bp
300bp
200bp
100bp
Tail tip
B cells
Tail tip
B cells
Tail tip
B cells
Tail tip
B cells
F4
R5
504bp
F3
R4
647 bp

A

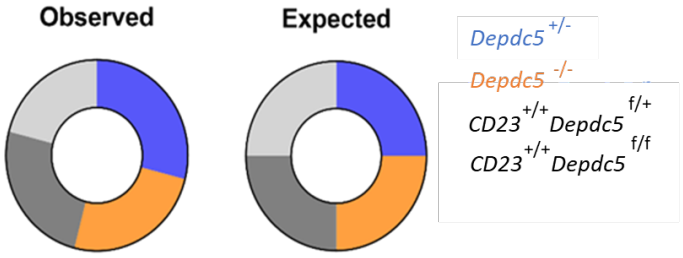

B

	Depdc5 +/-	Depdc5 -/-	CD23 +/+ Depdc5 f/+	CD23 +/+ Depdc5 f/f
Expected	25	25	25	25
Observed	25	21	29	25

Figure 3.6: Normal mendelian ratios observed in the F3 generation

Genotypes of mice from the *Depdc5*$^{f/f}$ x *CD23*$^{cre/+}$ *Depdc5*$^{+/-}$ inter-cross were determined by PCR. **(A)** Expected and observed numbers of offspring from the *Depdc5*$^{f/f}$ x *CD23*$^{cre/+}$ *Depdc5*$^{+/-}$ inter-cross. **(B)** Chi square test performed on 100 mice sampled from the litters. Number of mice per genotype enumerated in each genotype is indicated. N=100 mice (21-29 mice/genotype). Chi-squared test. p= [0.8863].

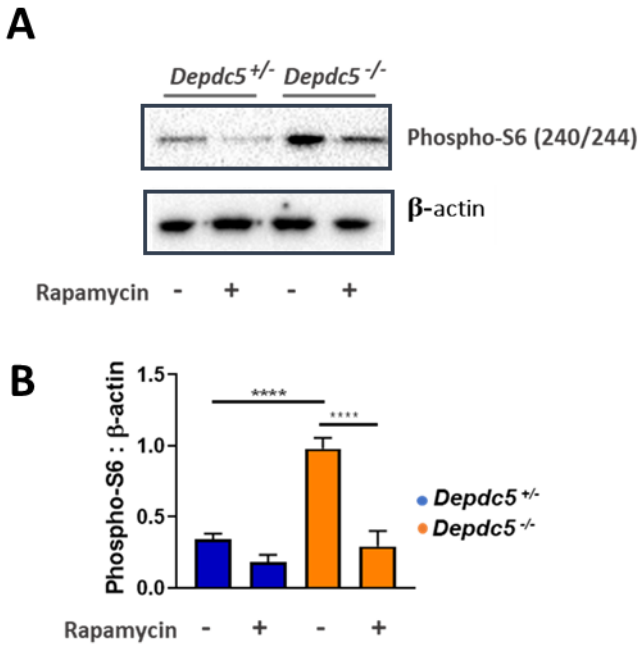

Figure 3.7: DEPDC5 loss increased the basal level of phospho-S6 in B cells

B cells ($CD43^-$) were purified from the SPs of *Depdc5*$^{+/-}$ and *Depdc5*$^{-/-}$ mice and then rested in incomplete media (- fetal calf serum) for 1 hour at 37°C. B cells were treated with or without 20μM rapamycin during this incubation. **(A)** phospho-S6 (34kD) and β-actin (40kD) protein levels were assessed by western blot, **(B)** bands were quantified using the ImageJ densitometric program, and phospho-S6 levels were normalized to β-actin protein. N=3-4/group, data are pooled from three independent similar experiments. The columns represent the mean ± SEM. A one-way ANOVA test was used for statistical analysis.

Figure 3.8: DEPDC5 loss did not impact development of B cells in the BM

BM cells from 8-12 week-old naive *Depdc5*$^{+/-}$ and *Depdc5*$^{-/-}$ mice were assessed for developmental B cell populations by flow cytometry. **(A)** Gating strategy for pre-B [B220^{+}CD2^{-}IgM^{-}], mature B cells [B220^{+}CD2^{+}IgD^{+}], pro-B cells [B220^{+}CD2^{+}IgD^{-} IgM^{-}] and immature B cells [B220^{+}CD2^{+}IgD^{-}IgM^{+}] in the BM. Representative flow cytometry **(B)** is shown with quantification **(C)** of developmental B cells in *Depdc5*$^{+/-}$ and *Depdc5*$^{-/-}$ mice. The columns represent the mean ± SEM. N=8 mice/group, data are pooled from two independent experiments. A one-way ANOVA test was used for statistical analysis.

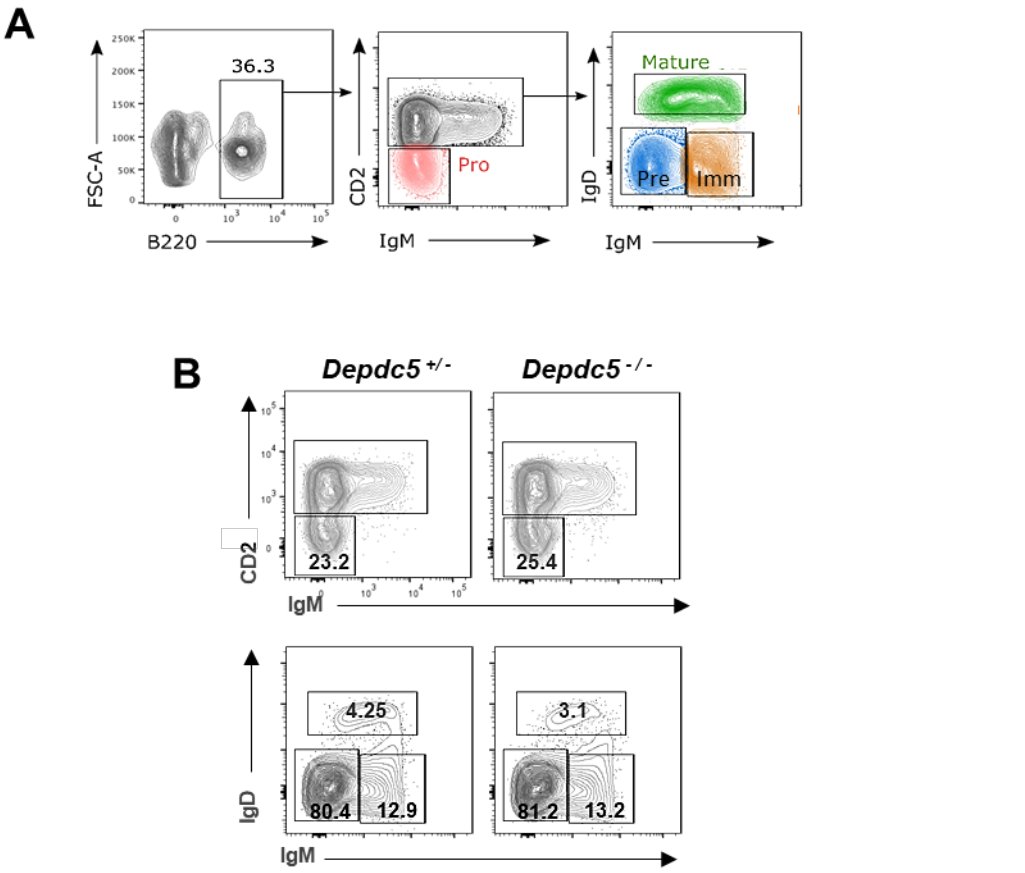
A
36.3
FSC-A
B220
CD2
IgM
Pro
IgD
Pre
Imm
Mature
B
Depdc5 +/-
Depdc5 -/-
23.2
25.4
4.25
3.1
80.4
12.9
81.2
13.2
C
% of B cell
# of cells
Immature
Mature
PreB
ProB
Depdc5 +/-
Depdc5 -/-

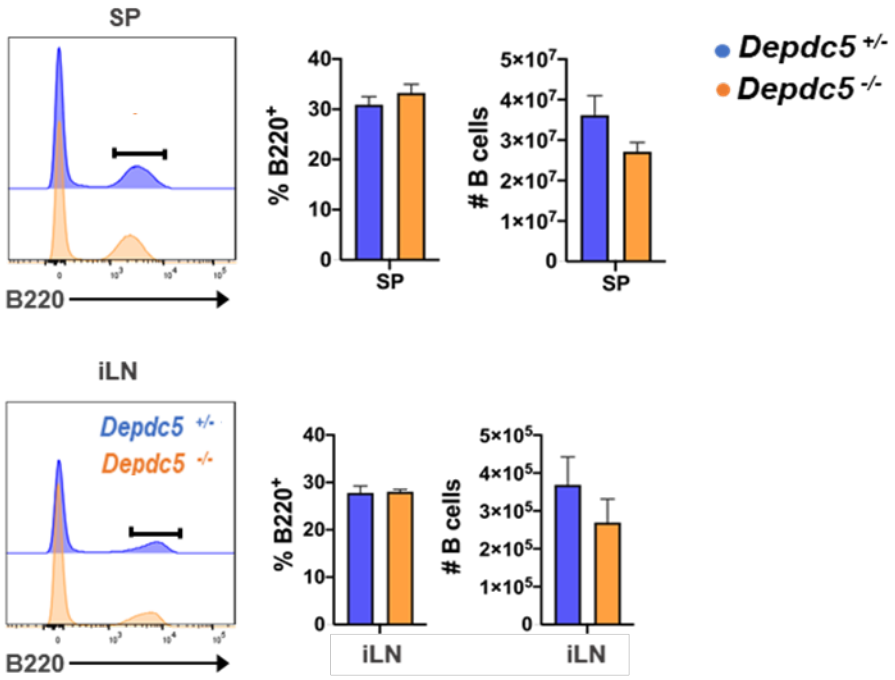

Figure 3.9: The size of the total B cell compartment at homeostasis in the SLOs was unaffected by *Depdc5* loss

SLOs from 8-12 week-old naive *Depdc5*$^{+/-}$ and *Depdc5*$^{-/-}$ mice were assessed for B cells by flow cytometry. Representative flow cytometry is shown with quantification of B cells (B220^{+}) from the SP and iLNs of *Depdc5*$^{+/-}$ and *Depdc5*$^{-/-}$ mice at homeostasis. N=8 mice/group, data are pooled from two independent experiments. The columns represent the mean ± SEM. A Mann-Whitney U-test was used for statistical analysis.

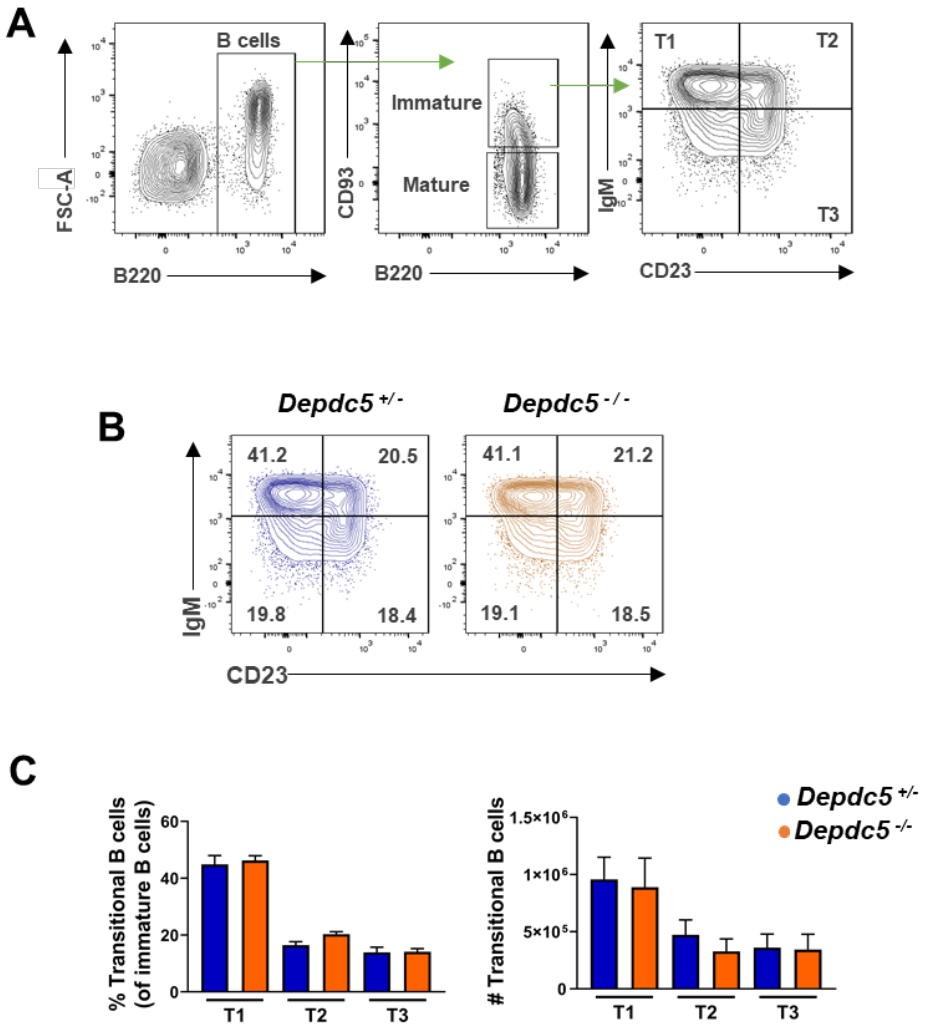

Figure 3.10: Loss of DEPDC5 did not affect transitional B cell frequencies in the SP

SPs from 8-12 week old naive *Depdc5*$^{+/-}$ and *Depdc5*$^{-/-}$ mice were assessed for transitional B cells by flow cytometry. **(A)** Gating strategy for T1 cells [B220^{+}CD93^{+}CD23^{-}IgM^{+}], T2 [B220^{+}CD93^{+}CD23^{+}IgM^{+}] cells and T3 [B220^{+}CD93^{+}CD23^{+}IgM^{-}] are shown. Representative flow cytometry **(B)** is shown with quantification **(C)** of T1, T2 and T3 B cells. The columns represent the mean ± SEM. N=10 mice/group, data are pooled from two independent experiments A one-way ANOVA test was used for statistical analysis.

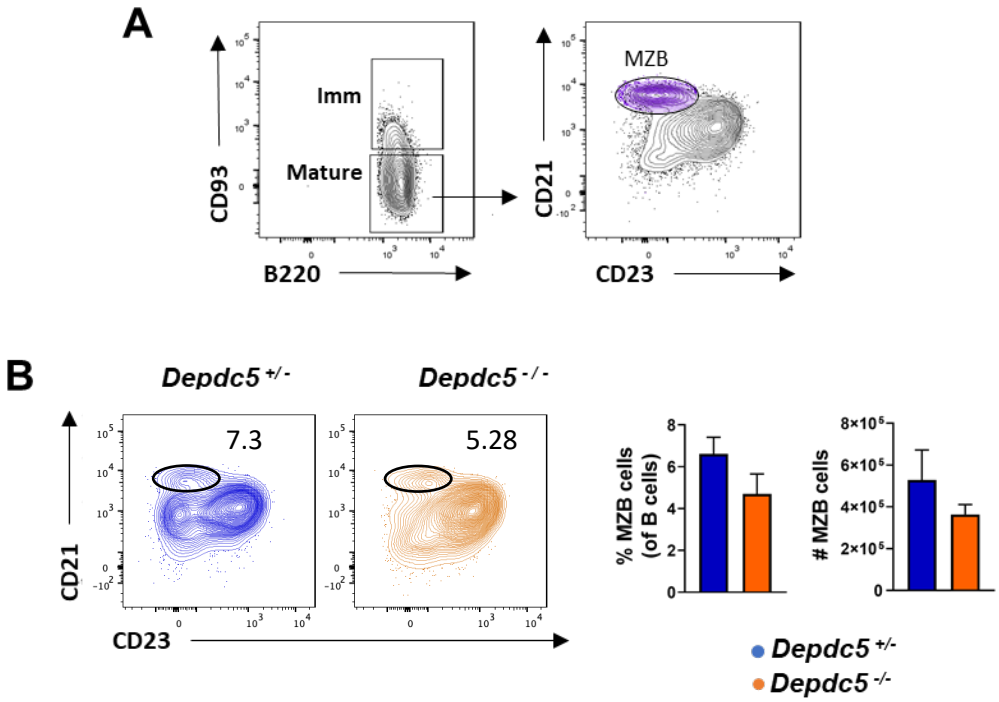

Figure 3.11: DEPDC5 loss did not affect MZB cell frequencies in the SP at homeostasis

SP from 8-12 week old naive *Depdc5*$^{+/-}$ and *Depdc5*$^{-/-}$ mice were assessed for MZB cells by flow cytometry. **(A)** Gating strategy for MZB [B220^{+}CD23^{lo}CD93^{-}CD2^{hi}] cell populations from the SP of *Depdc5*$^{+/-}$ and *Depdc5*$^{-/-}$ mice. **(B)** Representative flow cytometry is shown with quantification of MZB cells. The columns represent the mean ± SEM. N=10 mice/group, data are pooled from two independent experiments. A Mann-Whitney U-test was used for statistical analysis.

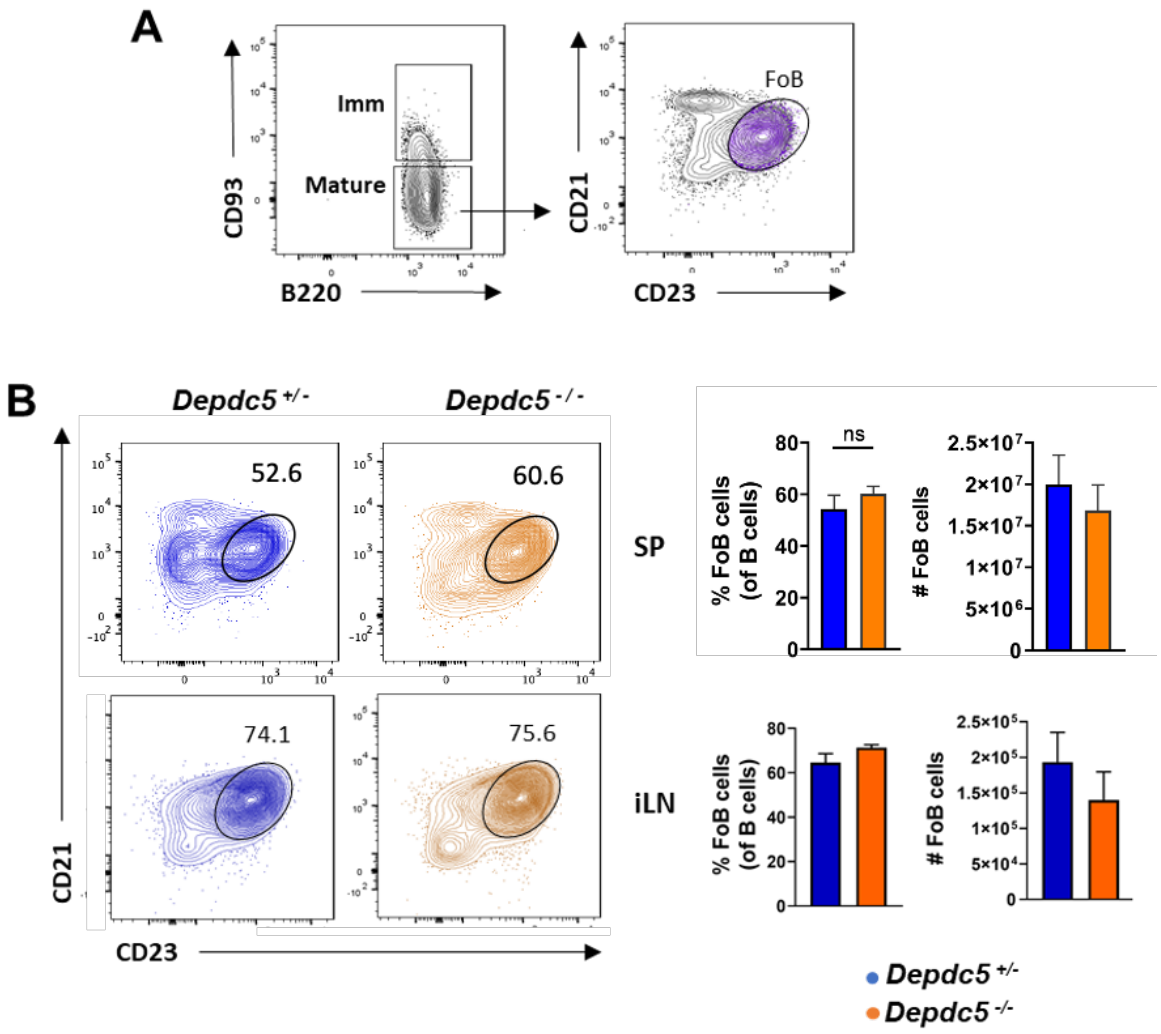

Figure 3.12: DEPDC5 deletion in B cells did not affect FoB cell frequencies in SP

SP from 8-12 week old naive *Depdc5*$^{+/-}$ and *Depdc5*$^{-/-}$ mice were assessed for FoB cells by flow cytometry. **(A)** Gating strategy for FoB (B220^{+}CD93^{-}CD23^{+}CD21$^{lo/mid}$) cell populations from the SP of *Depdc5*$^{+/-}$ and *Depdc5*$^{-/-}$ mice. **(B)** Representative flow cytometry is shown with quantification of FoB cells from *Depdc5*$^{+/-}$ and *Depdc5*$^{-/-}$ mice. N = 8-12/group, data are pooled from two to three experiments. The columns represent the mean ± SEM. A Mann-Whitney U-test was used for statistical analysis.

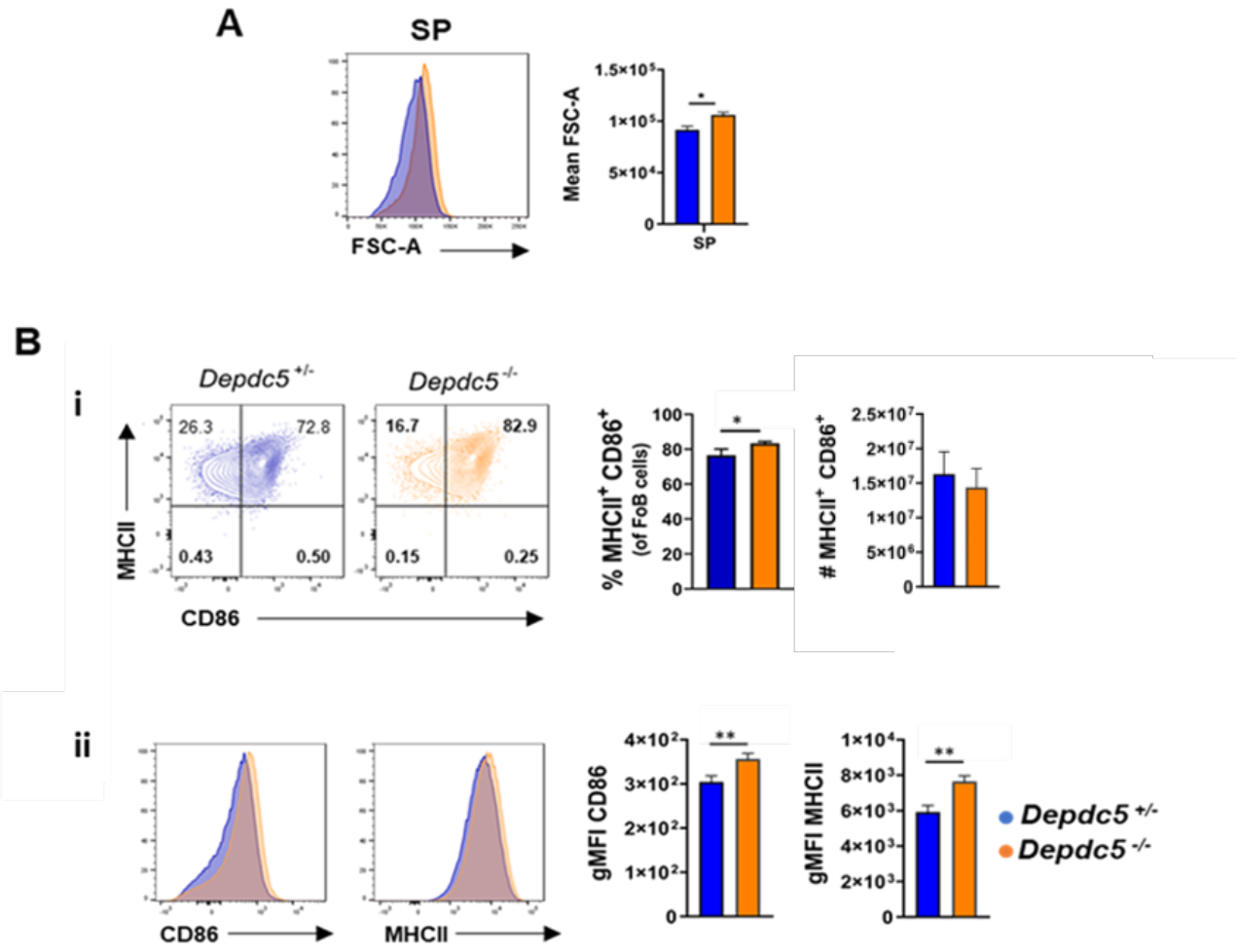

Figure 3.13: DEPDC5 regulates basal activation status of FoB cells

FoB cells from SP from 8-12 week old naive *Depdc5*$^{+/-}$ and *Depdc5*$^{-/-}$ mice were assessed for cell size and expression of activation markers by flow cytometry. Representative flow cytometry is shown with quantification of **(A)** FSC-A values and **(B)** MHCII and CD86 expression on FoB cells from *Depdc5*$^{+/-}$ and *Depdc5*$^{-/-}$ mice. N=6/group, data are pooled from two independent experiments. The columns represent the mean ± SEM. A Mann-Whitney U-test was used for statistical analysis.

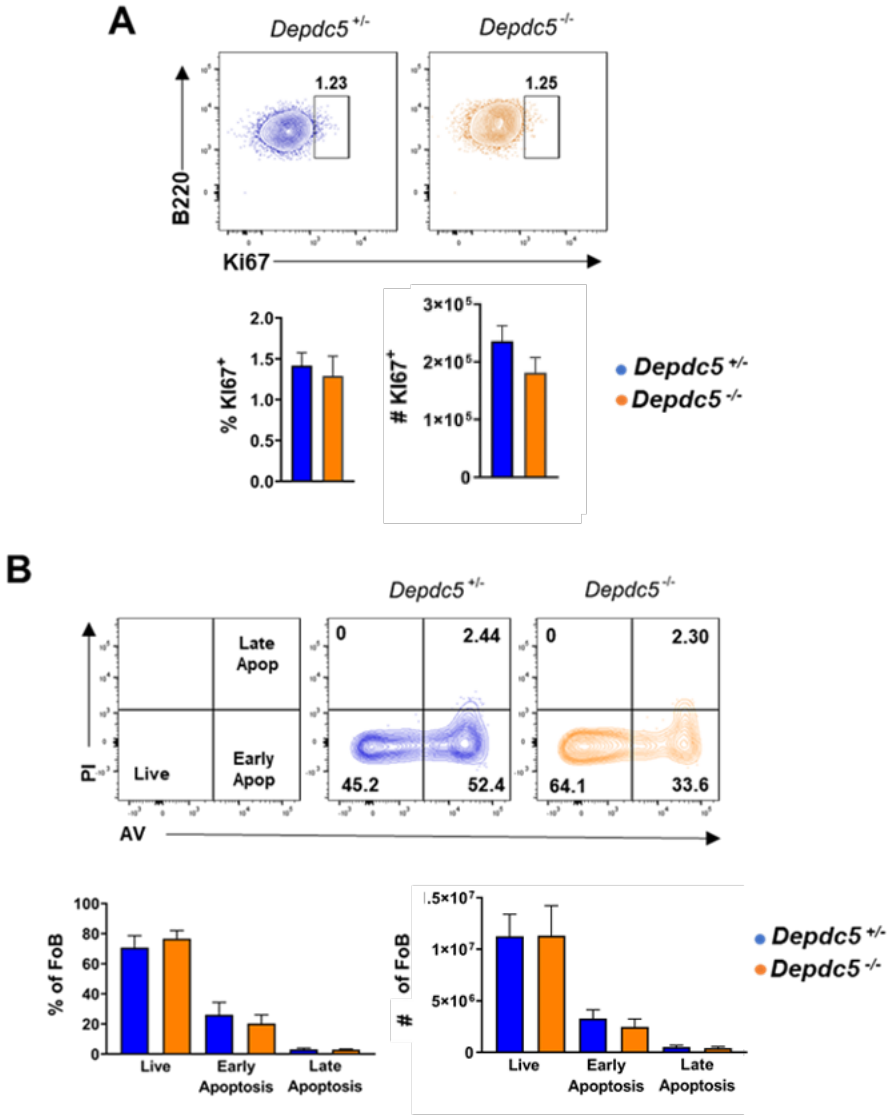

Figure 3.14: Deletion of DEPDC5 did not affect homeostatic proliferation or apoptosis of FoB cells

FoB cells from SPs from 8-12 week-old naive *Depdc5*$^{+/-}$ and *Depdc5*$^{-/-}$ mice were assessed for proliferation and apoptosis by flow cytometry. Representative flow cytometry is shown with quantification of **(A)** Ki67^{+} FoB cells and **(B)** live (AV^{-}PI^{-}), early apoptotic (AV^{+} PI^{-}) and late apoptotic (AV^{+}PI^{+}) FoB cells. The columns represent the mean ± SEM. N = 7-10 /group, data are pooled from 3 independent experiments. A Mann-Whitney U-test was used for statistical analysis in **(A),** and a one-way ANOVA test was used for statistical analysis in **(B).**

CHAPTER 4

Role of *Depdc5* in B cell activation

Chapter 4

Chapter 4

Role of *Depdc5* in B cell activation

4.1 Introduction

In the previous chapter, while no specific alterations were observed in the cellular aspects of the B cell compartment at homeostasis, a requirement for DEPDC5 for the regulation of metabolic quiescence, growth and activation state of resting mature B cells was demonstrated. This prompted the question of whether DEPDC5 plays a role in activation of B cells in an immune response. GCs are enriched for Ag-activated B cells undergoing intense proliferation, SHM and differentiation. GCB cells required stringent control of mTORC1 signalling to initiate and maintain optimal GC responses (Schwickert et al. 2014) (Raybuck et al. 2018) (Raybuck et al. 2018; Jones, Chernova, and Allman 2014; Li et al. 2017). Nutrient milieu impacted profoundly on mTOR signalling (Bar-Peled et al. 2013). However much remained to be explored as to how the various nutrient/mTOR modulators affected the GC reaction and consequently, adaptive humoral immunity. Thus, given the important role of DEPDC5 in linking AA sensing to mTORC1 signalling, the investigation in this chapter focussed first on the role of DEPDC5 in GC B cell biology.

4.2 *Depdc5* modulates mTORC1 activity in GCB cells

In the previous chapter it was established that *Depdc5* regulated mTORC1 activity in resting naïve B cells. In GCB cells, regulation of mTORC1 was known to be important for optimal anti-viral responses (Keating et al. 2013). As shown in the previous chapter, *Depdc5* regulated mTORC1 signalling in resting naïve B cells. Robust activation of mTORC1 in GCB cells led to activation of S6 kinase activity which resulted in phosphorylation of the ribosomal protein S6 (Ersching et al. 2017). To determine if *Depdc5* regulated mTORC1 activity in GCB cells, phospho-S6 levels were examined in *Depdc5*$^{+/-}$ and *Depdc5*$^{-/-}$ GCB cells during IAV infection. To this end, *Depdc5*$^{+/-}$ and *Depdc5*$^{-/-}$ mice were infected intranasally with X31 (H3N2) IAV to induce GC responses. GCB cells from the lung-draining mediastinal LN (medLN) were assessed for phospho-S6 by flow cytometry at D14 post-IAV infection. GCB cells from *Depdc5*$^{-/-}$ mice showed significantly increased levels of phospho-S6 compared to controls (**Figure 4.1**). These data indicated that DEPDC5 limits mTORC1 signalling in GCB cells.

4.3 *Depdc5* regulates GC expansion in response to viral challenge in the draining LN

4.3.1 DEPDC5 regulates GCB accumulation in the draining LN during IAV responses

IN challenge with IAV led to the drainage of viral Ag to the medLN, wherein anti-viral B cell responses are stimulated (Hamilton-Easton and Eichelberger 1995). As discussed in Chapter 1, numerous studies have shown that metabolic signalling plays a significant role in the B cell responses in IAV infection. *Depdc5*$^{+/-}$ and *Depdc5*$^{-/-}$ mice were infected IN with a sublethal dose of X31 IAV to elicit anti-viral humoral responses. This infectious did not lead to substantial weight loss or severe clinical signs. Notably, loss of DEPDC5 in B cells did not alter the clinical signs of infection in these mice, as *Depdc5*$^{-/-}$ mice showed very slight

weight loss and then full recovery following infection when compared to *Depdc5*$^{+/-}$ mice (**Figure 4.2**).

Next, to find if loss of *Depdc5* affected GCB cell formation, the generation of GCB cells in response to IAV infection was examined by flow cytometry every 7 days over a time-course of 21 days (**Figure 4.3**). The frequencies of GCBs in the medLN at D7 post-IAV infection were similar between *Depdc5*$^{+/-}$ and *Depdc5*$^{-/-}$ mice. However, at the later time-points of D14 and D21, GCBs in *Depdc5*$^{-/-}$ mice were significantly reduced compared to *Depdc5*$^{+/-}$ mice as a percentage of cells in the medLN. At D14, the total number of GCBs in *Depdc5*$^{-/-}$ medLN was also significantly reduced compared with their heterozygous counterparts. These data indicated that loss of DEPDC5 did not impair generation of GCB cells during early responses measured at D7. Instead, DEPDC5 was required for optimal GCB responses in the medLN later in the infection.

4.3.2 DEPDC5-deficiency impairs generation of anti-viral Ab-production and affinity maturation.

In addition to the role of mTORC1 for generation and maintenance of GCB responses, mTORC1 signalling had a significant role in the generation of Ab, CSR and SHM during T cell–dependent humoral responses (Zhang, Pruitt, et al. 2013; Jones et al. 2016; Chou et al. 2016; Chiu et al. 2019). To investigate whether DEPDC5 also regulated Ab production or class switching, *Depdc5*$^{+/-}$ and *Depdc5*$^{-/-}$ mice were infected with X31-IAV and serum was collected over the course of the infection every 7 days for 21 days and then assessed by ELISA to determine the levels of anti-X31 IgM and anti-X31 IgG Abs. Deletion of *Depdc5* had a significant impact on the anti-X31 IgM Ab response at days 14 and 21 post infection (but not D7), as observed by reduced anti-X31 IgM titres in *Depdc5*$^{-/-}$ mice compared to *Depdc5*$^{+/-}$ mice on D14 and D21 (**Figure 4.4**). In contrast, deletion of *Depdc5* had no significant impact on anti-X31 IgG responses observed at any of the timepoints analysed post-infection. This was surprising given the significant impact of DEPDC5 loss on GCB cells within the medLN during IAV infection. Therefore, the effect of DEPDC5 on the

generation of ASCs would have to be examined in greater detail to help understand the Ab responses during IAV infection.

The GC reaction facilitated generation of Ag-specific high-affinity Ab responses (Mendoza et al. 2018). As previously discussed, development of high affinity Ab was dependent on mTORC1 signalling (Keating et al. 2013; Zhang, Pruitt, et al. 2013; Ersching et al. 2017; Taketani et al. 1995; Matsumoto et al. 1996; Wang et al. 2000). To investigate the effect of DEPDC5 on affinity maturation, *Depdc5*$^{+/-}$ and *Depdc5*$^{-/-}$ mice were immunized with the hapten-carrier complex nitrophenyl-ovalbumin (NP-OVA), which allowed assessment of the affinity of the response based on binding of serum Ab to differentially haptenated carrier proteins using ELISA (Ersching et al. 2017). ELISAs were used to measure the circulating total anti-NP Abs (NP_{24}-BSA binding) and high-affinity anti-NP Ab (NP_2-BSA binding) in immunised mice and affinity maturation was calculated as the ratio of NP_2-binding: NP_{24}-binding Abs. IgG1 was the dominant isotype of Ab generated in response to NP- (Lalor et al. 1992), and thus was examined over the course of immunisation. A clear defect in the levels of total and high affinity IgG1 during NP-OVA immunisation was observed in *Depdc5*$^{-/-}$ mice compared to controls (**Figure 4.5**). Therefore, DEPDC5 also facilitates development of high-affinity IgG1 Ab responses to haptenated protein Ag.

4.3.3 The absence of DEPDC5 in B cells reduces ASC output

Metabolic sensitivity to nutrient availability ensures that sufficient AAs are present to provide fuel for protein synthesis, which was key for Ab generation. Disruption of mTORC1 signalling in B cells has led to reported defects in both the GCB compartment and Ab production (Raybuck et al. 2018; Zhang et al. 2011; Ersching et al. 2017; Iwata et al. 2017; Jones, Chernova, and Allman 2014). The GC facilitated development of high-affinity and isotype-switched ASCs which mediate secretion of effector Ab during the humoral response. To assess whether DEPDC5 played a role in modulating mTORC1 signalling in ASCs, the levels of phospho-S6 were measured by flow cytometry in ASCs from the medLN on D7 following IAV infection. In the absence of DEPDC5, phospho-S6 levels in ASCs were

significantly increased which indicated that DEPDC5 also modulates mTORC1 activity in the ASC compartment (**Figure 4.6**).

Next, to further assess the impact of *Depdc5*-deletion in B cells upon the ASC response, ASCs were quantified at D7 post-IAV infection in the medLN. Within the draining medLN, both the frequency and number of ASCs were significantly reduced in *Depdc5*$^{-/-}$ mice (**Figure 4.7**). CSR was also assessed through determining isotypes of Abs produced by the ASCs. The percentage of IgM^{+}, IgG^{+} and IgA^{+} ASCs were equivalent in *Depdc5*$^{-/-}$ and *Depdc5*$^{+/-}$ mice, however the total number of each population in and *Depdc5*$^{-/-}$ mice was significantly fewer due to the overall reduction in ASCs in *Depdc5*$^{-/-}$ mice described above (**Figure 4.8**). This was surprising, as the reduced number of IgG^{+} ASCs in *Depdc5*$^{-/-}$ mice was not associated with changes in anti-viral IgG in the serum of these mice.

To examine whether reduced general output of ASCs in *Depdc5*$^{-/-}$ mice could be a consequence of altered proliferation or survival of ASCs, these were also examined at D7 post-IAV infection. Although the total number of Ki67^{+} ASCs was reduced in *Depdc5*$^{-/-}$ mice the percentage of ASCs that expressed high levels of Ki67 was equivalent between *Depdc5*$^{+/-}$ and *Depdc5*$^{-/-}$ mice (**Figure 4.9A**), indicating that the amount of proliferation in this compartment was not generally impaired. The reduction in the total number of Ki67^{+} ASCs was reduced in *Depdc5*$^{-/-}$ mice likely reflected the significant reduction in ASC numbers from *Depdc5*$^{-/-}$ mice **(Figure 4.7)**. Further, the reduction in *Depdc5*$^{-/-}$ ASC generation could not be accounted for by measurable changes in the percentage of early or late apoptosis at this timepoint since AV and propidium iodide (PI) staining patterns for ASCs were also equivalent between both groups (**Figure 4.9B**). The reduction in the total number of live ASCs in *Depdc5*$^{-/-}$ mice was consistent with the ASC numbers from *Depdc5*$^{-/-}$ mice **(Figure 4.7)**. Together, these data indicated that ablation of DEPDC5 in B cells did not specifically impair the survival and proliferative capacity of ASCs during viral infection. Thus, it was most likely that in the absence of DEPDC5, fewer ASCs are generated during early responses to viral infection. Therefore, this study implicated a role for DEPDC5 in the generation, rather than the maintenance, of ASCs.

4.3.4 DEPDC5 promotes accumulation of GCBs by supporting their proliferation and survival

GCB cells undergo high rates of apoptosis and proliferation and regulators of mTORC1 have been shown to prevent metabolic collapse and apoptosis and promote proliferation during Ag-driven challenge. To understand whether reduced accumulation of DEPDC5-deficient GCB cells in the medLN was the result of reduced proliferation or increased apoptosis, these two cellular processes were measured during IAV infection in *Depdc5*$^{-/-}$ and *Depdc5*$^{+/-}$ mice. Firstly, to examine if DEPDC5 plays a role in regulating proliferation in GCB cells, Ki67 expression was assessed at D7, D14 and D21 post-IAV infection by flow cytometry. Proliferating GCB cells were demarcated as Ki67^{hi} cells. In the medLN, the frequencies and numbers of Ki67^{hi} GCB cells were equivalent between both groups at D7 (**Figure 4.10**). This indicated that there was no difference to early proliferation, which was consistent with the equivalent proportion and number of GCBs per group at this time (**Figure 4.3**). However, at D14 post-IAV infection, *Depdc5*$^{-/-}$ mice showed increased percentages of Ki67^{hi} GCB cells in the medLN. At D21, no difference in the proportions or numbers of proliferating Ki67^{hi} GCBs were apparent between *Depdc5*$^{+/-}$ and *Depdc5*$^{-/-}$ mice (**Figure 4.10**). The reduction in the number of Ki67^{+} GCBs in *Depdc5*$^{-/-}$ mice at D14 and D21 could have been the result of the initial defect in the GCB population observed in *Depdc5*$^{-/-}$ mice (**Figure 4.3**). These data indicated that DEPDC5 regulates GCB proliferation at D14 of the GC response against IAV infection and has a significant impact on sustaining the number of GCBs during infection.

To investigate the impact of DEPDC5 deletion on GCB cell survival in the medLN, apoptosis was examined at D14 post-IAV-infection, which was a time-point of the GC response when significant disruptions in GCB accumulation and proliferation occurred in *Depdc5*$^{-/-}$ mice. To analyse the nature of apoptosis in GCB cells, the AV and PI staining system was used again to identify cells that were live or undergoing early or late apoptosis. The frequency and number of live GCB cells was significantly reduced in the medLN of *Depdc5*$^{-/-}$ mice compared to *Depdc5*$^{+/-}$ mice (**Figure 4.11**). No differences were observed for early apoptotic GCB subsets between groups. However, a significant increase in the percentage GCB cells undergoing late apoptosis in *Depdc5*$^{-/-}$ mice was clearly detected (**Figure 4.11**). The significant reduction in GCB cells in *Depdc5*$^{-/-}$ mice at D14 may account

for the lack of significant increase in the number of late apoptotic GCB cells. Therefore, based upon the proportion of GCBs that were live or undergoing early or late apoptosis, these data indicated DEPDC5 was required to limit late stage apoptosis in GCBs. To study this in greater detail, a complimentary assay for apoptosis was used. To identify apoptotic GCB cells, a monoclonal Ab against active caspase-3 was used. Active caspase-3 (aCasp-3^{+}) was an executioner enzyme that regulates apoptosis by co-ordinating degradation of DNA and cytoskeleton proteins (McIlwain, Berger, and Mak 2013). At D14 post-IAV infection, there was a significant increase in the frequency of GCB cells within the medLN that were positive for aCasp-3 in *Depdc5*$^{-/-}$ mice compared to control mice (**Figure 4.12**). Similar to the lack of significant reduction in the number of late apoptotic GCBs in *Depdc5*$^{-/-}$ mice, there was no change in the number of aCasp-3^{+} GCBs within the medLN of in *Depdc5*$^{-/-}$ mice. Therefore, based upon these data DEPDC5 likely regulated susceptibility to apoptosis amongst GCB cells within the medLN at D14 of the IAV response.

mTORC1 signalling has been shown to contribute to polarisation of the GC in various studies (Ersching et al. 2017; Wray-Dutra et al. 2018). Therefore, it was examined whether loss of DEPDC5 in B cells affected the LZ to DZ ratio of GCB cells in response to IAV infection. The DZ:LZ ratio was examined using the markers CXCR4 and CD86 on GCB cells (Allen et al. 2004; Victora et al. 2010). Segregation of the GC can be distinguished by CXCR4^{+}CD86^{-} DZ cells and CXCR4^{-}CD86^{+} LZ cells. A study by the Cyster laboratory showed that in response to viral infection, DZ:LZ polarization reaches a peak at D14 (Allen et al. 2004). Thus, the impact of DEPDC5 on the LZ and DZ of the GC reaction was examined at D14 in both the medLN, and observations were also extended to D21. In the medLN, the DZ:LZ ratio of GCB cells in *Depdc5*$^{-/-}$ mice was comparable to the GCB cells of *Depdc5*$^{+/-}$ mice at both D14 and D21 (**Figure 4.13**). To understand whether the proliferative and apoptotic processes regulated by DEPDC5 in GCB cells were confined to the DZ or LZ, GC polarisation was investigated during IAV infection at D14. This time-point was selected firstly because it was established to be an optimal time for studying developed DZ:LZ zones during IAV infection (Allen et al. 2004) and secondly, because it was a timepoint when DEPDC5 deletion led to GCB dysregulation (**Figure 4.3**). An increased percentage of Ki67^{hi} GCB cells was observed in both LZ and DZ compartments in *Depdc5*$^{-/-}$ mice compared to

Depdc5$^{+/-}$ controls (**Figure 4.14**). The number of total number of Ki67^{+} DZ and LZ GCBs were reduced in *Depdc5*$^{-/-}$ mice at D14 and could have been the result of the initial defect in the GCB population observed in *Depdc5*$^{-/-}$ mice **(Figure 4.3)**. Therefore, the percentage of Ki67^{+} cells was likely a better indicator that *Depdc5*-dependent regulation of GCB cell proliferation was not confined to a particular compartment of the GC.

Cell survival was next examined in the LZ and DZ compartments to assess the influence of DEPDC5 on apoptosis of both LZ GCBs and DZ GCBs at D14. AV and PI staining showed that control *Depdc5*$^{+/-}$ mice had a significantly lower percentage and number of live (AV^{-}PI^{-}) GCB cells in the LZ and DZ compared to control mice (**Figure 4.15**). However, there was no significant change in the frequency or number of late-apoptotic LZ and DZ GCB cells was apparent in *Depdc5*$^{-/-}$ mice relative to controls. There did appear to be a trend towards the increase in late apoptotic GCB frequency in *Depdc5*$^{-/-}$ mice, but overall these data indicated that DEPDC5 has no significant impact on late apoptosis in either compartment. Perhaps the effect of DEPDC5 on late GCB apoptosis, which constituted a small percentage of total apoptotic cells, was slight enough that changes are only apparent on the GCB population as a whole. By using an alternative method of detecting all cells undergoing apoptosis (encompassing extrinsic [death ligand] and intrinsic [mitochondrial] pathways of apoptosis), a higher percentage of aCasp-3^{+} cells in the LZ and DZ were observed in *Depdc5*$^{-/-}$ mice relative to controls. However, no change in the number of aCasp-3^{+} cells DZ and LZ cells was observed between groups (**Figure 4.16**). Taken together, these results indicated that DEPDC5 did not limits apoptosis in a particular GC compartment, but rather affected apoptosis at the level of the GCB cell population.

4.4 Examination of DEPDC5 in iBALT-associated GCs

Acute viral infection leads to local and systemic activation of immune responses, which also leads to changes in the host metabolome (Chandler et al. 2016). In particular, the metabolic pathways that are upregulated within lungs infected with respiratory viruses have been reported to change over the course of infection (Chandler et al. 2016) which was discussed in detail in Chapter 1. However, GC responses at this site are of lesser magnitude and display delayed kinetics compared to the development of GCs in the medLN (Tan et al. 2019). Thus, to improve the overall understanding of how DEPDC5-mediated regulation of nutrition affects GC responses to viral infection, iBALT-associated GC responses at the primary site of infection in the lung were examined in *Depdc5*$^{-/-}$ mice.

4.4.1 DEPDC5 regulates GCB accumulation within the lung

To study iBALT-associated GCB response in response to infection, *Depdc5*$^{+/-}$ and *Depdc5*$^{-/-}$ mice were infected intranasally with X31 IAV. The GCB cell responses in the lung were assessed at D7, D14 and D21 in order to compare GCB cell responses in the iBALT to the medLN. Consistent with reports of delayed GC kinetics in the lung compared to medLN (Tan et al. 2019), *Depdc5*$^{+/-}$ mice responded to IAV infection with a delayed accumulation of GCBs in the lung compared to the medLN. Further, the magnitude of the pulmonary GC response was of significantly reduced magnitude compared to the peak GC response in the medLN (**Figure 4.17, Figure 4.3**). GCB responses in the lung on D7 were of similar magnitude between *Depdc5*$^{+/-}$ and *Depdc5*$^{-/-}$ mice. However, at D14 post-infection, *Depdc5*$^{-/-}$ mice showed an increased percentage and number of GCB cells in the lung compared to control mice. This was in stark contrast to the results previously seen in medLN where loss of DEPDC5 profoundly reduced frequencies of GCB cells following IAV infection at this time-point (**Figure 4.3**). By D21, GCB cells in the lungs of mice in both groups reached equivalent levels. Overall, these data indicated that DEPDC5 did not affect the generation of GCB cells in lungs during early responses to IAV at D7. Instead, DEPDC5 limited the accumulation of GCB cells in the lung at later time-points in the course of infection. Further, these data also showed that *Depdc5* elicits differential effects on GCB cell kinetics in the

lung and medLN. This was potentially due to the site-specific differences in microenvironments with respect to AA availability and GC development in each site (Boyden, Legge, and Waldschmidt 2012) and was discussed in more detail in Chapter 5.

Deletion of DEPDC5 was previously shown to increase GCB cell proliferation in the draining medLN, which prompted an examination of proliferation in the context of pulmonary GCs. IAV infection led to graded Ki67 responses in pulmonary GCBs in mice at D7 and D14 post-IAV infection, with low, mid and high levels of Ki67 expression apparent on GCB cells (**Figure 4.18**). This likely reflects GCB cells undergoing different levels of proliferation depending on their source and stage of development in the iBALT (Rangel-Moreno et al. 2007; Tan et al. 2019), which can lead to varied cycling rates amongst the GCB population. *Depdc5*$^{+/-}$ and *Depdc5*$^{-/-}$ mice were observed to possess similar frequencies and numbers of Ki67^{hi} GCBs within the lung at D7. However, at D14 the frequency and number of Ki67^{hi} GCB cells in *Depdc5*$^{-/-}$ lungs were elevated compared to those in *Depdc5*$^{+/-}$ lungs. Lung GCBs from both groups had similar Ki67 expression profiles at D21 post-infection. The percentage of proliferating GCB cells in *Depdc5*$^{-/-}$ mice at D14 were equivalent to those proliferating in lungs of control mice at D21, perhaps indicating an accelerated level of proliferation in the absence of DEPDC5 during the pulmonary GC response. These results collectively showed that DEPDC5 restrained GCB proliferation in the lung at D14 post-IAV infection, and that in its absence GCB cells accumulated at an accelerated rate in the lung compared to controls.

The earlier observation of increased GCB cells on D14 in the lungs of IAV-infected mice lacking B cell expression of DEPDC5 and the fact that DEPDC5 was shown in other experiments to regulate GCB survival in the draining medLN led to an investigation of whether cell survival was affected by loss of DEPDC5 in the context of pulmonary GCs. In the lung on D14, there was a significant increase in the percentage and total number of live GCB cells in *Depdc5*$^{-/-}$ compared to *Depdc5*$^{+/-}$ mice (**Figure 4.19**). This was likely a result of the higher GCB proliferation observed in the absence of DEPDC5, coupled with limited apoptosis of GCB cells during the response in the lung. A significant reduction in the percentage of early apoptotic GCB cells was also observed in *Depdc5*$^{-/-}$ mice, however the number of early apoptotic cells in *Depdc5*$^{-/-}$ mice was not significantly reduced. No significant change in late apoptotic GCBs were observed between groups. Furthermore,

equivalent levels of aCasp-3^{+} GCB cells were observed within *Depdc5*$^{+/-}$ and *Depdc5*$^{-/-}$ mice (**Figure 4.20**). Together these results indicated that DEPDC5 likely did not affect apoptosis of GCBs in the lung, and rather inhibits GCB cell apoptosis in a site-specific manner. This may explain why an increase in GCB cells within the lung of *Depdc5*$^{+/-}$ mice are observed, while GCB cells were reduced in the medLN in the absence of DEPDC5.

GCs in the iBALT are less structured and more diffuse compared to GCs in the LNs, meaning the DZ and LZ areas in these structures overlap and are less well defined (Tan et al. 2019). The contribution of mTORC1 activity to DZ and LZ polarisation in iBALT GCs has not been described in the literature to date. Therefore, it was tested whether DEPDC5 influences GC polarisation in the lung by comparing DZ:LZ ratios in the lungs of mice infected with IAV as well as proliferation and apoptosis of DZ and LZ GCB cells. On day D14 and D21 post-infection, DZ:LZ ratios in lung GCB cells were equivalent between *Depdc5*$^{+/-}$ and *Depdc5*$^{-/-}$ mice. (**Figure 4.21**). The proliferation and apoptosis of LZ and DZ cells in iBALT GCB cells was also assessed. Consistent with the findings in the mesLN, increased frequencies of both LZ and DZ GCB cells were Ki67^{hi} in *Depdc5*$^{-/-}$ mice compared to *Depdc5*$^{+/-}$ controls (**Figure 4.22**). This data shows that DEPDC5 restrains GCB proliferation globally, rather than in a specific compartment. Within the lung, AV and PI staining of lung GCB cells showed a higher frequency and number of live DZ and LZ cells in *Depdc5*$^{-/-}$ mice compared to their *Depdc5*$^{+/-}$ counterparts (**Figure 4.23**), consistent with observations in the total GCB lung population (**Figure 4.19**). Further, changes in the frequencies and numbers early and late apoptotic LZ and DZ cells in *Depdc5*$^{-/-}$ mice were comparable to the trends observed in the total GCB lung population (**Figure 4.19**). There were equivalent levels of aCasp-3^{+} DZ and LZ GCB cells when compared between *Depdc5*$^{+/-}$ and *Depdc5*$^{-/-}$ groups (**Figure 4.24**), similar to what was observed in total GCB cells (**Figure 4.20**). These data indicated that DEPDC5 did not likely impact the survival or polarisation of DZ and LZ GCB cells in the lung, rather DEPDC5 loss increases the proliferation of both DZ and LZ GCBs within iBALT associated GCs.

4.5 Examination of DEPDC5 in chronic GCs

The PP and mesLN within the GALT are nutrient-rich sites of chronic GCs (Casola and Rajewsky 2006) due to their proximity to the gut microbiome and nutrients (Reboldi and Cyster 2016). Starvation and re-feeding studies have reported that nutritional signals regulate B cell maturation and GCB apoptosis within the PP (Nagai et al. 2019) (de Jonge et al. 2002). Further, hypoxia-labelling studies have shown that GCs in the PPs are not as susceptible to nutrient-deprivation compared to primary sites of immunisation in peripheral tissues (Raybuck et al. 2018). However, as discussed within Chapter 1 the reported role of mTORC1 and nutritional regulators of mTORC1 in GALT-associated GCB cells has been variable and not extensively explored. To this end, the role of DEPDC5 was examined within PPs and mesLN which drain food-Ags and nutrients from the GIT. Given that DEPDC5 acts to suppress mTORC1 in the absence of AAs, it was hypothesised that DEPDC5 would be redundant for regulating GCB responses in nutrient-rich sites such as the PP and mesLNs.

4.5.1 *Depdc5* has minimal impact on GC in a chronic setting

The GCB cell responses in mesLN and PP were assessed in *Depdc5*$^{+/-}$ and *Depdc5*$^{-/-}$ mice at homeostasis. Analysis of chronic GCs within the mesLN and PP of *Depdc5*$^{+/-}$ and *Depdc5*$^{-/-}$ mice showed an equivalent proportion and number of GCB cells between both groups (**Figure 4.25**). This indicates that the AA-mTORC1 signalling axis controlled by DEPDC5 was dispensable for regulation of GCB cell responses in GALT-associated GCs. Consistent with this finding, the frequency and number of proliferating GCB cells, defined as Ki67^{hi}, were also unchanged in the absence of DEPDC5 in both the mesLN and PP (**Figure 4.26**). Furthermore, the frequencies of GCB cells actively undergoing apoptosis (aCasp-3^{+}) in these GALT-associated tissues were similar in *Depdc5*$^{+/-}$ and *Depdc5*$^{-/-}$ mice (**Figure 4.27**). These data suggest that DEPDC5 was not required to regulate apoptosis and proliferation in GCB cells within the PP and mesLN, consistent with the unaltered number of GCB cells in the absence of DEPDC5. Analysis of GC polarisation within these chronic GC sites showed that DEPDC5 did not impact DZ:LZ ratios (**Figure 4.28**), similar to the results seen with respect to GC polarization following IAV infection. This suggested that in response to both complex

IAV Ag and food-borne Ag, DEPDC5 played a redundant role in regulating GC polarisation or no role at all.

Overall, these results indicated that DEPDC5 did not affect chronic GALT-associated GCB responses. Further analyses found that ASC production in the mesLN and PP was similar between both *Depdc5*$^{+/-}$ and *Depdc5*$^{-/-}$ mice in frequency and number (**Figure 4.29**). Consistent with these findings, proliferation (**Figure 4.30**) and apoptosis (**Figure 4.31**) of ASCs was not affected by the loss of DEPDC5. While this was similar to the effect of DEPDC5 deletion on ASC survival and proliferation during acute IAV infection within the medLN, it led to different outcomes in terms of ASC accumulation. This suggested that while DEPDC5 may be involved in the generation of ASCs within the medLN during IAV infection, it was dispensable in GALT-associated GCs. Further, there could have been a difference between GC and ASC generation in acute versus chronic situations. For example, there was no effect following DEPDC5 loss when PCs were assessed in the context of long-term accumulation in the GALT, whereas DEPDC5 had a primary effect on the early and acute generation of medLN-associated ASCs where pre-existing ASCs were not present. Together these findings indicated that DEPDC5 loss did not impair or alter GC responses and ASC output under chronic stimulation of GCB cells in GALT-associated tissues.

4.6 Conclusion

The data in this chapter has established the following findings:

- Loss of DEPDC5 increased phospho-S6 levels, a key indicator of mTORC1 activity, in GCB cells from mesLN of IAV infected mice.

- DEPDC5 regulates proliferation and apoptosis in GCB cells in a site-specific manner in response to IAV-infection; differentially influencing GCB turnover and the kinetics of GCB accumulation within the medLN and lung. However, it did not regulate polarisation of the GC response.

- Within the medLN, DEPDC5 did not affect ASC survival, proliferation or isotype switching. Thus, it was most likely that generation of ASCs was compromised by loss of DEPDC5 at this site.

- Significantly reduced anti-viral IgM Ab responses were observed circulating in the serum of *Depdc5*$^{-/-}$ mice challenged with IAV, perhaps due to reduced IgM^{+} ASCs. But no change in anti-viral IgG, potentially due to intact pools of IgG^{+} ASCs generated in the lung or generation/CSR within X31-specific ASCs, as only total medLN-ASCs were assessed. Given DEPDC5 was observed to differentially affect GCBs within the medLN and lung, it was possible ASC responses within the lung may respond differently to DEPDC5 mediated regulation.

- Ab affinity maturation was attenuated in *Depdc5*$^{-/-}$ mice following immunisation with NP-OVA.

- There were no apparent alteration in the development or maintenance of DEPDC5-deficient GCB cells or ASCs within chronic GALT-associated GCs.

Together, these data revealed a novel role for the AA-mTORC1 checkpoint, DEPDC5 for the regulation of GCB and resulting ASC responses during the acute phase of virally induced GC reactions in draining LN, but not in a chronic setting in nutrient-rich mucosal tissue or iBALT. These data will be discussed in more detail in Chapter 5.

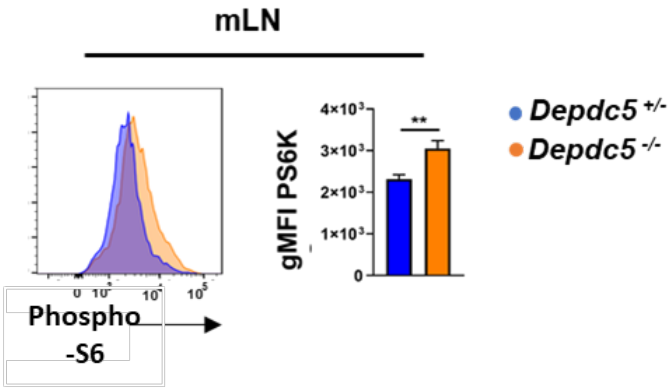

Figure 4.1: DEPDC5 regulated phospho-S6 expression in GCB cells

Depdc5$^{+/-}$ and *Depdc5*$^{-/-}$ mice were infected IN with X31(100 $TCID_{50}$). The medLN was analysed by flow cytometry at D14 for phospho-S6 expression in GCBs (pre-gated on GCBs). Representative flow cytometry is shown with quantification of phospho-S6 expression (geometric mean fluorescent intensity) in GCB cells from the medLN at D14 post-IAV infection in *Depdc5*$^{+/-}$ and *Depdc5*$^{-/-}$ mice. The columns represent the mean ± SEM. N = 8 per group pooled from two independent experiments. A Mann-Whitney U test was applied for statistical analysis.

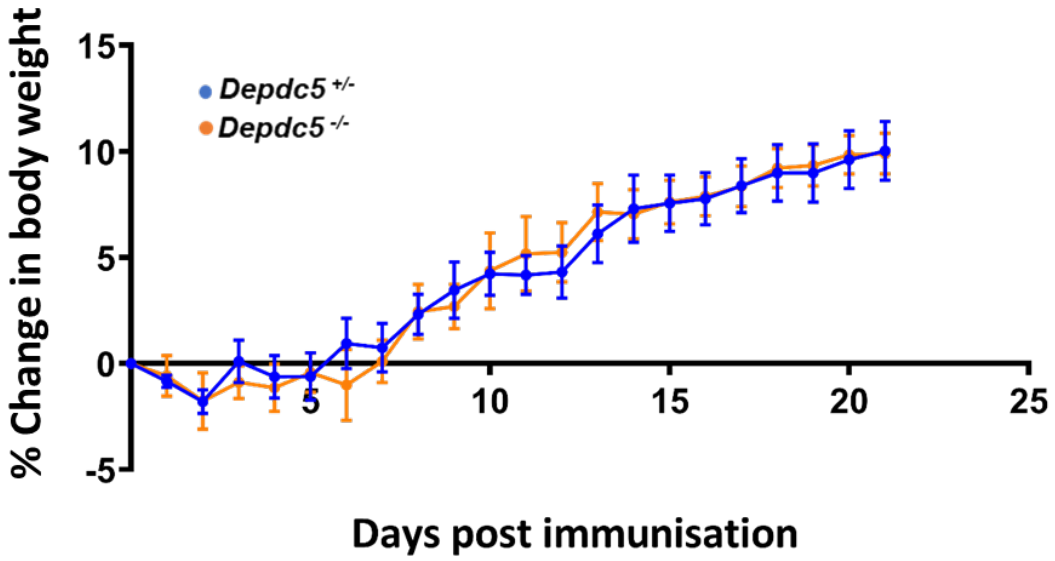

Figure 4.2: Loss of DEPDC5 did not affect mouse weight following sub-lethal IAV infection

Depdc5$^{+/-}$ and *Depdc5*$^{-/-}$ mice were infected IN with X31(100 $TCID_{50}$). The change in body weight was measured over 21 days. Percentage weight loss of *Depdc5*$^{+/-}$ and *Depdc5*$^{-/-}$ following IN IAV infection was calculated as [*(DX weight – D0 weight)/D0 weight)*100*]. The data set represent the represent the mean ± SEM. N = 7 mice per group, pooled from two independent experiments. The data were tested for statistical differences by 2-way ANOVA.

Figure 4.3: Loss of DEPDC5 delayed GCB accumulation in the medLN during IAV infection

Depdc5$^{+/-}$ and *Depdc5*$^{-/-}$ mice were infected IN with X31(100 $TCID_{50}$). The medLN was analysed for flow cytometry at D7, D14 and D21 to measure GCB populations. Representative flow cytometry **(A)** is shown with quantification **(B)** of *Depdc5*$^{+/-}$ and *Depdc5*$^{-/-}$ GCB ($B220^{+}CD38^{-}CD95^{+}$) cells from the medLN at D7, 14 and 28 post-IAV infection. The columns represent the mean ± SEM. D7 = N12/group, D14 = N18/group and D21 = 24/group, pooled from at 2-3 independent experiments. A one-way ANOVA test was used for statistical analysis.

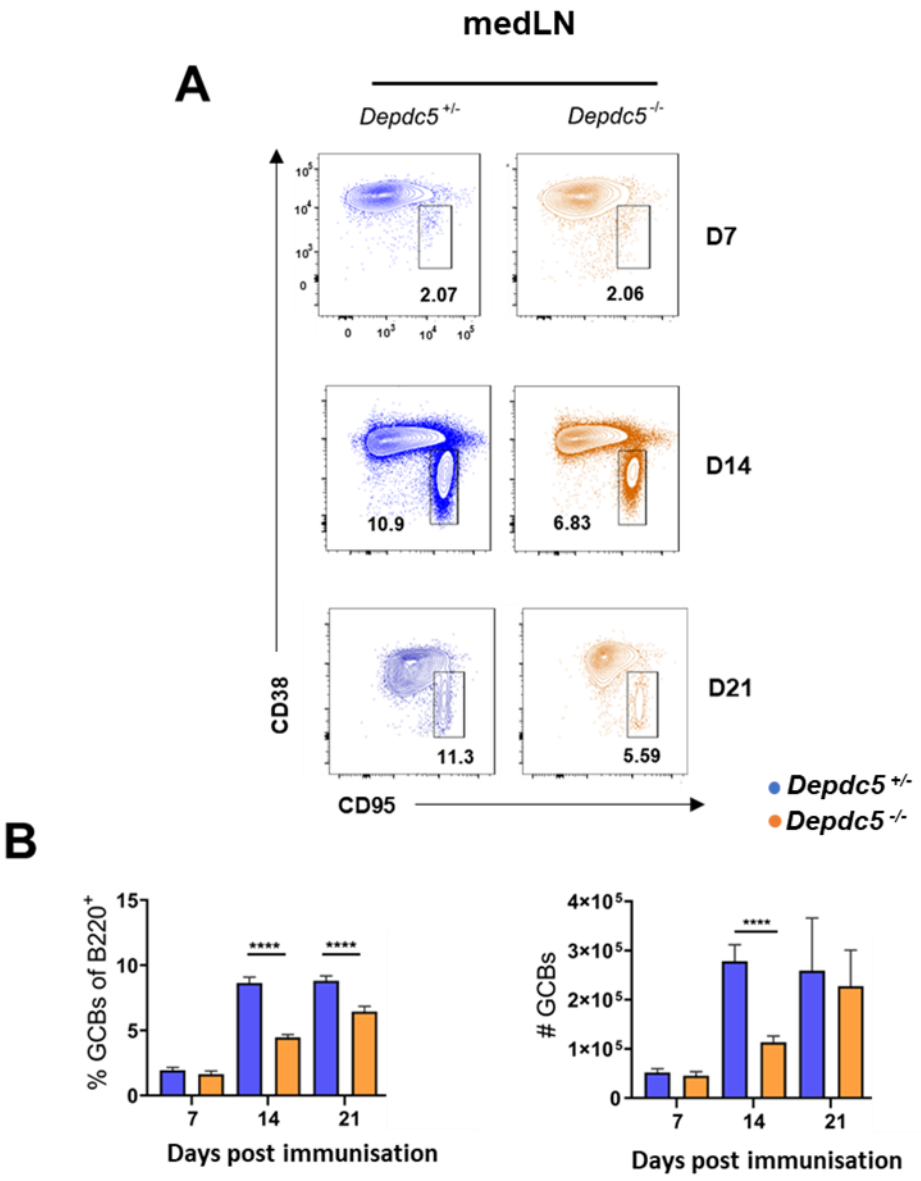
medLN
A
Depdc5 +/-
Depdc5 -/-
D7
D14
D21
2.07
2.06
10.9
6.83
11.3
5.59
CD38
CD95
Depdc5 +/-
Depdc5 -/-
B
% GCBs of B220+
Days post immunisation
GCBs
Days post immunisation
****

Figure 4.4: DEPDC5 deletion reduced anti-viral IgM serum responses during IAV infection

Depdc5$^{+/-}$ and *Depdc5*$^{-/-}$ mice were infected IN with X31(100 $TCID_{50}$). Serum was isolated at D7, D14 and D21 post infection. Samples were analysed by ELISA to assess circulating levels of anti-X31 IgM and anti-X31 IgG Ab in *Depdc5*$^{+/-}$ and *Depdc5*$^{-/-}$ serum at **(A)** D7, **(B)** D14 and **(C)** D21 post-IAV infection. The columns represent the mean ± SEM. N= 4-8 per group, pooled from two independent experiments (D7 N=4/group, D14 N=8/group and D21 N=6/group). A one-way ANOVA test was used to test for statistical analysis.

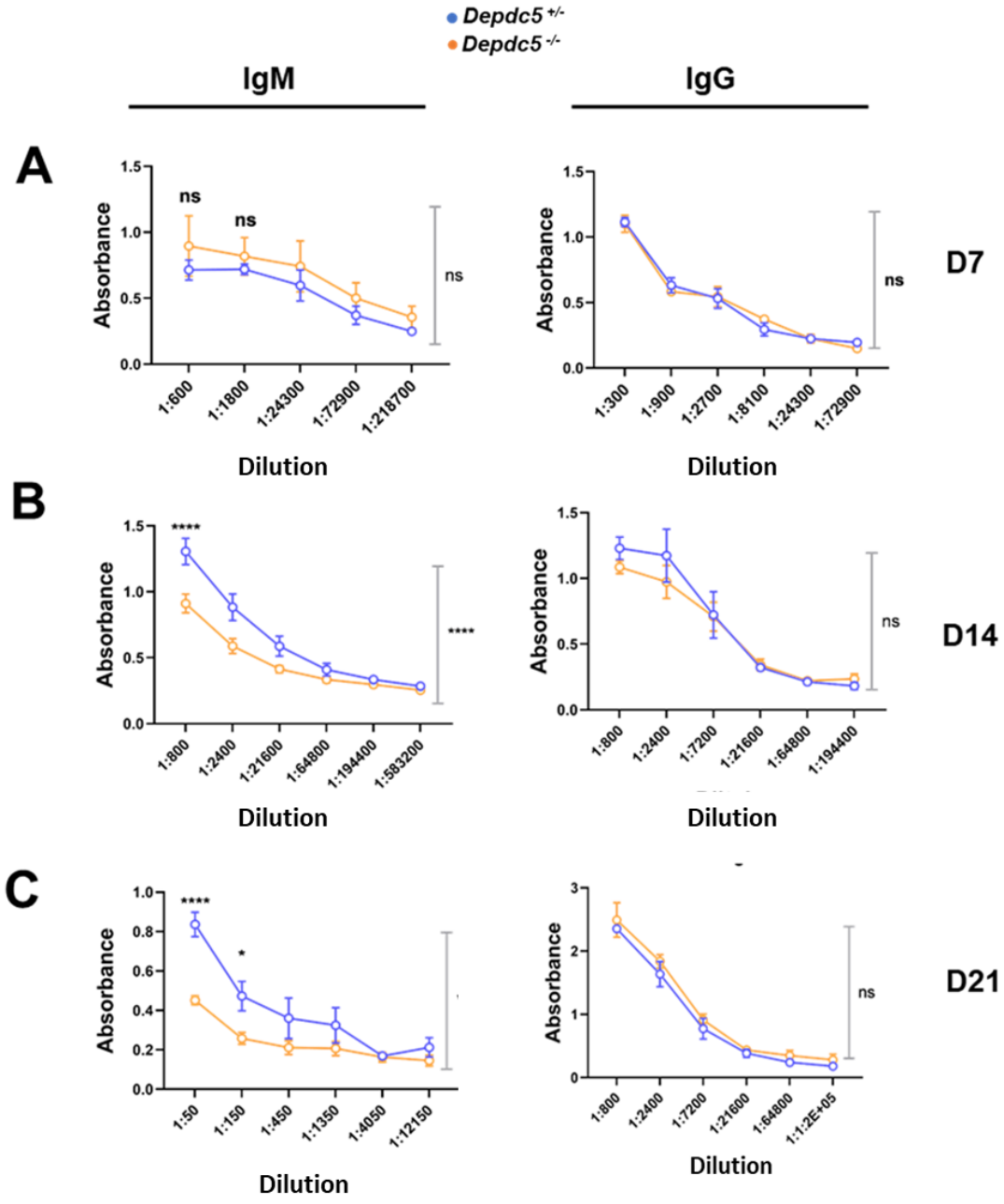
Depdc5 +/-
Depdc5 -/-
IgM
IgG
A
B
C
D7
D14
D21
Absorbance
Dilution
ns
****
*
1:600
1:1800
1:24300
1:72900
1:218700
1:300
1:900
1:2700
1:8100
1:800
1:2400
1:7200
1:21600
1:64800
1:194400
1:583200
1:50
1:150
1:450
1:1350
1:4050
1:12150
1:1:2E+05

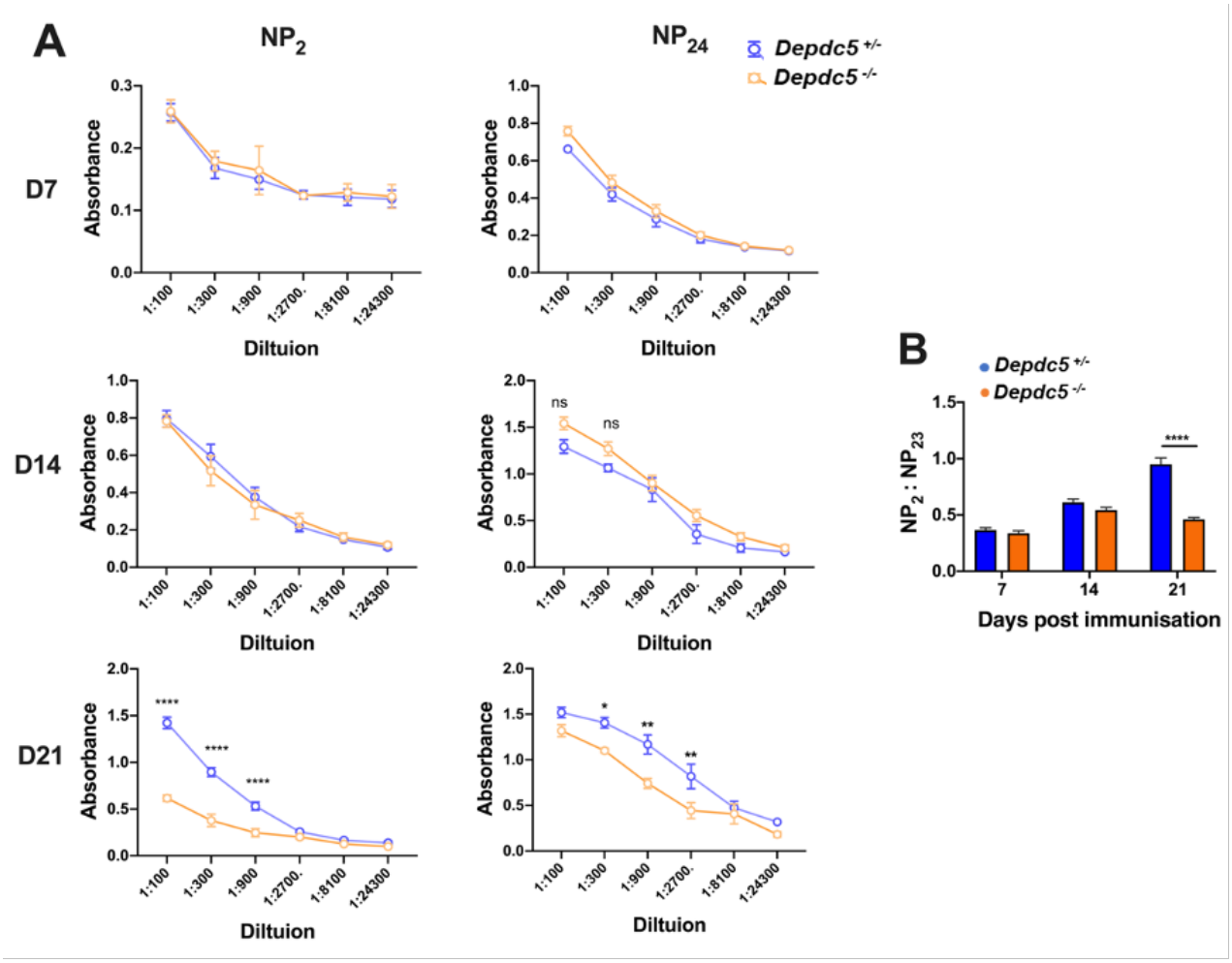

Figure 4.5: Loss of DEPDC5 reduced affinity of anti-NP IgG1 responses

Depdc5$^{+/-}$ and *Depdc5*$^{-/-}$ mice were immunized IP with NP-OVA. Serum was isolated at D7, D14 and D21 post NP-OVA immunization. Samples were analysed by ELISA to determine Ab affinity maturation. A) anti-NP IgG1 Ab titres and B) Ratio of NP2:NP24 for anti-NP IgG1 Ab in *Depdc5*$^{+/-}$ and *Depdc5*$^{-/-}$ immunized with NP-OVA. The columns represent the mean ± SEM. N= 5/group per time point, pooled from two independent experiments. The data were tested for statistical differences by one-way ANOVA.

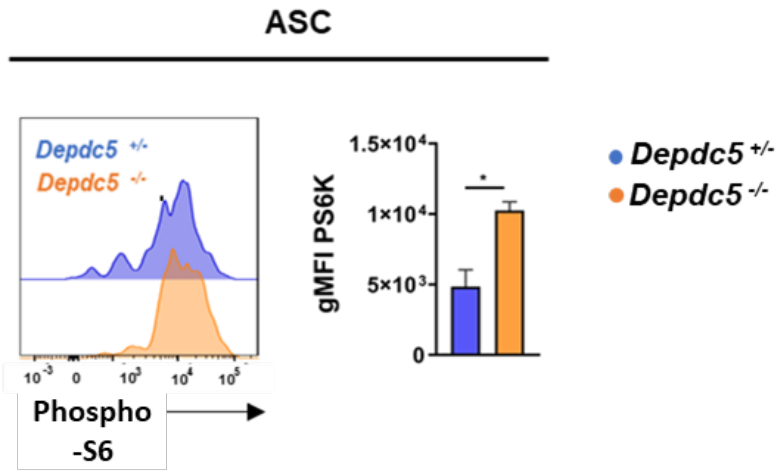

Figure 4.6: DEPDC5 regulated phospho-S6 expression in ASCs

Depdc5$^{+/-}$ and *Depdc5*$^{-/-}$ mice were infected IN with X31(100 $TCID_{50}$). The medLN was analysed for flow cytometry at D7. phospho-S6 expression was assessed in ASCs by flow cytometry (Pre-gated on ASCs). Representative flow cytometry is shown with quantification (gMFI) of phospho-S6 expression in ASCs cells from the medLN at D7 post-IAV infection in *Depdc5*$^{+/-}$ and *Depdc5*$^{-/-}$ mice. The columns represent the mean ± SEM. N=5/group, pooled from two independent experiments. A Mann-Whitney U test was applied for statistical analysis.

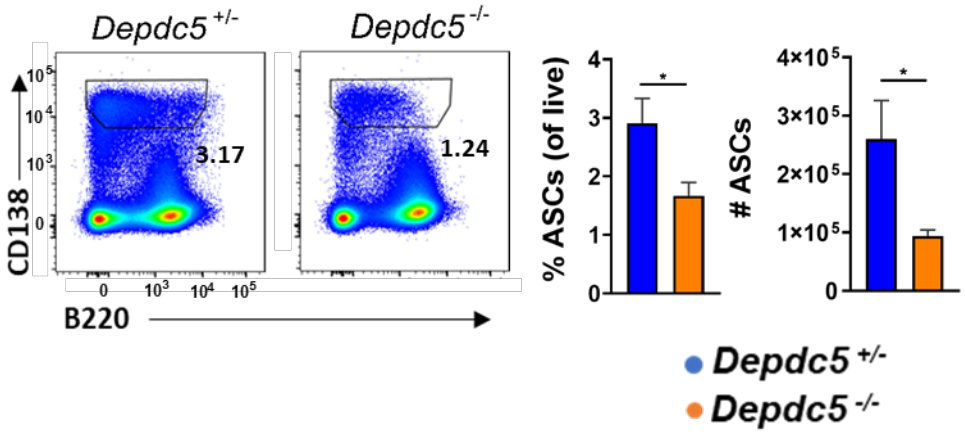

Figure 4.7: Deletion of DEPDC5 reduced ASC frequencies in the medLN during IAV infection

Depdc5$^{+/-}$ and *Depdc5*$^{-/-}$ mice were infected IN with X31(100 $TCID_{50}$). The medLN was analysed for flow cytometry at D7. ASCs were assessed by flow cytometry (Pre-gated on live cells). Representative flow cytometry is shown with quantification of ASCs from the medLN from *Depdc5*$^{+/-}$ and *Depdc5*$^{-/-}$ mice at D7 post-IAV infection. N= 5/group, pooled from two independent experiments. The columns represent the mean ± SEM. A Mann-Whitney U test was applied for statistical analysis.

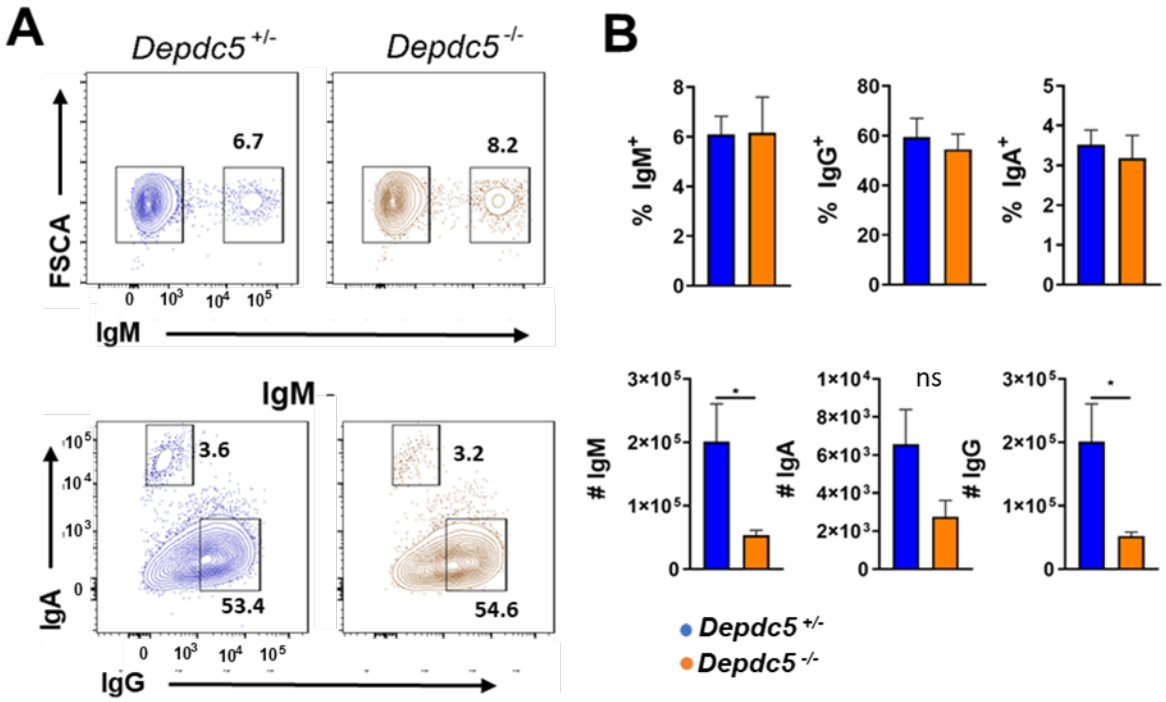

Figure 4.8: Deletion of DEPDC5 did not alter ASC isotype switching

Depdc5$^{+/-}$ and *Depdc5*$^{-/-}$ mice were infected IN with X31(100 $TCID_{50}$). The medLN were analysed for flow cytometry at D7. Ab isotypes (IgM, IgG and IgA) within the ASC compartment were analysed (Pre-gated on ASCs). Representative flow cytometry **(A)** is shown with quantification **(B)** of IgM^+, IgG^+ and IgA^+ ASCs. N= 5/ group, pooled from two independent experiments. The columns represent the mean ± SEM. A Mann-Whitney U test was applied for statistical analysis.

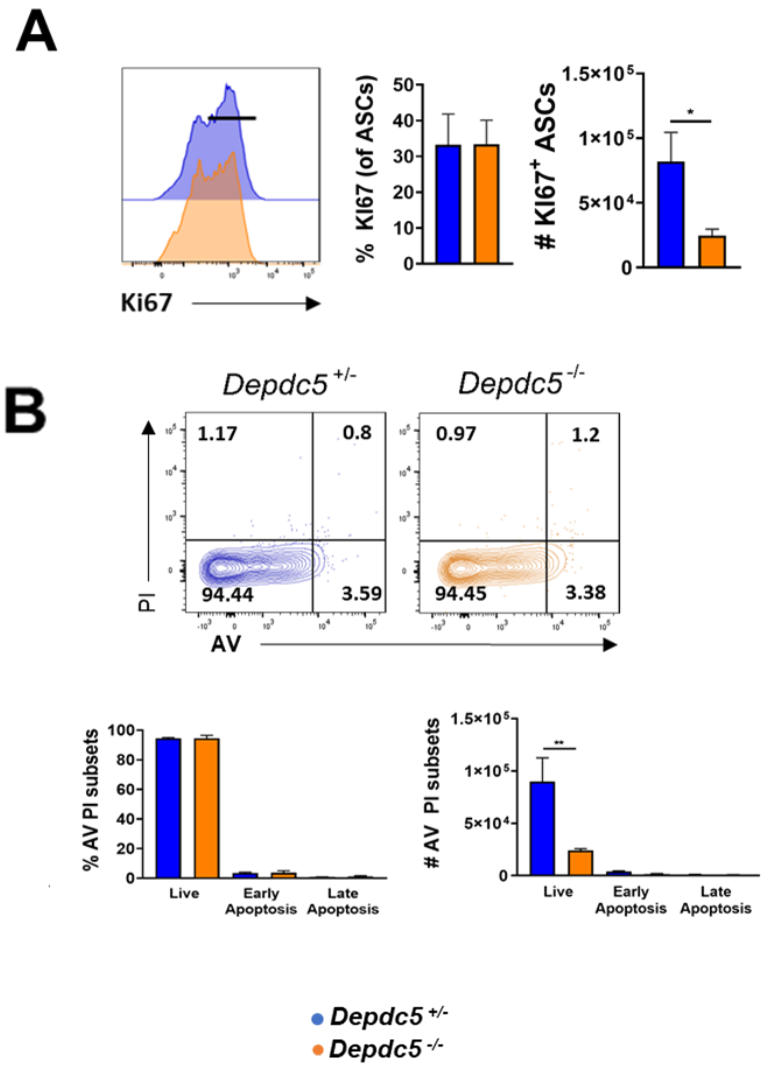

Figure 4.9: DEPDC5 deletion did not affect proliferation or apoptosis of ASCs at in the medLN during IAV infection

Depdc5$^{+/-}$ and *Depdc5*$^{-/-}$ mice were infected IN with X31(100 $TCID_{50}$). Lungs were analysed for flow cytometry at D14. Proliferating ($Ki67^+$), live (AV^-PI^-), early apoptotic (AV^+PI^-) and late apoptotic (AV^+PI^+) populations in the ASC compartment were assessed (pre-gated on ASCs). Representative flow cytometry and quantification of **(A)** $Ki67^+$ ASCs and **(B)** live, early apoptotic and late apoptotic ASCs. N= 5/group, pooled from two independent experiments. The columns represent the mean ± SEM. A) Mann-Whitney test. B) A one-way ANOVA test was used for statistical analysis.

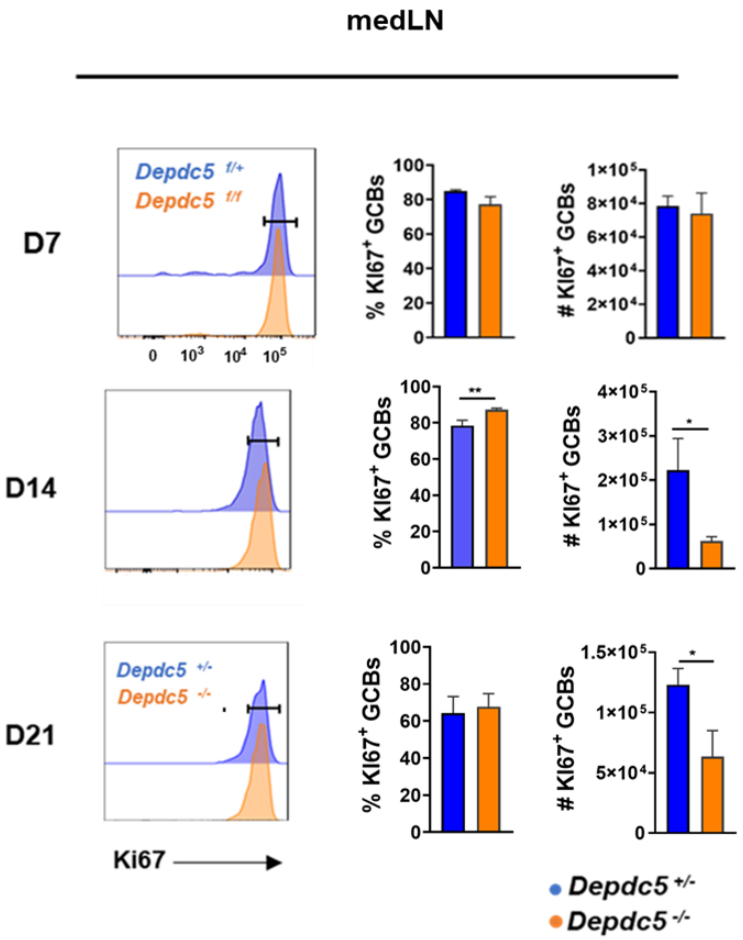

Figure 4.10: DEPDC5 deletion transiently increased GCB proliferation in the medLN at peak of GCB response in the medLN following IAV infection

Depdc5$^{+/-}$ and *Depdc5*$^{-/-}$ mice were infected IN with X31(100 $TCID_{50}$). The medLN were analysed for flow cytometry at D7. D14 and D21. Ki67^{+} populations in the GCB compartment was assessed (pre-gated on GCB cells). Representative flow cytometry is shown with quantification of Ki67^{hi} GCB cells from the medLN at D7, 14 and 21 post-IAV infection in *Depdc5*$^{+/-}$ and *Depdc5*$^{-/-}$ mice. The columns represent the mean ± SEM. D7 N=4/group, D14.group N=10 and D21 N=10/group), pooled from at least two independent experiments. A Mann-Whitney U test was applied for statistical analysis.

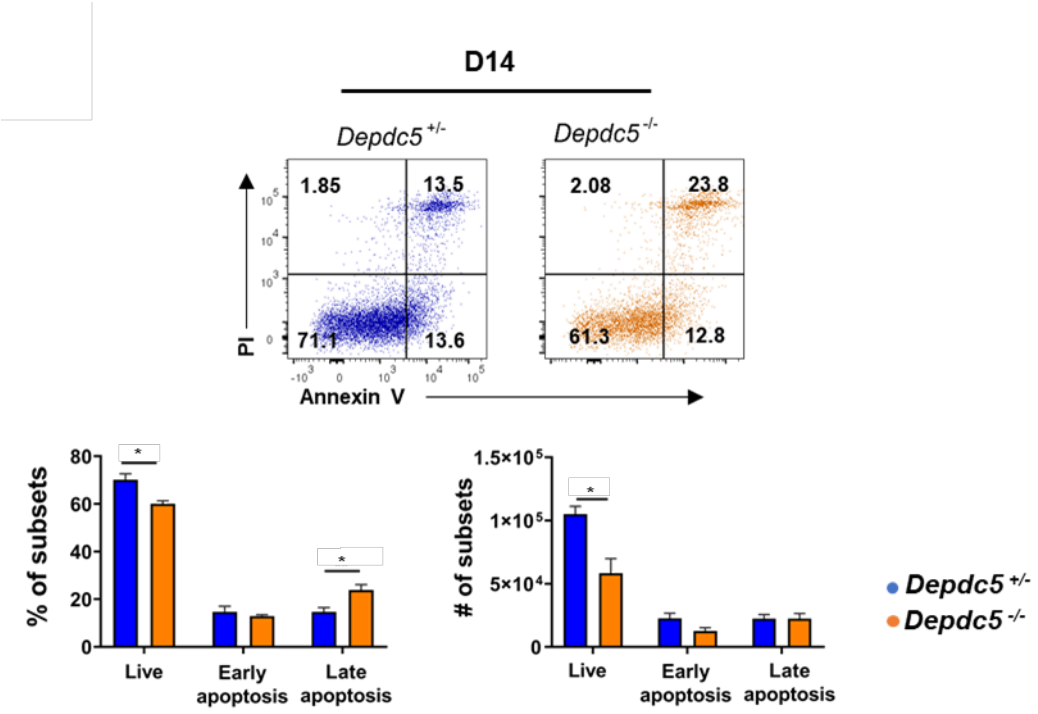

Figure 4.11: DEPDC5 deletion increased late stage GCB cell apoptosis at peak of the GC

Depdc5$^{+/-}$ and *Depdc5*$^{-/-}$ mice were infected IN with X31(100 $TCID_{50}$). The medLN was analysed for flow cytometry at D14. Live (AV^{-} PI^{-}), early apoptotic (AV^{+} PI^{-}) and late apoptotic (AV^{+} PI^{+}) populations in the GCB compartment was assessed (pre-gated on GCB cells). Representative flow cytometry is shown with quantification of these GCB populations at D14 post-IAV infection from *Depdc5*$^{+/-}$ and *Depdc5*$^{-/-}$ mice. N= 6/group, pooled from two independent experiments. The columns represent the mean ± SEM. A Mann-Whitney U test was used for statistical analysis to compare groups within each population.

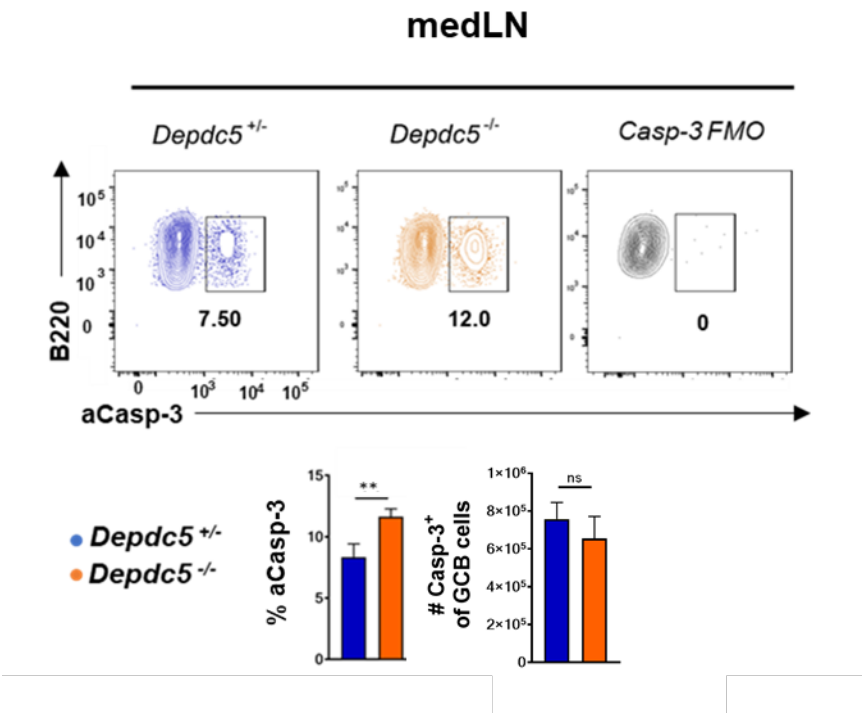

Figure 4.12: DEPDC5 deletion increased apoptosis in GCB cells at peak of GCB response to IAV in the medLN

Depdc5$^{+/-}$ and *Depdc5*$^{-/-}$ mice were infected IN with X31(100 $TCID_{50}$). The medLN was analysed for flow cytometry at D14. aCasp-3^{+} populations in the GCB compartment was assessed (pre-gated on GCB cells). Representative flow cytometry is shown with quantification of aCasp-3^{+} in GCB cells from the medLN at 14 post-IAV infection in *Depdc5*$^{+/-}$ and *Depdc5*$^{-/-}$ mice. The columns represent the mean ± SEM. N= 5 -7/group, pooled from two independent experiments. A Mann-Whitney U test was used for statistical analysis.

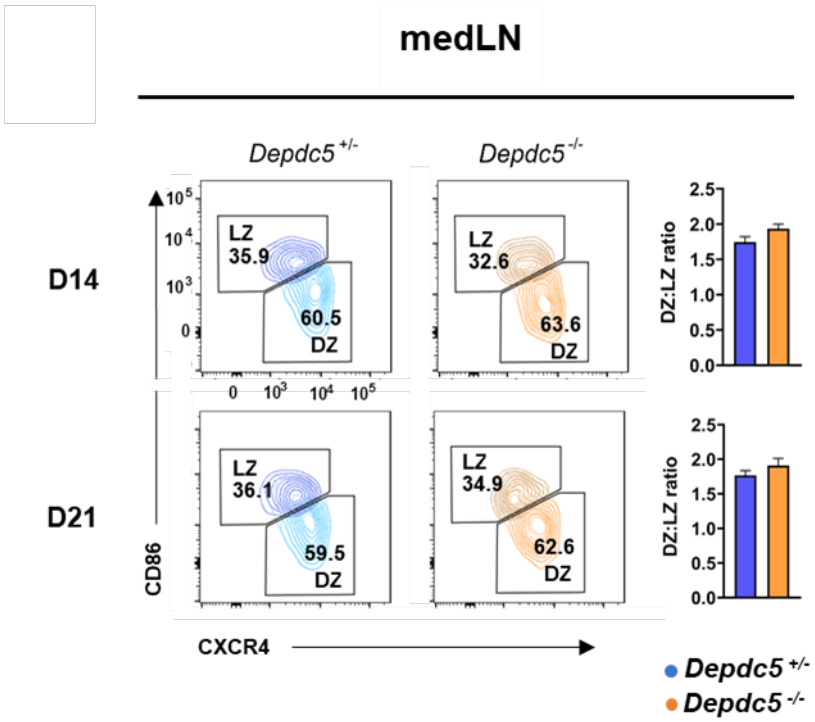

Figure 4.13: DEPDC5 deletion did not affect GC polarisation within the medLN during the response to IAV infection

Depdc5$^{+/-}$ and *Depdc5*$^{-/-}$ mice were infected IN with X31(100 $TCID_{50}$). The medLN was analysed for flow cytometry at D14 and D21. Representative flow cytometry is shown with quantification of the DZ:LZ ratio (DZ and LZ pre-gated on GCBs). The columns represent the mean ± SEM. D14 N=10 and D21 N=10/group, pooled from at least two independent experiments. A Mann-Whitney U test was applied for statistical analysis.

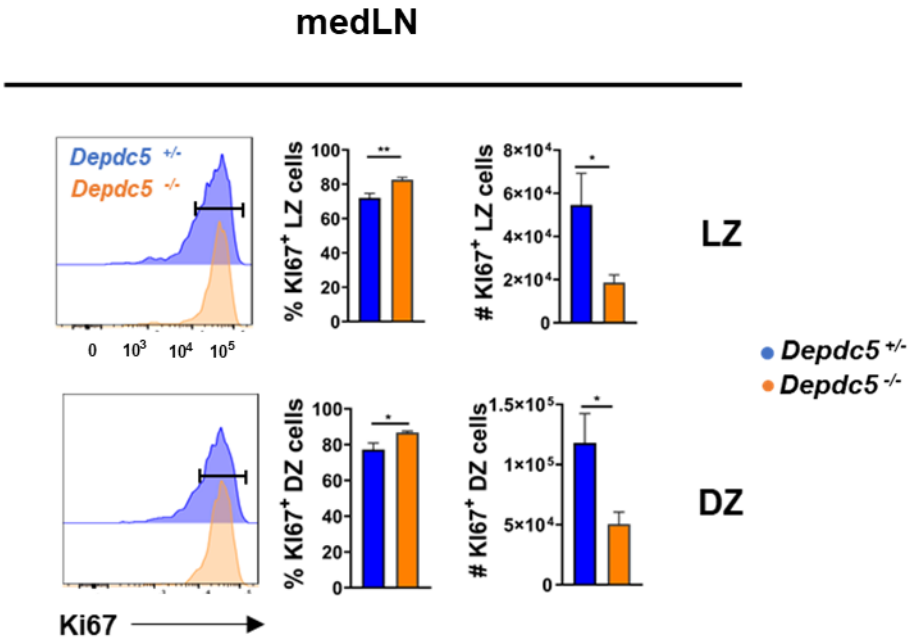

Figure 4.14: DEPDC5 deletion transiently increased LZ and DZ cell proliferation in the medLN during peak GC response to IAV

Depdc5$^{+/-}$ and *Depdc5*$^{-/-}$ mice were infected IN with X31(100 $TCID_{50}$). The medLN was analysed for flow cytometry at D14. Ki67^{+} populations in the DZ and LZ compartment was assessed (pre-gated on LZ and DZ GCBs). Representative flow cytometry is shown with quantification of Ki67^{hi} LZ (CXCR4^{-}CD86^{+} GCBs) and DZ (CXCR4^{+}CD86^{-} GCBs) cells from the medLN at D14 post-IAV infection of *Depdc5*$^{+/-}$ and *Depdc5*$^{-/-}$ mice. The columns represent the mean ± SEM. N= 5-6/group, pooled from two independent experiments. A Mann-Whitney U test was applied for statistical analysis.

Figure 4.15: DEPDC5 deletion did not affect apoptosis specifically in LZ and DZ cells at peak of GC response in the medLN during IAV infection

Depdc5$^{+/-}$ and *Depdc5*$^{-/-}$ mice were infected IN with X31(100 $TCID_{50}$). The medLN was analysed for flow cytometry at D14. Live ($AV^{-}PI^{-}$), early apoptotic ($AV^{+}PI^{-}$) and late apoptotic ($AV^{+}PI^{+}$) populations in the DZ and LZ compartment was assessed (DZ and LZ pre-gated on GCBs). Representative flow cytometry is shown with quantification of live, early apoptotic and late apoptotic in the LZ and DZ cells from the medLN at d14 post-IAV infection of *Depdc5*$^{+/-}$ and *Depdc5*$^{-/-}$ mice. The columns represent the mean ± SEM. N= 5-6/group, pooled from two independent experiments. A Mann-Whitney U test was used for statistical analysis to compare groups within each population.

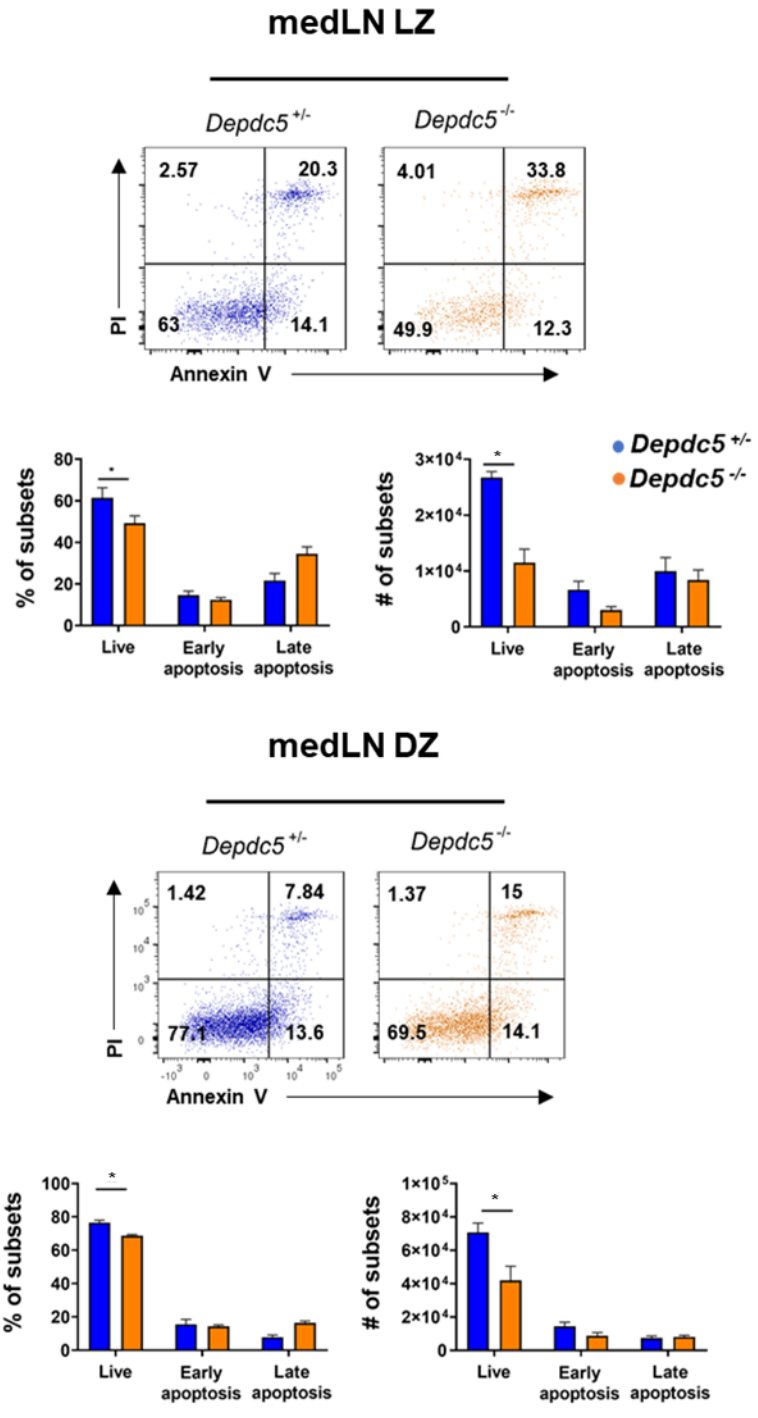
medLN LZ
Depdc5 +/-
Depdc5 -/-
2.57
20.3
63
14.1
4.01
33.8
49.9
12.3
PI
Annexin V
% of subsets
# of subsets
Live
Early apoptosis
Late apoptosis
medLN DZ
1.42
7.84
77.1
13.6
1.37
15
69.5
14.1

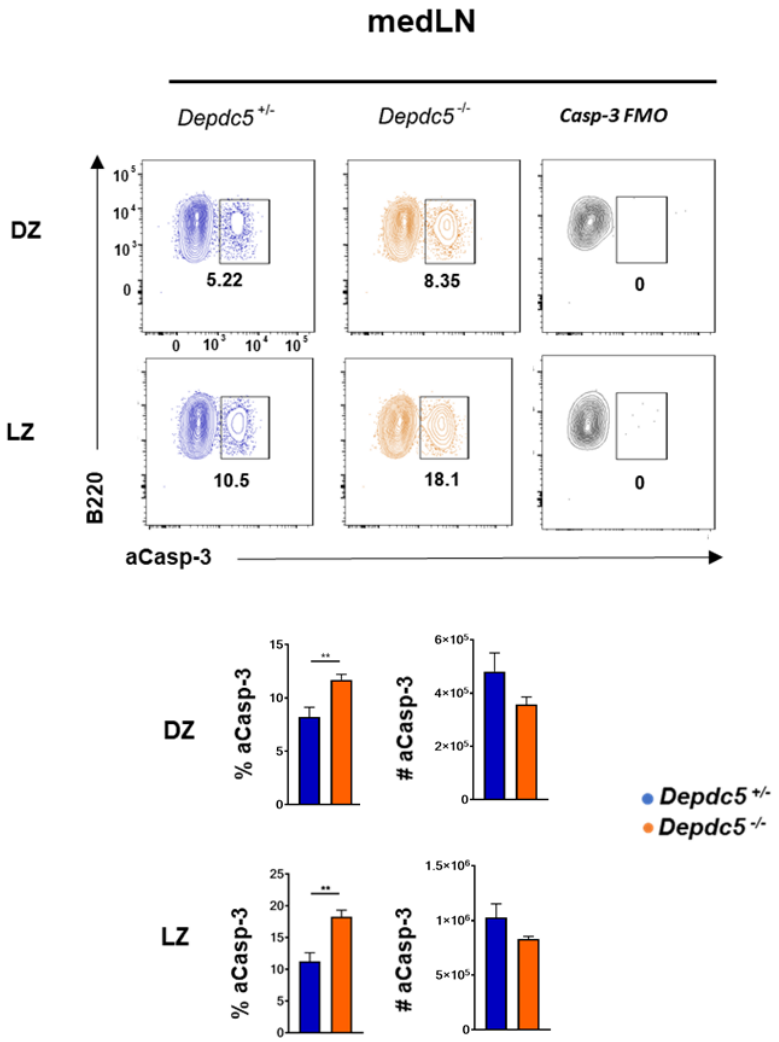

Figure 4.16: DEPDC5 deletion increased apoptosis amongst LZ and DZ cells in the medLN during peak GC response to IAV infection

Depdc5$^{+/-}$ and *Depdc5*$^{-/-}$ mice were infected IN with X31(100 $TCID_{50}$). The medLN was analysed for flow cytometry at D14. aCasp-3^{+} populations in the DZ and LZ compartment was assessed (pre-gated on LZ and DZ GCBs). Representative flow cytometry is shown with quantification of aCasp-3^{+} LZ (CXCR4^{-}CD86^{+} GCBs) and DZ (CXCR4^{+}CD86^{-} GCBs) cells from the medLN at D14 post-IAV infection of *Depdc5*$^{+/-}$ and *Depdc5*$^{-/-}$ mice. N= 6/group, pooled from two independent experiments. The columns represent the mean ± SEM. A Mann-Whitney U test was applied for statistical analysis.

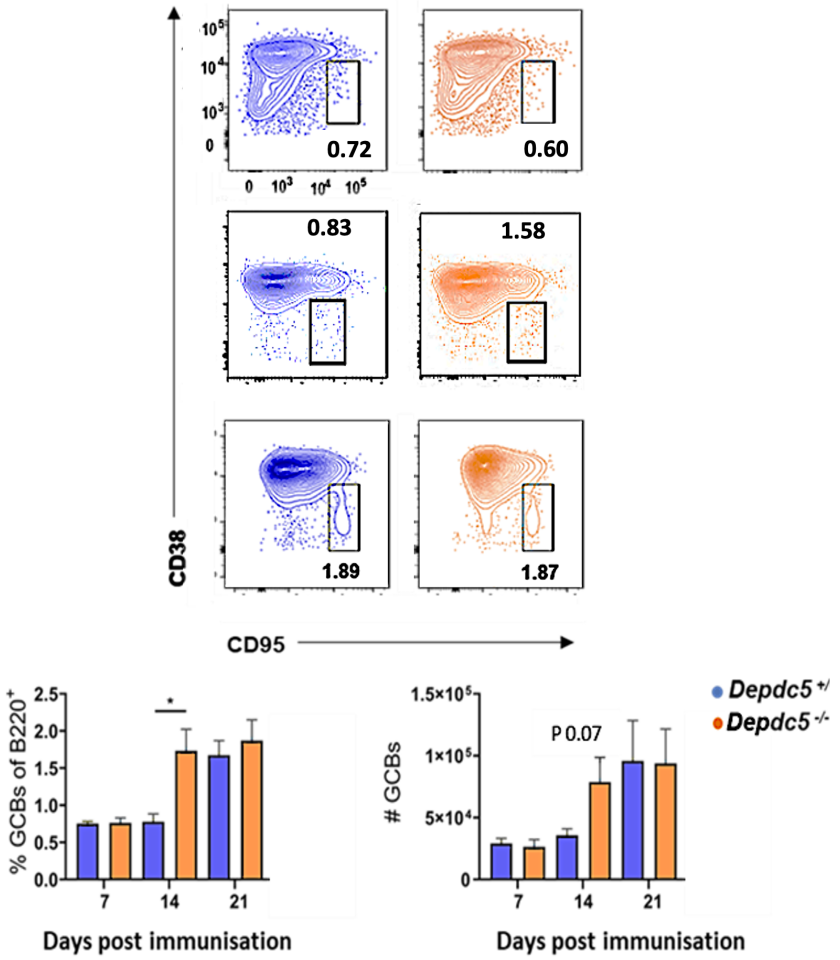

Figure 4.17: DEPDC5 loss accelerated GCB accumulation in the lung during IAV responses

Depdc5$^{+/-}$ and *Depdc5*$^{-/-}$ mice were infected IN with X31(100 $TCID_{50}$). Lungs were analysed for flow cytometry at D7, D14 and D21. Representative flow cytometry is shown with quantification of GCB ($B220^{+}CD38^{-}CD95^{+}$) cells from the medLN at D7, 14 and 28 post-IAV infection of *Depdc5*$^{+/-}$ and *Depdc5*$^{-/-}$ mice. The columns represent the mean ± SEM. D7 N=12/group, D14 N=18/group and D21 N=23/group, pooled from at least two independent experiments. A one-way ANOVA test was used for statistical analysis.

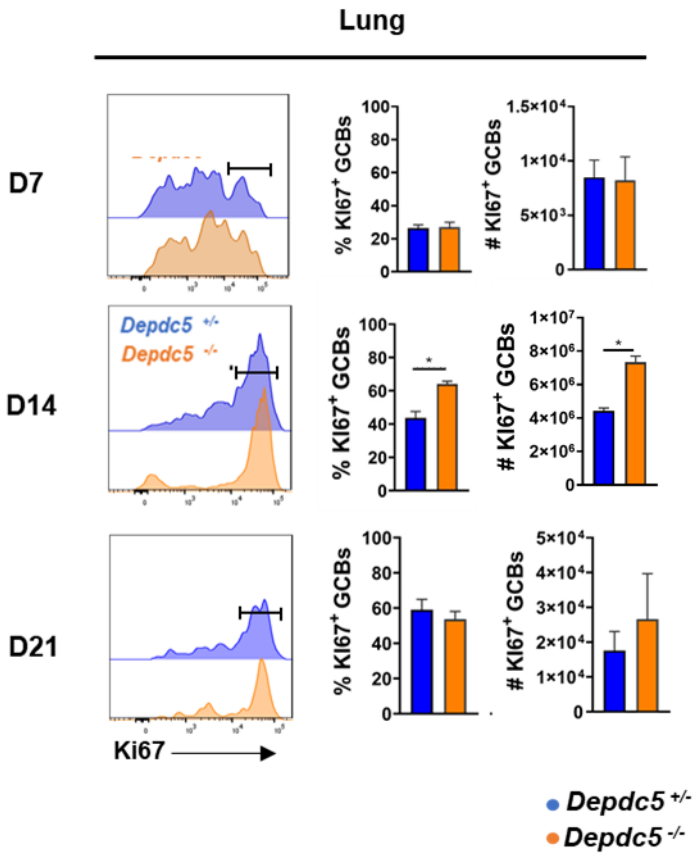

Figure 4.18: Loss of DEPDC5 enhanced GCB proliferation at peak of GC response in the lung following IAV infection.

Depdc5$^{+/-}$ and *Depdc5*$^{-/-}$ mice were infected IN with X31(100 $TCID_{50}$). Lungs were analysed for flow cytometry at D7, D14 and D21. Ki67^{+} populations in the GCB compartment were assessed (pre-gated on GCB cells). Representative flow cytometry and quantification of Ki67^{+} GCBs at D7, 14 and 21 post-IAV infection in the lung of *Depdc5*$^{+/-}$ and *Depdc5*$^{-/-}$ mice. The columns represent the mean ± SEM. D7 N=4/group, D14 N=10/group and D21 N=10/group, pooled from four independent experiments. A Mann-Whitney U test was applied for statistical analysis.

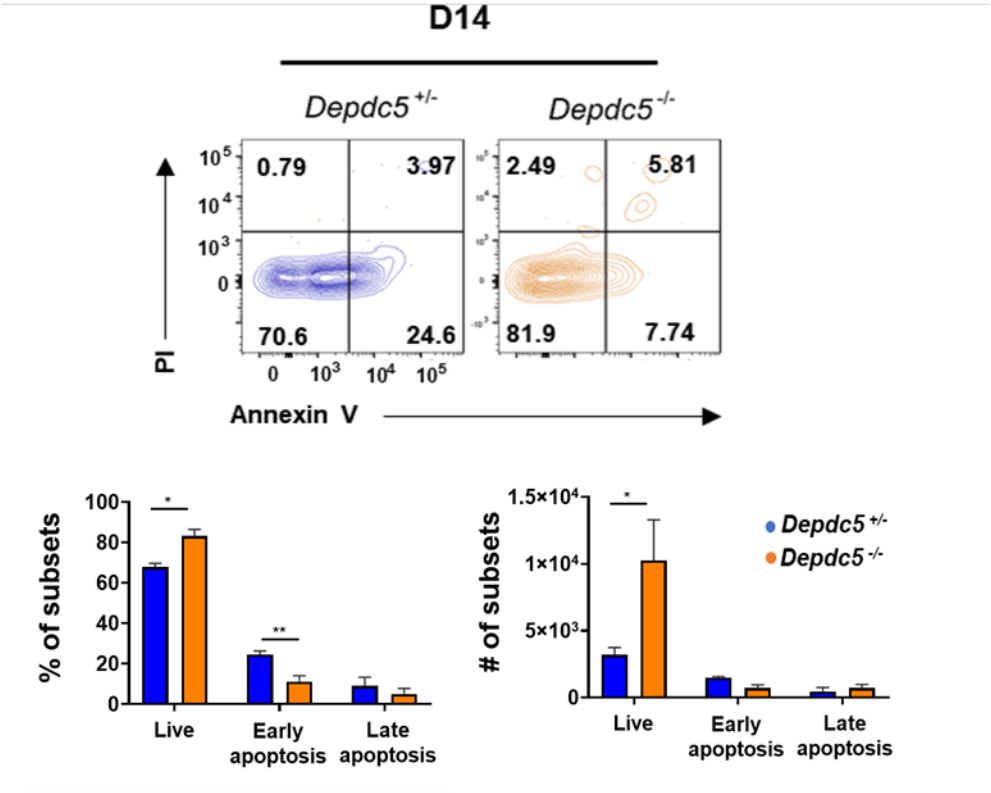

Figure 4.19: DEPDC5 loss did not affect apoptosis of GCB cells in the lung following IAV infection

Depdc5$^{+/-}$ and *Depdc5*$^{-/-}$ mice were infected IN with X31(100 $TCID_{50}$). Lungs were analysed for flow cytometry at D14. Live ($AV^{-}PI^{-}$), early apoptotic ($AV^{+}PI^{-}$) and late apoptotic ($AV^{+}PI^{+}$) populations in the GCB compartment was assessed (pre-gated on B cells). Representative flow cytometry and quantification of live, early apoptotic and late apoptotic GCBs at D14 cells from the lung of *Depdc5*$^{+/-}$ and *Depdc5*$^{-/-}$ mice. The columns represent the mean ± SEM. N= 6/group, pooled from two independent experiments. A one-way ANOVA test was used for statistical analysis.

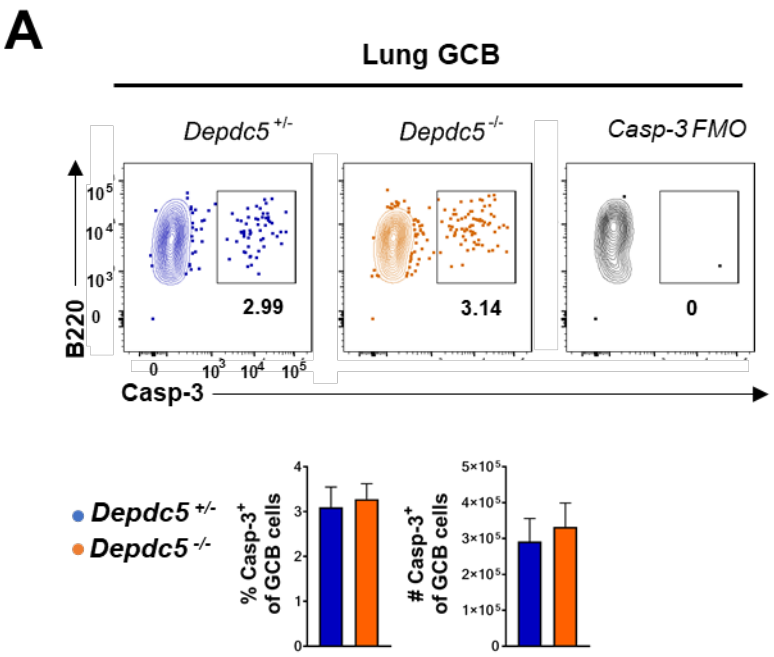

Figure 4.20: DEPDC5 did not affect active apoptosis in GCB cells at peak humoral response in the lung during IAV responses

Depdc5$^{+/-}$ and *Depdc5*$^{-/-}$ mice were infected IN with X31(100 $TCID_{50}$). Lungs were analysed for flow cytometry at D14. aCasp-3^{+} populations in the GCB compartment was assessed (pre-gated on B cells). Representative flow cytometry is shown with quantification of aCasp-3^{+} GCB cells from the lung of *Depdc5*$^{+/-}$ and *Depdc5*$^{-/-}$ mice at D14. The columns represent the mean ± SEM. N= 6 -7/group, pooled from two independent experiments. A Mann-Whitney U test was applied for statistical analysis.

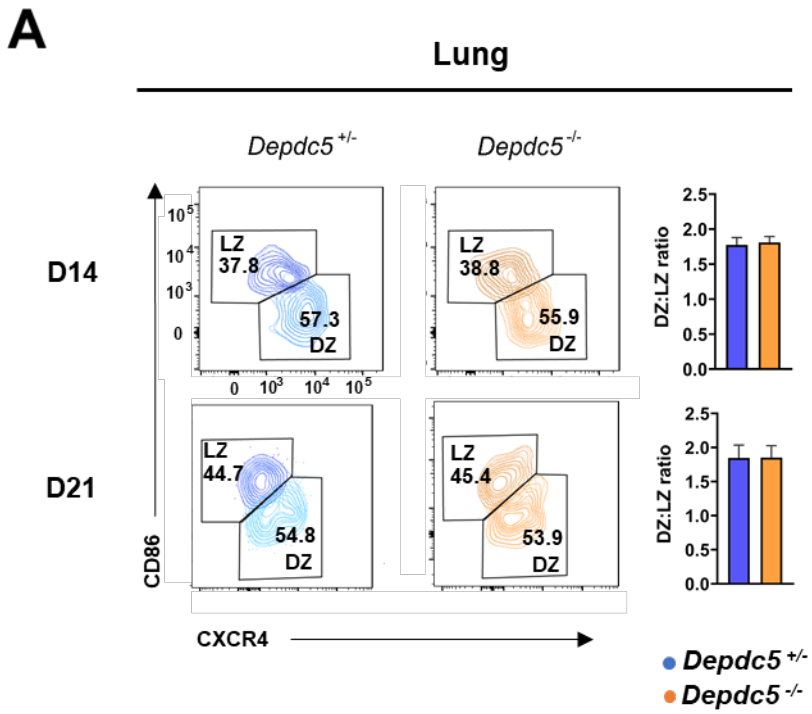

Figure 4.21: DEPDC5 did not affect GC polarisation during responses within the lung following IAV infection

Depdc5$^{+/-}$ and *Depdc5*$^{-/-}$ mice were infected IN with X31(100 $TCID_{50}$). Lungs were analysed for flow cytometry at D14 and D21. DZ:LZ ratios were assessed (DZ and LZ pre-gated on GCBs). The columns represent the mean ± SEM. D14 N=10 and D21 N=10 per group in total, pooled from two to four independent experiments. A Mann-Whitney U test was applied for statistical analysis.

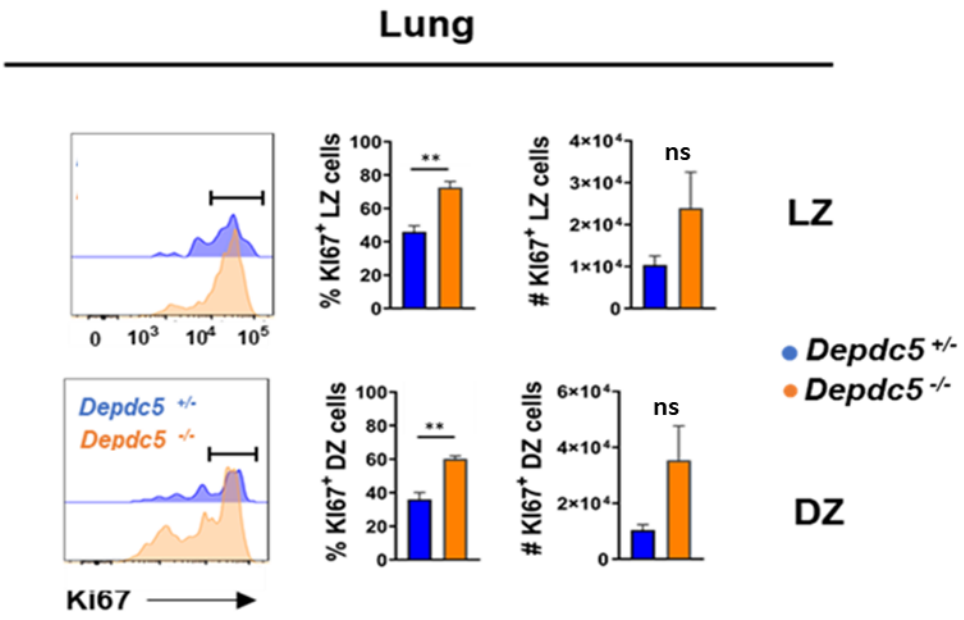

Figure 4.22: DEPDC5 inhibited LZ and DZ proliferation at peak of GC response in the lung following IAV infection

Depdc5$^{+/-}$ and *Depdc5*$^{-/-}$ mice were infected IN with X31(100 $TCID_{50}$). Lungs were analysed for flow cytometry at D14. Ki67^{+} populations in the DZ and LZ compartment was assessed (pre-gated on LZ and DZ GCBs). Representative flow cytometry is shown with quantification of Ki67^{+} **(i)** LZ (CXCR4^{-}CD86^{-} GCBs) and **(ii)** DZ (CXCR4^{-}CD86^{-} GCBs) cells from the lung of *Depdc5*$^{+/-}$ and *Depdc5*$^{-/-}$ mice at D14. The columns represent the mean ± SEM. N= 5-6 per group/pooled from two independent experiments. A Mann-Whitney U test was applied for statistical analysis.

Figure 4.23: DEPDC5 deletion increased LZ and DZ cell survival in the lung following IAV infection

Depdc5$^{+/-}$ and *Depdc5*$^{-/-}$ mice were infected IN with X31(100 $TCID_{50}$). Lungs were analysed for flow cytometry at D14. Live (AV^- PI^-), early apoptotic (AV^+ PI^-) and late apoptotic (AV^+ PI^+) populations in the DZ and LZ compartment was assessed (pre-gated on LZ and DZ GCBs). Representative flow cytometry is shown with quantification of live, early apoptotic and late apoptotic in the LZ ($CXCR4^-CD86^-$ GCBs) and DZ ($CXCR4^-CD86^-$ GCBs) cells from the lung of *Depdc5*$^{+/-}$ and *Depdc5*$^{-/-}$ mice at D14. The columns represent the mean ± SEM. N= 5-6/group, pooled from two independent experiments. A Mann-Whitney U test was applied for statistical analysis.

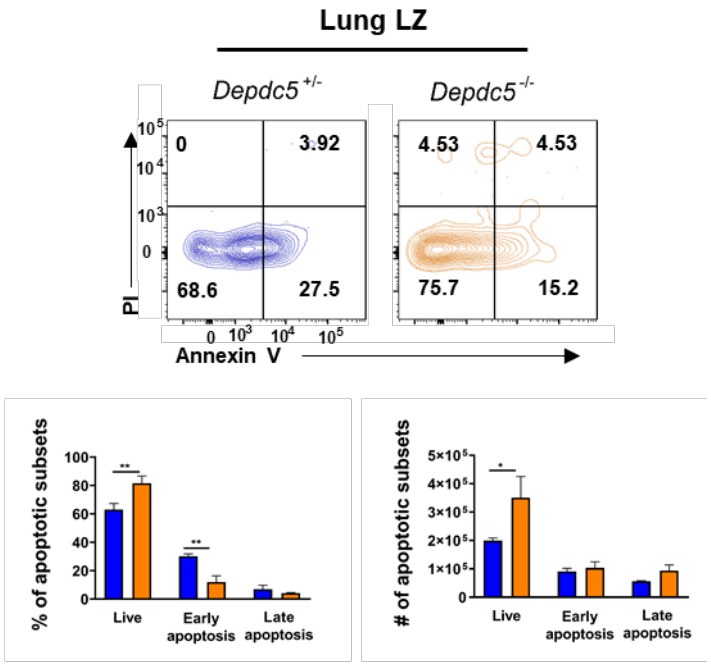

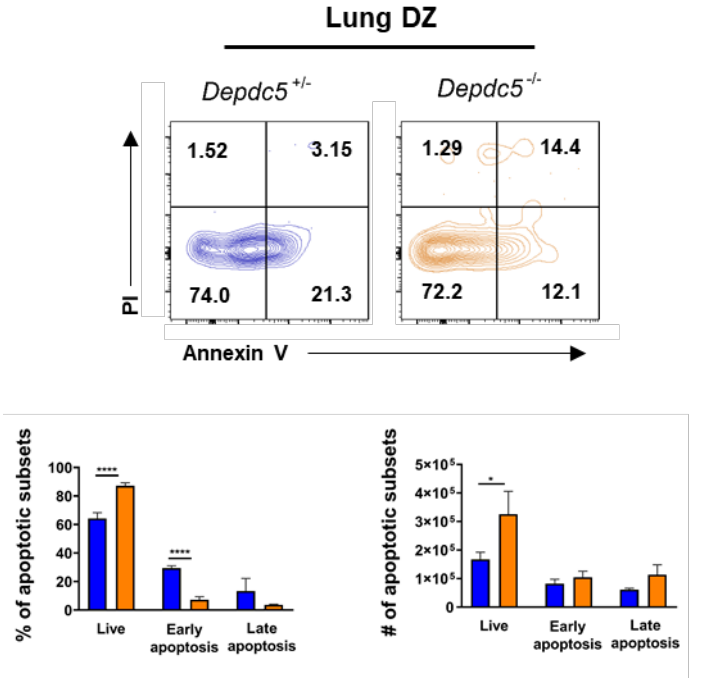

● Depdc5 +/-
● Depdc5 -/-

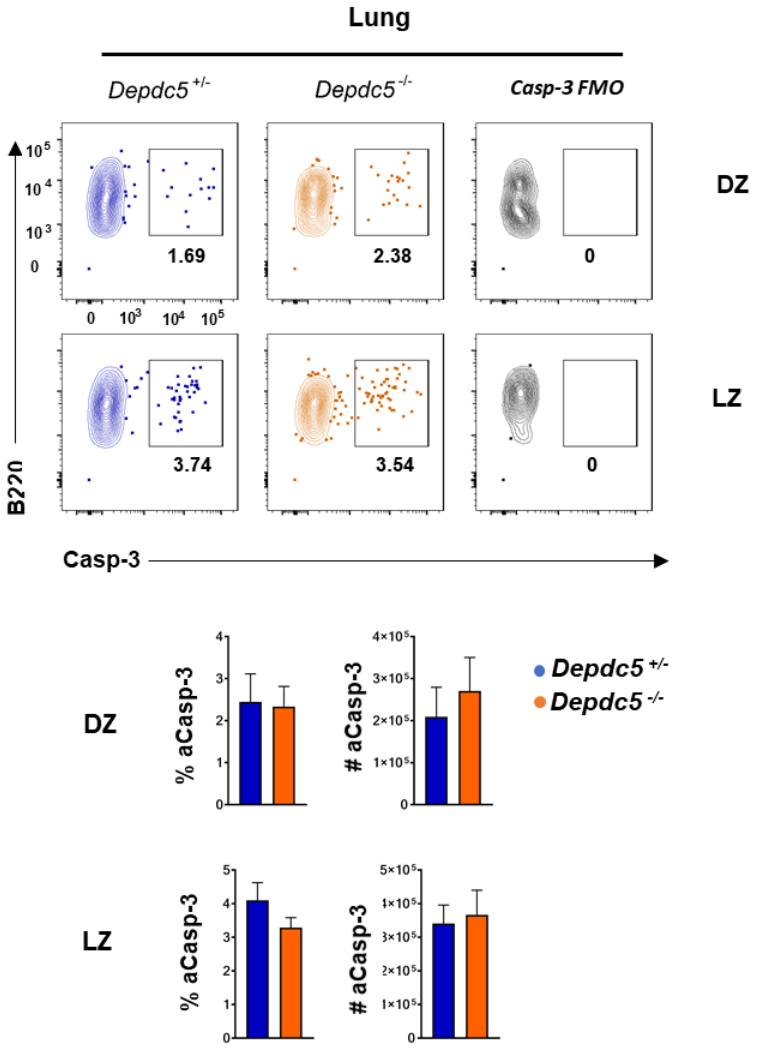

Figure 4.24: DEPDC5 did not affect active apoptosis in LZ and DZ cells at peak of GC in the lung following IAV infection

Depdc5$^{+/-}$ and *Depdc5*$^{-/-}$ mice were infected IN with X31(100 $TCID_{50}$). Lungs were analysed for flow cytometry at D14. aCasp-3^{+} populations in the DZ and LZ compartment was assessed (pre-gated on LZ and DZ GCBs). Representative flow cytometry is shown with quantification of aCasp-3^{+} in the LZ (CXCR4^{-}CD86^{-} GCBs) and DZ (CXCR4^{-}CD86^{-} GCBs) cells from the lung of *Depdc5*$^{+/-}$ and *Depdc5*$^{-/-}$ mice at D14. The columns represent the mean ± SEM. N= 5-6/group, pooled from two independent experiments. A Mann-Whitney U test was applied for statistical analysis.

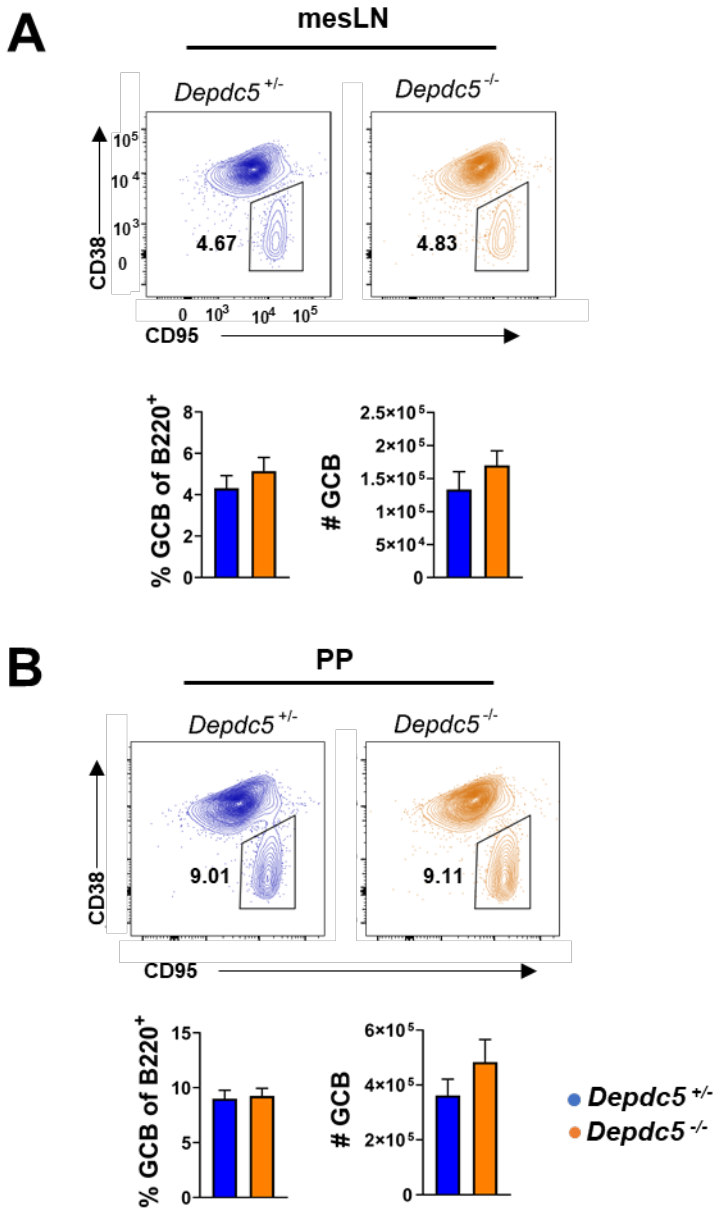

Figure 4.25: DEPDC5 loss did not affect GCB cells in chronic GCs

PP and mesLN from 8-12 week old naive *Depdc5*$^{+/-}$ and *Depdc5*$^{-/-}$ mice. Representative flow cytometry is shown with quantification of GCBs (pre-gated on total B cells) from the **(A)** mesLN and **(B)** PP of *Depdc5*$^{+/-}$ and *Depdc5*$^{-/-}$ mice. The columns represent the mean ± SEM. N= 20-22/group, pooled from two independent experiments. A Mann-Whitney U test was applied for statistical analysis.

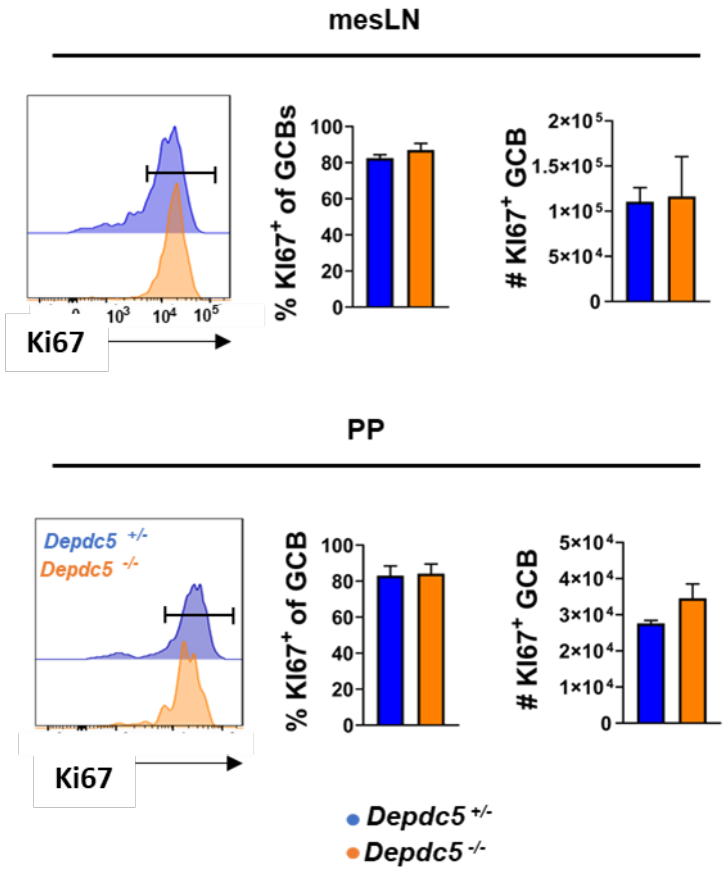

Figure 4.26: DEPDC5 loss did not affect GCB proliferation in chronic GC reactions

PP and mesLN from 8-12 week old naive *Depdc5*$^{+/-}$ and *Depdc5*$^{-/-}$ mice. Representative flow cytometry is shown with quantification of Ki67^{+} GCBs (pre-gated on B cells) from the mesLN and PP from from *Depdc5*$^{+/-}$ and *Depdc5*$^{-/-}$ mice. The columns represent the mean ± SEM. N= 6-16/group, pooled from two independent experiments. A Mann-Whitney U test was applied for statistical analysis.

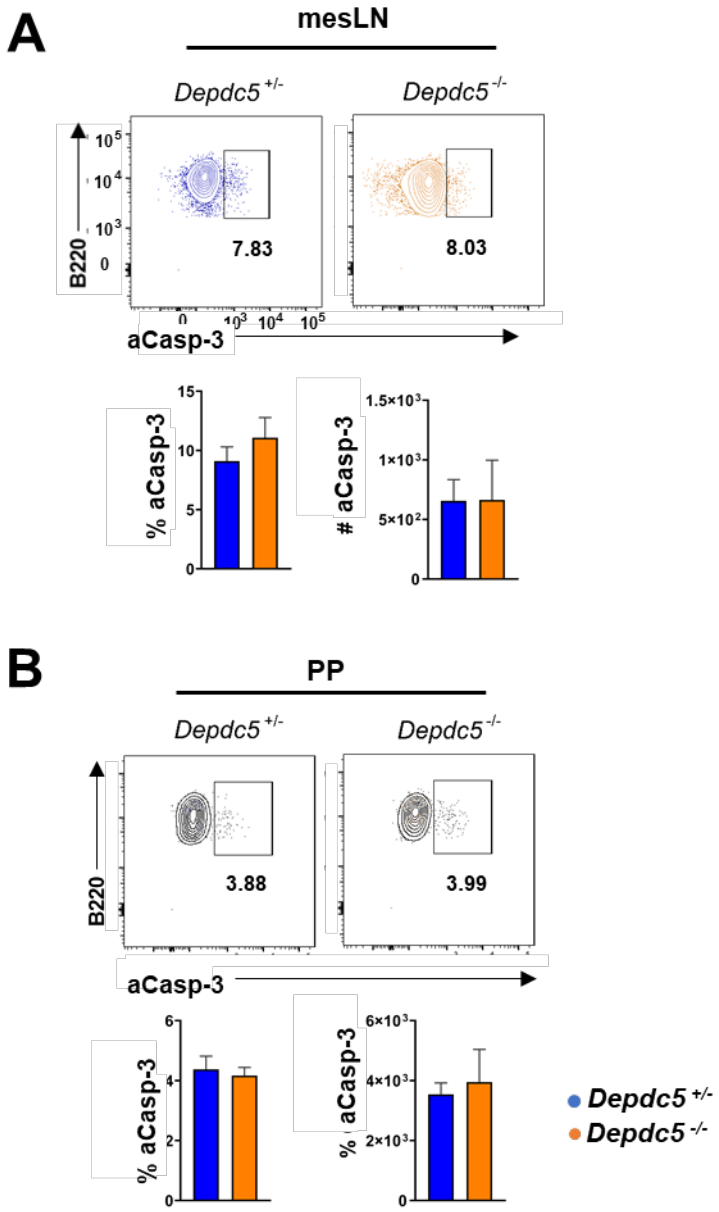

Figure 4.27: DEPDC5 loss did not affect GCB apoptosis in chronic GC reactions

PP and mesLN from 8-12 week old naive *Depdc5*$^{+/-}$ and *Depdc5*$^{-/-}$ mice. Representative flow cytometry is shown with quantification of aCasp-3^{+} GCBs (pre-gated on B cells) from the **(A)** mesLN and **(B)** PP from *Depdc5*$^{+/-}$ and *Depdc5*$^{-/-}$ mice. The columns represent the mean ± SEM. N= 4/group, pooled from two independent experiments. A Mann-Whitney U test was applied for statistical analysis.

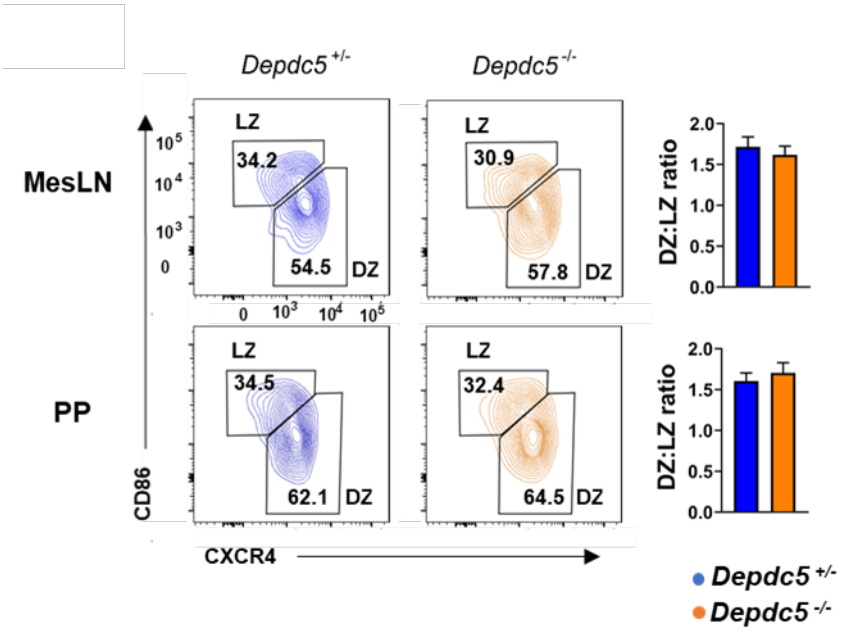

Figure 4.28: DEPDC5 loss did not affect GCB polarisation in chronic GC reactions

PP and mesLN from 8-12 week old naive *Depdc5*$^{+/-}$ and *Depdc5*$^{-/-}$ mice. Representative flow cytometry is shown with quantification of the DZ:LZ ratio (DZ and LZ pre-gated on GCBs) from the mesLN and PP from *Depdc5*$^{+/-}$ and *Depdc5*$^{-/-}$ mice. N= 8/group, pooled from two independent experiments. The columns represent the mean ± SEM. A Mann-Whitney U test was applied for statistical analysis.

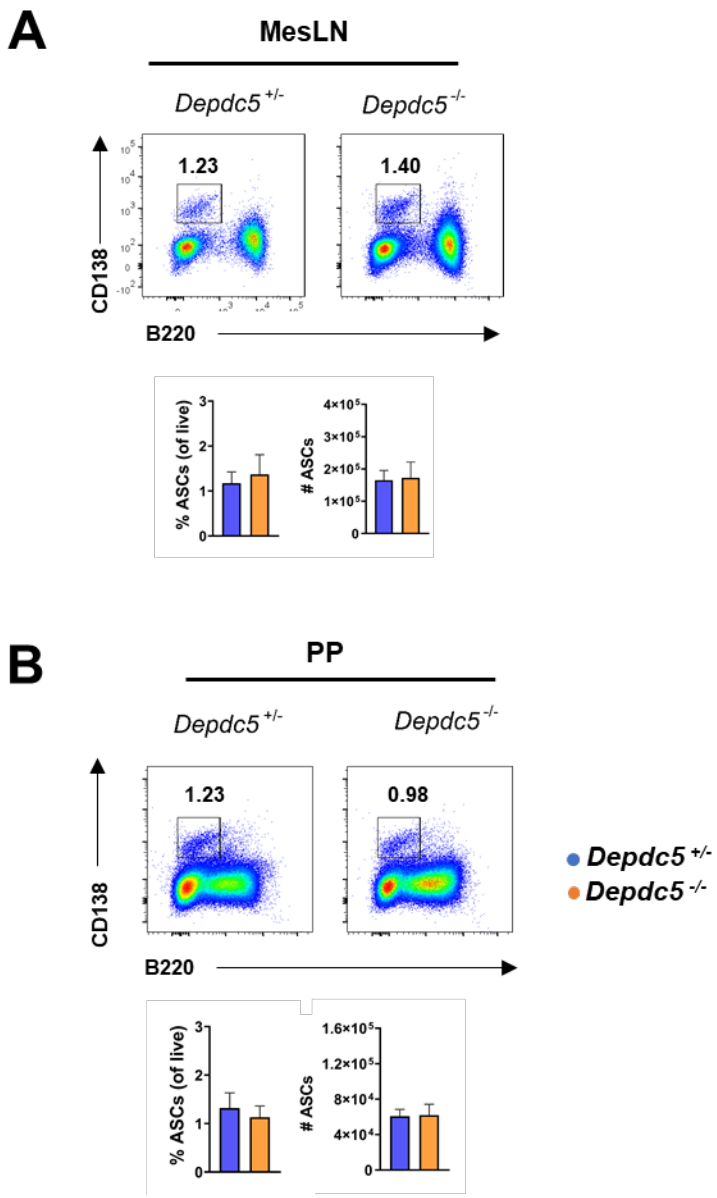

Figure 4.29: DEPDC5 loss did not affect ASCs in the mesLN and PP

PP and mesLN from 8-12 week old naive *Depdc5*$^{+/-}$ and *Depdc5*$^{-/-}$ mice. Representative flow cytometry is shown with quantification of ASCs (pre-gated on live cells) from the **(A)** mesLN and **(B)** PP from *Depdc5*$^{+/-}$ and *Depdc5*$^{-/-}$ mice. The columns represent the mean ± SEM. N= 8-12/group, pooled from two independent experiments. A Mann-Whitney U test was applied for statistical analysis.

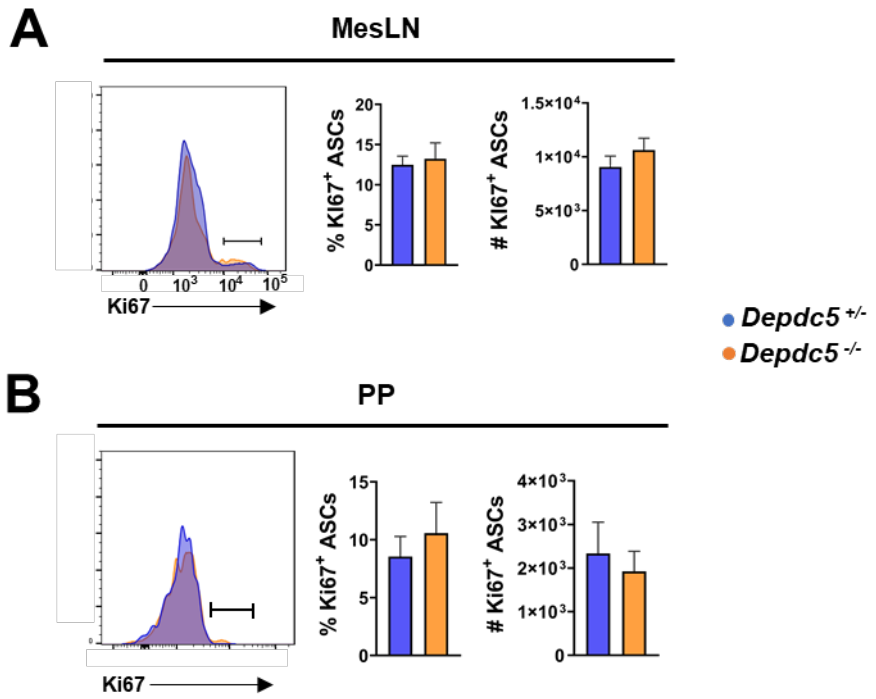

Figure 4.30: DEPDC5 loss did not affect ASC proliferation in the mesLN and PP

PP and mesLN from 8-12 week old naive *Depdc5*$^{+/-}$ and *Depdc5*$^{-/-}$ mice. Representative flow cytometry is shown with quantification of Ki67^{+} ASCs (pre-gated on ASCs) from the **(A)** mesLN and **(B)** PP from of *Depdc5*$^{+/-}$ and *Depdc5*$^{-/-}$ mice. N= 4-6/group, pooled from two independent experiments. The columns represent the mean ± SEM. A Mann-Whitney U test was applied for statistical analysis.

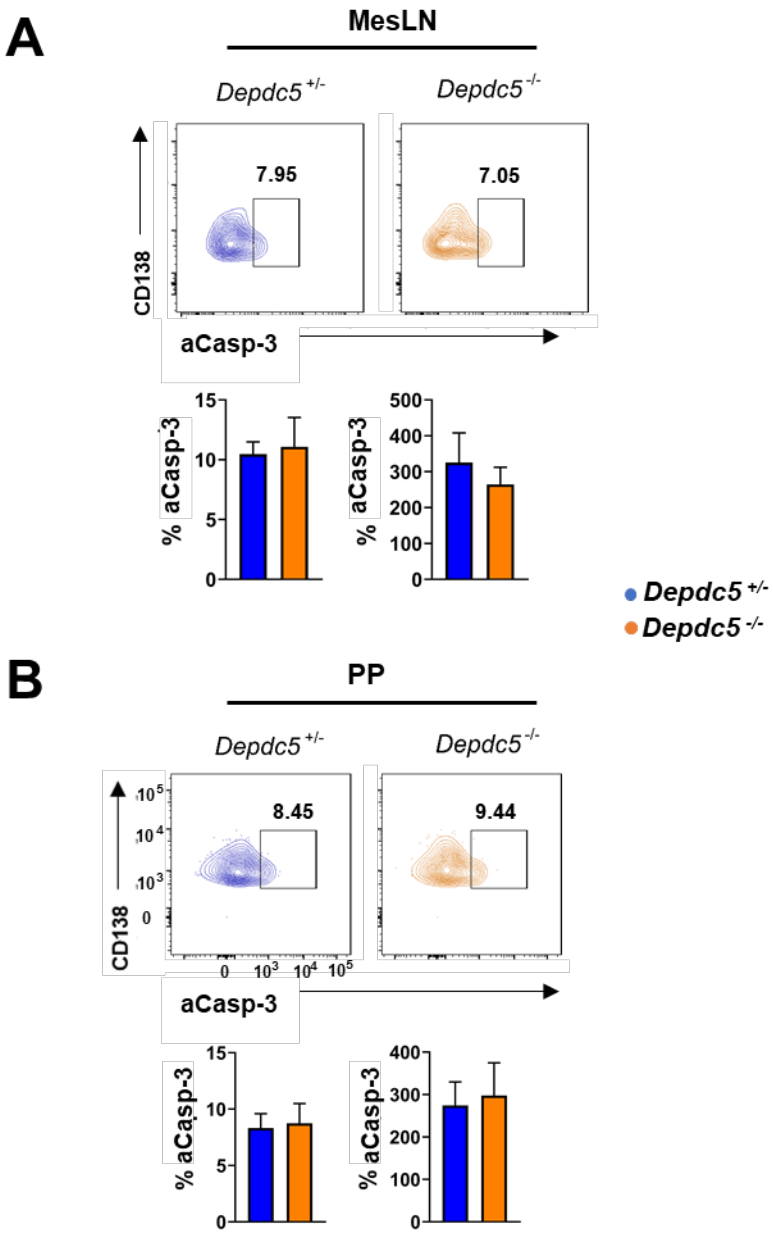

Figure 4.31: DEPDC5 l did not affect ASC apoptosis in the mesLN and PP

PP and mesLN from 8-12 week old naive *Depdc5*$^{+/-}$ and *Depdc5*$^{-/-}$ mice. Representative flow cytometry is shown with quantification of aCasp-3^{+} ASCs (pre-gated on ASCs) from the **(A)** mesLN and **(B)** PP from of *Depdc5*$^{+/-}$ and *Depdc5*$^{-/-}$ mice. The columns represent the mean ± SEM. N= 4/group, pooled from two independent experiments. A Mann-Whitney U test was applied for statistical analysis.

Chapter 5

CHAPTER 5
Discussion

Chapter 5

Chapter 5

Discussion

5.1 Introduction

The overarching aim of this project is to determine the role of DEPDC5 in B cells during homeostasis and following Ag-driven activation. Through understanding the role of DEPDC5 in B cells, this study may more broadly determine whether AA sensing in B cells plays a significant role in their biology. In a broader context, understanding the pathways which regulate B cells and Ab responses are central for informing the design of vaccines and therapeutics for autoimmunity. The AA-mTORC1 axis was first implicated in B cell biology when it was found that stimulation of the BCR *in-vitro* promoted leucine uptake and expression of leucine transporters in B cells (Cho et al. 2016). Furthermore, sufficient leucine levels are required by B cells for the activation of mTORC1 by the BCR *in-vitro* (Cho et al. 2016). A study by Ersching *et al*. that emerged during the course of this investigation reported that the AA-mTORC1 axis influenced GCB metabolism, polarisation and high affinity Ab production (Ersching et al. 2017). This indicates that the AA-mTORC1 signalling axis is indeed required for B cell activation and optimal humoral responses. However, unanswered questions remain about the impact of AA-mTORC1 signalling in the maintenance of naïve B cells and GCB populations, and in the regulation of GCB proliferation, apoptosis and Ab responses. Furthermore, a limitation in the study by Ersching *et al*. is the examination of GCs is limited to responses to model Ags rather than against more physiologically relevant and complex infectious Ags. Moreover, there is currently a lack of information concerning the role of specific components of the mTORC1 pathway, for example, DEPDC5 in B cell biology. Thus, the present study focusses on investigating the role of DEPDC5 in regulating AA-mTORC1 signalling during both B cell homeostasis and activation in the context of viral infection and in GALT-associated chronic stimulation of GCs.

5.2 Role of DEPDC5 in naive B cells

Naïve B cells are maintained in a metabolically quiescent state in order to restrain growth, ribosomal biogenesis, mTORC1 signalling and aerobic respiration (Farmer et al. 2019). The role of mTORC1 signalling in naïve B cells is shown to be important in murine and human studies (Benhamron and Tirosh 2011; Iwata et al. 2017; Suzuki et al. 2003; Ci et al. 2015; Farmer et al. 2019). Hyperactivation of mTORC1 in B cells led to a significant reduction in numbers of naïve FoB cells in those studies. This effect is attributed to a distinct block between the stages of transitional and FoB cell development (Benhamron and Tirosh 2011; Ci et al. 2015; Farmer et al. 2019). In a separate study, Suzuki *et al*. suggests that hyperactivation of mTORC1 in B cells may promote the migration of FoB cells out of the SLOs (Suzuki et al. 2003). However, those studies focused centrally on the role of glucose/insulin-mTORC1 signalling pathways in naïve B cells. While it is shown that mTORC1 pathways are important for maintaining B cell homeostasis, the specific signals that regulate the activity of mTORC1 in naïve B cells have not been fully investigated. Studies have, however, examined the role of AAs in T cells, and found that naive T cells require ATP energy from the TCA cycle and oxidative phosphorylation (OXPHOS) to promote homeostatic growth and survival (as reviewed by (Ren et al. 2017)). AAs are required for maintaining naive $CD8^+$ T cell growth and size, but were not required for their survival (Pearson, Silva, and Seddon 2012). Uptake of leucine is not required for normal T cell development (Sinclair et al. 2013). These previous studies have highlighted the need for a deeper understanding of the AA-mTORC1 axes in naïve B cell biology.

This current study shows for the first time that DEPDC5 regulates naïve B cell growth, metabolism and expression of activation markers, demonstrating that DEPDC5 activity, and therefore the AA-mTORC1 pathway, is likely required to maintain metabolic quiescence in naïve B cells. However, at homeostasis the numbers of FoB cells remains constant in the absence of *Depdc5* in B cells. This work contrasts observations made in glucose/insulin-mTORC1 signalling B cell studies and provides evidence that different nutrient-metabolic signalling axes have distinct roles in B cell homeostasis. It is postulated

that increased mTORC1 signalling in the absence of DEPDC5 in mature B cells stimulates the activation signals that normally initiate growth and expression of activation markers in B cells. The present study lays the foundation for further assessment of whether AA signalling and B cell activation signals intersect during metabolic signalling. The use of BCR activation reporting systems, such as the Nurr77 transgenic mouse (Mueller, Matloubian, and Zikherman 2015) could be useful in examining this in the context of changing AA availability or through the use of B cells which lack AA transporter expression, such as the system previously described in Tregs (Sinclair et al. 2013). Overall, the present research strongly indicates that there is a previously undetermined role for AA-mTORC1 signalling in naive B cells which is entirely distinct from the reported role of glucose/insulin-mTORC1 signalling in this compartment.

5.3 Role of DEPDC5 following Ag-driven B cell activation

As discussed previously, mTORC1 activity is implicated in GCB cell differentiation, maintenance, polarisation, cell cycling, growth and CSR (Wray-Dutra et al. 2018; Raybuck et al. 2018; Jones, Chernova, and Allman 2014; Li et al. 2017; Mendoza et al. 2018). As mentioned above, during the present study, Ersching *et al*. provided evidence that the AA-mTORC1 signalling axis plays a role in B cell activation and GC polarisation. However, important unanswered questions remain about the effects of AA-mTORC1 signalling in the maintenance, proliferation and survival of GCB cell populations. Furthermore, whether the interplay between AAs and mTORC1 following B cell activation are relevant in more physiologically relevant settings had not been previously been examined.

Ag from the upper respiratory tract drains to the medLN and is therefore the main site of immune priming following IN IAV infection. The IAV model chosen is an excellent model of acute infection, inflammation, and of early B cell activation (Coro, Chang, and Baumgarth 2006). Moreover, when injury is sustained in the lung following IAV infection, the formation of iBALT occurs and it functions as a tertiary lymphoid organ (Moyron-Quiroz et al. 2004) which is suggested to contribute to chronic immune activation and hence the damage to the lung in IAV (recently reviewed by (Lam and Baumgarth 2019)). The IAV model therefore

provides an opportunity to examine GCB cell response in both the draining LN and the site of infection. B cell responses associated with the iBALT are delayed relative to the initiation of immune responses in the draining LNs, as there is a lag time prior to iBALT formation within the lung (Moyron-Quiroz et al. 2004). The results of the present study determined that DEPDC5, and therefore likely the AA-mTORC1 signalling pathway, is required for optimal GCB responses within the draining LNs and the lung during IAV infection. In this model of IAV infection, loss of DEPDC5 in B cells led to a reduction in GCB cells in the medLN and an apparent increase in the accumulation of lung-associated GCBs during infection. Of relevance, in homeostatic settings, GC responses in GALT-associated tissues are maintained in a chronically-activated state by continual exposure to gut-derived Ag (Shroff, Meslin, and Cebra 1995). However, during homeostasis, DEPDC5 is shown to dispensable for maintenance of GCBs in the mesLN and PP. Taken together, these data indicate that DEPDC5 differentially regulates GCB biology across different models and tissues. Indeed, DEPDC5 is shown to differentially affect the proliferation and apoptosis of GCBs in these various contexts. Within the medLN, loss of DEPDC5 in mature B cells increased both proliferation and apoptosis in GCB cells. However, within the lung GCB cell proliferation is increased following DEPDC5 loss, while apoptosis is unaffected. High levels of Ki67 expression are associated with cells undergoing rapid cycling, indicating that elevated Ki67 expression in GCB cells following the loss of DEPDC5 promoted proliferation (Miller et al. 2018). Variation in Ki67 expression is likely due to the varying rates of Ki67 degradation and synthesis across the GCB population, due to the unique experiences of each individual whether it be the timing of or signalling strength of activation, thus leading to a spectrum of Ki67 expression. These observations could be explained by dynamic changes in AA availability across different sites during infection or by metabolic adaptation of B cells to different niches. In addition, differences in B cell activation within the medLN could drive enhanced egress of DEPDC5-deficient B cells from this site and promote their entry into peripheral tissues, such as the lung, thereby increasing their number. This could be tested by intravenous labelling of circulating B cells over the course of infection to determine if there is an increase in DEPDC5-deficient B cell egress from the mLN as described in (Allie et al. 2019).

Prior to the present study, the role of AA-mTORC1 signalling in GCB cell biology had not previously been examined in the context of either IAV infection or chronic stimulation within the GALT. Indeed, the precise role that mTORC1-mediated metabolic signalling plays in GALT-associated GCBs is unclear due to contrasting results reported in the field (Ci et al. 2015; Benhamron and Tirosh 2011). Ci *et al*. reports that hyperactivation of mTORC1 in the absence of TSC1 had no effect on GCB cells in the PP (Ci et al. 2015). In contrast, Benhamron *et al*. reported that this TSC1 deletion significantly reduced GCB cells in the PPs (Benhamron and Tirosh 2011). Despite both studies examining the glucose/insulin-mTORC1 pathway using the same methodology, variability in GCB responses were still observed. It is possible that these different results could arise from variability in the co-housing of experimental groups, diet or animal house microbiota. Co-housing has previously been shown to impact mouse physiology significantly (Caruso et al. 2019). These previous findings highlight the need for caution in interpreting GALT-associated GCB studies, and indicate that well-controlled multi-institute studies may be required to robustly examine the role of this pathway in regulation of immune cell populations.

Another possibility is that AA availability differs across various tissues and changes over the course of IAV infection. If AA availability is restricted, enhanced GCB cell proliferation caused by DEPDC5 loss may be detrimental to the cell and result in enhanced apoptosis, thus reducing the GCB cell population. This would fit with the data in the present study in the medLN. Alternatively, if sufficient AAs are present in the microenvironment during intense proliferation, loss of DEPDC5 would be of no consequence if its role is to sense AA starvation. This may explain the finding in this study that deletion of DEPDC5 did not alter GCB cells in the GALT, as it could be expected that higher nutrient levels would be available here as it is the site of nutrient absorption. However, more work will be required to quantify bioavailable AAs in local tissue microenvironments to resolve these issues. Despite extensive research there are no data available which comparatively quantify AAs and metabolites across different tissue sites, during both homeostasis and infection. Despite this, some conclusions can be tentatively drawn from previous studies. Silver *et al*. indicates that

relative to other metabolites within the lung, the availability of AAs is limited (Silver et al. 2019). A separate study finds the concentration of free AAs within the lung is only 10 – 17% of the total concentration of AAs detected in plasma of mice (Subashchandrabose et al. 2009). In the context of H1N1 IAV infection, high-resolution metabolomics (HRM) is used to identify metabolic pathways associated with murine lungs. Pyrimidine and purine nucleotide metabolism, lipid metabolism, and AA metabolism were all significantly elevated within the lung during IAV infection (Chandler et al. 2016). Cross-examination of metabolomics across mouse sera, lung tissue and BALF at different time-points following IAV infection revealed spatiotemporal differences in metabolic pathways, for example those involved in AA metabolism (Cui et al. 2016). Many of these metabolites were also found to be associated with viral-induced changes in pulmonary surfactant during the host response to infection (Cui et al. 2016). Taken together, these studies show that AA availability has spatiotemporal variability wherein AAs are typically in limited availability in peripheral tissues. Similarly, there is spatiotemporal variability in the cellular metabolic pathways that are active, and these are influenced by the stress of infection. Therefore, the observation that DEPDC5 deletion impacted GCB cell levels differently within different tissues could be explained by variation in the microenvironment or nutrient availability between specific niches. However, this postulation does not explain the increase in DEPDC5-deficient GCB cells within the lung in response to infection. It could be that DEPDC5 is redundant for GCB cells in the lung, as in the GALT, and that the increase in DEPDC5-deficient GCB cells observed in the lung could be directly associated with changes in the medLN. Key chemokine receptors important for migration and entry to the lung parenchyma during infection could be identified by intravascular staining of B cells and sorting the vascular negative B cells from the lungs of *Depdc5*$^{+/-}$ or *Depdc5*$^{-/-}$ mice. A comparison of chemokine receptor and adhesion molecules will identify candidate targets which can be knocked out in these B cells and provide insight into how DEPDC5 deficient B cells may be migrating more into the lung. A significant loss in the number of GCB cells in the medLN does coincide with elevated numbers of GCB cells in the lung following DEPDC5 loss in mature B cells. Of potential relevance, it has previously been shown that high levels of AAs stimulate mTORC1-mediated cell migration (Rhoads et al. 2006). Therefore, examining migration of B cells during infection following DEPDC5 loss would be informative. It is proposed that an inter-organ analysis of metabolites

and AAs should be performed during both homeostasis and infection, in addition to the metabolic control of migration from different sites. This can be examined in the context of acute infection including IAV, and chronic responses such as in the GALT or in a chronic infectious settings like LCMV. Such experiments could be the subject of a future study.

Context-specific effects of AA-mTORC1 signalling in GCBs could also reflect distinct transcriptional and functional profiles of GCB cells between different sites. In response to viral challenge, tissue-specific defects in B cell migration, function and differentiation have been observed across LNs, SP and mesLNs (Peruchon et al. 2009). Further, development of GCs occurred at different rates across the mesLN and SP in response to viral infection (Peruchon et al. 2009). Additionally, these tissue-specific changes are not restricted to B cells. For example, Tregs have been shown to adapt to lymphoid and barrier tissues, wherein subpopulations of Treg cells at each site present conserved and distinct expression programs in humans and mice (e.g. metabolic programming, proliferation and cytokine production) (Miragaia et al. 2019). DCs have also been shown to possess distinct transcriptional, phenotypic and functional profiles between the PPs and SP (Iwasaki and Kelsall 1999). Collectively, these data indicate that immune cells have the capacity to adapt to their tissue environment to express tissue-specific transcriptional programs and functions. It would be interesting to examine whether B cells associated with the GALT have metabolically adapted to withstand fluctuations in AA levels, due to the importance of B cell responses in maintaining gut homeostasis. Mechanisms have been identified that control intestinal inflammation in response to acute AA starvation using an mTORC1-independent mechanism in $CD11c^+$ APCs and intestinal epithelial cells (Ravindran et al. 2016). Mechanisms have been identified that control intestinal inflammation in response to acute AA starvation using an mTORC1-independent mechanism in $CD11c^+$ APCs and intestinal epithelial cells (Ravindran et al. 2016). These cells use the general control nonderepressible 2 (GCN2) kinase to halt protein synthesis when AA levels are low. Ravindran and colleagues demonstrated that during intestinal inflammation, loss of GCN2 in CD11c+ APCs ked to enhanced ROS and inflammasome within these cells and allowed them to promote elevated Th17 responses. When dietary AA were limited, GCN2 KO mice were also protected from disease and Th17-mediated inflammation. Thus, AA sensor, GCN2 was shown to significantly regulate intestinal inflammation. In B cells, this alternative pathway has not

been examined and it would be interesting to understand the interplay between both DEPDC5 and GCN2 aa-sensing pathways on cellular function. Further, what this study by Ravindran and colleagues highlights is inflammation or dysbiosis in the intestine could exacerbate the metabolic effects of AA-regulation in B cell biology. For example, aberrantly activated B cells accumulate in the mLN in Crohn's disease and recirculate systemically (Timmermans et al. 2016; Olson et al. 2004). It is therefore hypothesized that the effects of DEPDC5 may be more apparent in B cells within this setting and could be the focus of future work. Further mTORC1-dependent and mTORC1-independent AA sensing mechanisms could work cooperatively.

To confirm this, transcriptional analysis of GCB cells from lymphoid and non-lymphoid tissues could be used to identify tissue-specific heterogeneity amongst GCB cells. These data could collate with the previously proposed experiments to characterize tissue-specific nutrient availability and metabolic pathways, in order to comprehensively characterise whether GCB cells metabolically adapt to the nutritional environment of their tissue niche. Thus, the future experiments proposed to understand if B cells metabolically adapt to tissue specific niches would involve first the assessment of metabolic microenvironments by microscopy to assess regions of hypoxia, reactive oxygen species and amino acids availability. Once metabolic microenvironments have been identified, B cells (or any cell of interest) can be isolated from the metabolic niche and outside of the metabolic niche by laser capture for transcriptional analysis. A transcriptional comparison of B cells within and outside the metabolic niche will identify whether B cells alter their function according to nutrient availability or presence of metabolites. These data can then inform testable and non-biased hypothesises that can be studied further using knock out models of metabolic pathways or functional pathways that are altered in B cells occupying metabolic niches. Further, these experiments can be conducted in a variety of tissues in different infectious settings to understand if metabolic niches vary across tissue sites in terms of nutrients, hypoxia, reactive oxygen species availability and the frequency or size of these niches. This will help with our understanding of the metabolic landscape and relationship to B cell activity across different sites, and whether particular tissues are more susceptible to nutrient loss during infection compared to other tissues.

In the current study, polarisation of the GC response is unaffected by DEPDC5 loss during either IAV induced- or GALT-associated GC responses. This is in direct contrast to the findings in a study by Ersching *et al*. which showed that NP-induced GCs favoured a DZ:LZ ratio following disruption of the AA-mTORC1 signalling axis. This discrepancy may be attributable to the different models of Ag-driven B cell activation used in these studies and differences in the methods used to disrupt AA sensing in B cells between the two studies. Therefore, the data in the present study suggests that the effect of AA-mTORC1 signalling on GC polarisation may not be relevant in a setting where complex Ags, such as viral infection and microbial/food Ag in the gut, initiate GC responses. Thus, the data generated in the present study question whether AA-mTORC1 signalling plays a significant and physiologically relevant role in GC polarisation.

In summary, the present study has identified that DEPDC5 has distinct roles in GCB cell regulation and raises interesting questions for tissue-specific regulation of the B cell response through the AA-mTORC1 axis. Furthermore, it is the first study to examine the relevance of AA-mTORC1 regulation in GCBs within physiologically relevant settings through disruption of this axis due to loss of DEPDC5.

5.4 Regulation of the Ab response by DEPDC5

The generation of high-affinity Abs is important for clearance of pathogens and relies on optimal proliferation of GCB cells in order to undergo BCR SHM and affinity maturation (Chen, Zhai, et al. 2018; Gitlin, Shulman, and Nussenzweig 2014). T cell-dependent signals modulate the degree of clonal expansion and cell division, which directly impacts hypermutation and selection of high affinity clones (Gitlin et al. 2015; Gitlin, Shulman, and Nussenzweig 2014). Ersching *et al*. recently showed that AA-mTORC1 signalling is essential for the generation of high affinity Ab responses (Ersching et al. 2017). However, important questions remain as to the effect of the AA-metabolic signalling on

the generation of ASCs and production of Abs in a physiologically relevant context. Understanding the regulation of Ab responses during humoral immunity is essential for development of therapies and vaccines. Therefore, the role of AA-mTORC1 signalling in ASC generation and Ab production is examined during this current study in the context of IAV infection in the B cell-specific *DEPDC5* knockout mouse.

The present study showed significant defects in the ability of B cells to mount a high-affinity Ab response to haptenated protein Ag when mTORC1 activity is uncoupled from AA sensing via deletion of DEPDC5. This strongly supports the role of AA-mTORC1 in the generation of high affinity Ab responses and fits with previously published data (Ersching et al. 2017). Moreover, these results are also consistent for the broader role of mTORC1 hyperactivation in defective affinity maturation (Ersching et al. 2017; Keating et al. 2013; Chou et al. 2016).

Early research has shown that mTORC1 inhibition delayed the onset of CSR and elevated IgM production (Omori et al. 2006). More recent work has found inhibition of mTORC1 activity reduced CSR and ASC formation (Limon et al. 2014). Additionally, the impact of hyperactive mTORC1 activity is shown to affect Ig CSR and has led to variable outcomes in Ig switching (Wray-Dutra et al. 2018; Ci et al. 2015). When taken together, these findings indicate a role for mTORC1 signalling in Ig CSR. In the present study, in the context of IAV infection, DEPDC5 did not affect CSR in ASCs generated early during the IAV response within the medLN. This indicates that the AA-mTORC1 pathway plays a redundant role in this process. However, the requirement for AAs in CSR could be further examined through the loss of AA-transporters in B cells as this would potentially expose more subtle aspects of this system.

Previous studies have reported that acute inhibition of mTORC1 or complete loss of mTORC1 ablated newly formed ASCs and GCs (Jones et al. 2016), and hyperactivation of mTORC1 in B cells promoted ASC differentiation (Wray-Dutra et al. 2018; Benhamron et al. 2015). The present study puts forward a previously unknown role for AA-mTORC1 signalling in the formation of early ASC responses and IgM production in

the context of IAV infection. A significant reduction in the number and frequency of ASCs is observed in DEPDC5 deficient mice at D7 post-IAV infection within the medLN. Reduced levels of circulating anti-viral IgM at the peak of the humoral response to viral infection were also apparent. However, unexpectedly, there is no impact of DEPDC5 deletion on circulating anti-viral IgG. The impact of DEPDC5 loss on early anti-viral IgM responses may have potentially been masked by alternative sources of Ag-induced IgM production, for example from the B1-a compartment (Baumgarth 2016). As circulating anti-viral IgM levels increased during infection, the impact of DEPDC5 deletion may have become more prominent. The significant reduction in the number of IgG^+ ASCs in mice with DEPDC5-deficient B cells is not consistent with the finding that anti-viral IgG levels were unchanged in serum. It is possible, that because GCB responses in the lung were accelerated despite deficiencies in the medLN in mice with DEPDC5-deficient B cells, that ASCs were also increased in the lung and that this compensated for the reduction in medLN ASCs. However, despite multiple attempts, ASCs were unable to be assessed in the lung due to technical issues as degradation of the CD138 epitope following tissue digestion is apparent. Future experiments using the Blimp-1-GFP reporter (Kallies et al. 2004; Tellier et al. 2016) should allow tracking ASCs at greater resolution. Further, assessing the impact of DEPDC5 specifically on virus-specific ASCs could determine the degree to which Ag-specific ASC populations were affected, as only Ag-specific serum Ab levels were evaluated. Additionally, the D7 time-point may only capture the effect of DEPDC5 on GC-independent ASCs, whereas it is possible GC-dependent ASC production later during the infectious response may be intact and contribute to IgG secretion. Given IgM responses are largely initiated independent of the GC, this may explain the discrepancies in Ab responses affected.

It is important to understand how AA-mTORC1 signalling may contribute to the loss of ASCs. The present research found that proliferation or apoptosis within the ASC compartment is unaffected by DEPDC5 loss in B cells. It is therefore likely that DEPDC5 (and therefore perhaps AA-mTORC1) signalling affects ASC differentiation. BCR activation with CD40 ligation leads to translocation of canonical NF-κB subunits RelA

and c-Rel in activated B cells. RelA is involved in PC differentiation while c-Rel is required for GC maintenance (Heise et al. 2014). Therefore, if the AA-mTORC1 regulatory pathway modulates CD40/BCR signalling, it may inherently also affect ASC differentiation via NF- κB. To examine this, the effect of AA-mTORC1 signalling on APC-specific TFs and programs could be examined following B cell activation. Further, the effect of AA-mTORC1 signalling on ASCs derived from both GC-independent or GC-dependent pathways could be determined.

Together, this current study of DEPDC5 in B cells corroborates the report that AA-mTORC1 signalling plays a significant role in the generation of high affinity responses (Ersching et al. 2017). Furthermore, this present study highlights a previously unknown role for the DEPDC5 and perhaps the AA-mTORC1 signalling pathway in the development of ASCs, but not for CSR. These findings lay the foundation for future experiments to discover the mechanistic basis of these observations greater detail to provide further insight into the role of nutrient sensing and metabolic adaptations in B cell biology.

5.5 Clinical implications

The findings of this study may have applications in a clinical setting. As discussed previously, a complex relationship exists between nutrition, infection and immunity. Protein malnutrition is a significant risk factor for diseases, such as IAV and secondary immune deficiencies (Taylor et al. 2013; Ritz et al. 2008) and supplementation of diets with protein is shown to restore optimal immunity in response to IAV. Furthermore, poor induction of vaccine-induced Ab responses to IAV vaccination is associated with malnutrition in the elderly (Bellei et al. 2006). However, few studies have examined the mechanistic basis for the contribution of nutrients to the B cell response. The present study has shown that DEPDC5-mediated regulation of AA-mTORC1 nutritional axes is required for optimal B cell responses during viral infection. If specific nutritional-metabolic axes can be identified as important for anti-viral responses, targeted AA treatments could potentially be designed and administered alongside vaccination or given

to at-risk individuals during infection to promote viral clearance and reduce mortality. More broadly, nutrient deficiencies are a global health issue, hence understanding how immunometabolism contributes to compromised immune responses and vaccine-induced responses could improve the development of metabolic-reprogramming interventions, and open avenues for novel treatment strategies.

5.6 Conclusion

This project has presented new insights into the role of DEPDC5, a nutritional checkpoint regulator of AA-mTORC1 signalling in humoral immunity. A novel conditional *Depdc5* B cell-specific knock-out mouse generated during this project established a role for DEPDC5 as a negative regulator of mTORC1 in B cells. At homeostasis, formation of the mature B cell compartment is not discernibly affected by disruption of the DEPDC5. However, quiescence in naive FoB cells is perturbed by the loss of DEPDC5 as evidenced by increased biomass, hyperphosphorylation of S6 ribosomal protein and elevated expression of B cell activation markers. Examination of DEPDC5 in a clinically relevant model of B cell activation (IAV) revealed that GCB cell responses in the draining medLN were significantly attenuated when DEPDC5 is lost in mature B cells. This disruption is associated with the defective generation of ASCs within the medLN and altered anti-viral IgM Ab responses. This reveals a potential role for DEPDC5 in B cells in mounting an optimal anti-viral humoral response. It is important to note that the findings above are specific to GCBs in the medLNs, as a significant acceleration in GCB cell responses is observed in the lung. Examination of *Depdc5* deletion in B cells revealed limited impact on GCB biology in the GALT. This indicates a tissue- or context-specific role for DEPDC5 regulation in B cell biology. Overall, this project establishes potential new roles for DEPDC5, and by extension likely the AA-mTORC1 pathway, in the regulation in humoral immunity.

The study supports the following model by which DEPDC5 may regulate B cell responses (**Figure 5.1**):

The absence of DEPDC5 renders B cells unable to detect reduced nutrient availability in specific microenvironments, leading to constitutive mTORC1 hyperactivity in B cells. This metabolic change disrupts the enforced quiescent state in naive B cells at rest in homeostatic settings. This likely also contributes to increased basal levels of B cell activation, which relies on the intersection of Ag-driven BCR/CD19 signalling with the mTORC1 pathway. This suggested DEPDC5 contributes to maintenance of a quiescent state in B cells. Perturbing B cell homeostasis, as modelled here using acute IAV infection, typically stimulates Ag-driven B cell activation and GCB cell formation. Crucially, this relies on sufficient nutrients to fuel the increased metabolic signalling and cell differentiation processes. DEPDC5 is an AA-sensitive regulator of metabolism, and acts to suppress metabolic activity when AAs are limited. This effectively prevents metabolic collapse and death of B cells in nutrient depleted conditions. In the absence of DEPDC5, GCB cell proliferation is significantly enhanced in medLN, which is an effect associated with constitutive mTORC1 activity. Functional DEPDC5 is also found to limit apoptosis in GCB cells during acute viral infection in draining SLOs. As stated above, absence of DEPDC5 renders B cells insensitive to nutrient availability changes, thus they are unable to halt metabolism when AAs become depleted during the metabolically demanding response to viral infection. As a result, they are forced down an apoptosis pathway as there are insufficient nutrients to support continued proliferative programs. Conversely, functional DEPDC5 limits this GCB cell apoptosis. Interestingly, the same phenomenon is not observed in TLOs within the lung during the same viral infection scenario. Potentially, nutrients may be more readily available and/or depleted at a slower rate between different tissues, thus altering the requirement for DEDPC5 mediated regulation for B cells and leading to tissue-specific outcomes. In further support of this, DEPDC5 function is found to be completely dispensable in the context of GALT-associated B cell responses. If B cells associated with the GALT are metabolically adapted to withstand constant AA fluctuations (due to irregularly timed food intake and variable nutritional content), DEPDC5 function would be rendered redundant. This project also demonstrated that DEPDC5 is required for normal Ab generation within the medLN during viral infection and contributes to the understanding that AA-mTORC1 axes are needed to generate high affinity Ab to haptenated Ag. While further work is required to elucidate the effect of DEPDC5 on the Ab response in various niches (due

to the tissue-specific effects outlined above), this proposed model of DEPDC5 function represents an interesting and novel mode of nutritional metabolic regulation in B cell responses. Further exploration of this facet of B cell regulation may aid the development of effective anti-viral therapies and novel interventions to improve human health and immunity in the future.

Figure 5.1: Proposed model of DEPDC5 regulation of B cell responses

DEPDC5 modulates mTORC1 activity in B cells, which exerts tissue-specific specific effects of GCB cells and ASCs during homeostasis and infection. Nutrient availability within specific tissues may impact whether hyperproliferation and metabolic activity induced by DEPDC5 loss is appropriately fuelled. Metabolic adaptation of B cells to SLOs at the interface of nutrient absorption may adopt multiple robust programs for nutritional control of

mTORC1, consequently making DEPDC5 redundant. Moreover, DEPDC5 is required for generation of high affinity Abs through modulation of mTORC1 activity.

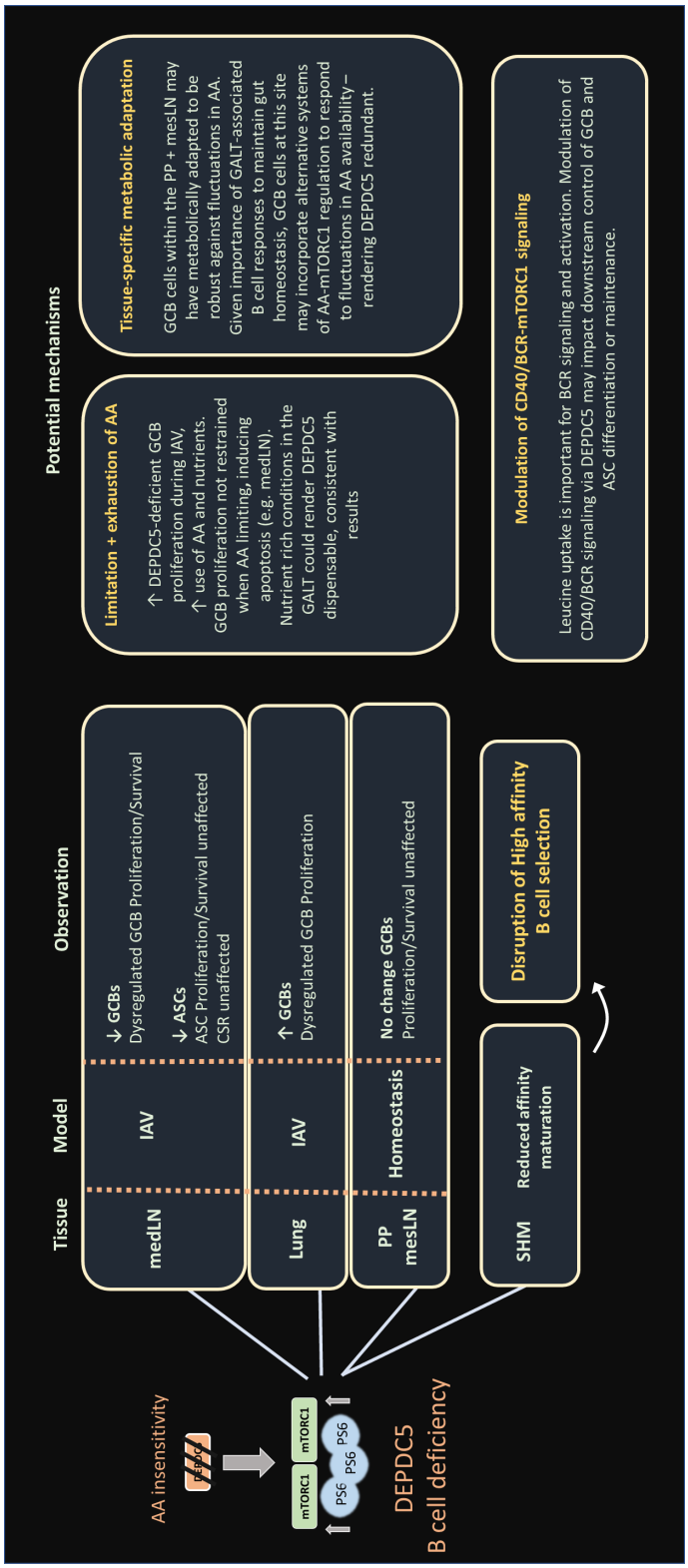
AA insensitivity
DEPDC5
B cell deficiency
mTORC1
mTORC1
PS6
PS6
PS6
Tissue
Model
Observation
medLN
IAV
↓ GCBs
Dysregulated GCB Proliferation/Survival
↓ ASCs
ASC Proliferation/Survival unaffected
CSR unaffected
Lung
IAV
↑ GCBs
Dysregulated GCB Proliferation
PP mesLN
Homeostasis
No change GCBs
Proliferation/Survival unaffected
SHM
Reduced affinity maturation
Disruption of High affinity B cell selection
Potential mechanisms
Limitation + exhaustion of AA
↑ DEPDC5-deficient GCB proliferation during IAV, ↑ use of AA and nutrients. GCB proliferation not restrained when AA limiting, inducing apoptosis (e.g. medLN). Nutrient rich conditions in the GALT could render DEPDC5 dispensable, consistent with results
Tissue-specific metabolic adaptation
GCB cells within the PP + mesLN may have metabolically adapted to be robust against fluctuations in AA. Given importance of GALT-associated B cell responses to maintain gut homeostasis, GCB cells at this site may incorporate alternative systems of AA-mTORC1 regulation to respond to fluctuations in AA availability – rendering DEPDC5 redundant.
Modulation of CD40/BCR-mTORC1 signaling
Leucine uptake is important for BCR signaling and activation. Modulation of CD40/BCR signaling via DEPDC5 may impact downstream control of GCB and ASC differentiation or maintenance.

CHAPTER 6

References

Chapter 6

References

Abbott, R. K., M. Thayer, J. Labuda, M. Silva, P. Philbrook, D. W. Cain, H. Kojima, S. Hatfield, S. Sethumadhavan, A. Ohta, E. L. Reinherz, G. Kelsoe, and M. Sitkovsky. 2016. 'Germinal Center Hypoxia Potentiates Immunoglobulin Class Switch Recombination', *J Immunol*, 197: 4014-20.

Adler, L. N., W. Jiang, K. Bhamidipati, M. Millican, C. Macaubas, S. C. Hung, and E. D. Mellins. 2017. 'The Other Function: Class II-Restricted Antigen Presentation by B Cells', *Front Immunol*, 8: 319.

Adolfsson, J., O. J. Borge, D. Bryder, K. Theilgaard-Monch, I. Astrand-Grundstrom, E. Sitnicka, Y. Sasaki, and S. E. Jacobsen. 2001. 'Upregulation of Flt3 expression within the bone marrow Lin(-)Sca1(+)c-kit(+) stem cell compartment is accompanied by loss of self-renewal capacity', *Immunity*, 15: 659-69.

Akkaya, M., J. Traba, A. S. Roesler, P. Miozzo, B. Akkaya, B. P. Theall, H. Sohn, M. Pena, M. Smelkinson, J. Kabat, E. Dahlstrom, D. W. Dorward, J. Skinner, M. N. Sack, and S. K. Pierce. 2018. 'Second signals rescue B cells from activation-induced mitochondrial dysfunction and death', *Nat Immunol*, 19: 871-84.

Allen, C. D., K. M. Ansel, C. Low, R. Lesley, H. Tamamura, N. Fujii, and J. G. Cyster. 2004. 'Germinal center dark and light zone organization is mediated by CXCR4 and CXCR5', *Nat Immunol*, 5: 943-52.

Allen, C. D., T. Okada, H. L. Tang, and J. G. Cyster. 2007. 'Imaging of germinal center selection events during affinity maturation', *Science*, 315: 528-31.

Allie, S. R., J. E. Bradley, U. Mudunuru, M. D. Schultz, B. A. Graf, F. E. Lund, and T. D. Randall. 2019. 'The establishment of resident memory B cells in the lung requires local antigen encounter', *Nat Immunol*, 20: 97-108.

Allman, D., R. C. Lindsley, W. DeMuth, K. Rudd, S. A. Shinton, and R. R. Hardy. 2001. 'Resolution of three nonproliferative immature splenic B cell subsets reveals multiple selection points during peripheral B cell maturation', *J Immunol*, 167: 6834-40.

Anderson, M. P. 2018. 'DEPDC5 takes a second hit in familial focal epilepsy', *J Clin Invest*, 128: 2194-96.

Bachmann, M. F., and R. M. Zinkernagel. 1997. 'Neutralizing antiviral B cell responses', *Annu Rev Immunol*, 15: 235-70.

Bannard, O., R. M. Horton, C. D. Allen, J. An, T. Nagasawa, and J. G. Cyster. 2013. 'Germinal center centroblasts transition to a centrocyte phenotype according to a timed program and depend on the dark zone for effective selection', *Immunity*, 39: 912-24.

Bar-Peled, L., L. Chantranupong, A. D. Cherniack, W. W. Chen, K. A. Ottina, B. C. Grabiner, E. D. Spear, S. L. Carter, M. Meyerson, and D. M. Sabatini. 2013. 'A Tumor suppressor complex with GAP activity for the Rag GTPases that signal amino acid sufficiency to mTORC1', *Science*, 340: 1100-6.

Baracho, G. V., M. H. Cato, Z. Zhu, O. R. Jaren, E. Hobeika, M. Reth, and R. C. Rickert. 2014. 'PDK1 regulates B cell differentiation and homeostasis', *Proc Natl Acad Sci U S A*, 111: 9573-8.

Baumgarth, N. 2016. 'B-1 Cell Heterogeneity and the Regulation of Natural and Antigen-Induced IgM Production', *Front Immunol*, 7: 324.

Beirowski, B., K. M. Wong, E. Babetto, and J. Milbrandt. 2017. 'mTORC1 promotes proliferation of immature Schwann cells and myelin growth of differentiated Schwann cells', *Proc Natl Acad Sci U S A*, 114: E4261-E70.

Bellei, N. C., E. Carraro, A. Castelo, and C. F. Granato. 2006. 'Risk factors for poor immune response to influenza vaccination in elderly people', *Braz J Infect Dis*, 10: 269-73.

Benhamron, S., S. P. Pattanayak, M. Berger, and B. Tirosh. 2015. 'mTOR activation promotes plasma cell differentiation and bypasses XBP-1 for immunoglobulin secretion', *Mol Cell Biol*, 35: 153-66.

Benhamron, S., and B. Tirosh. 2011. 'Direct activation of mTOR in B lymphocytes confers impairment in B-cell maturation andloss of marginal zone B cells', *Eur J Immunol*, 41: 2390-6.

Bergqvist, P., A. Stensson, L. Hazanov, A. Holmberg, J. Mattsson, R. Mehr, M. Bemark, and N. Y. Lycke. 2013. 'Re-utilization of germinal centers in multiple Peyer's patches results in highly synchronized, oligoclonal, and affinity-matured gut IgA responses', *Mucosal Immunol*, 6: 122-35.

Bi, Y., G. Liu, and R. Yang. 2011. 'mTOR regulates T-cell differentiation and activation in immunity and autoimmunity', *Crit Rev Eukaryot Gene Expr*, 21: 313-22.

Bioley, G., J. Monnerat, M. Lotscher, C. Vonarburg, A. Zuercher, and B. Corthesy. 2017. 'Plasma-Derived Polyreactive Secretory-Like IgA and IgM Opsonizing Salmonella enterica Typhimurium Reduces Invasion and Gut Tissue Inflammation through Agglutination', *Front Immunol*, 8: 1043.

Boothby, M. R., E. Hodges, and J. W. Thomas. 2019. 'Molecular regulation of peripheral B cells and their progeny in immunity', *Genes Dev*, 33: 26-48.

Boyden, A. W., K. L. Legge, and T. J. Waldschmidt. 2012. 'Pulmonary infection with influenza A virus induces site-specific germinal center and T follicular helper cell responses', *PLoS One*, 7: e40733.

Breitfeld, D., L. Ohl, E. Kremmer, J. Ellwart, F. Sallusto, M. Lipp, and R. Forster. 2000. 'Follicular B helper T cells express CXC chemokine receptor 5, localize to B cell follicles, and support immunoglobulin production', *J Exp Med*, 192: 1545-52.

Brink, R., D. Paus, K. Bourne, J. R. Hermes, S. Gardam, T. G. Phan, and T. D. Chan. 2015. 'The SW(HEL) system for high-resolution analysis of in vivo antigen-specific T-dependent B cell responses', *Methods Mol Biol*, 1291: 103-23.

Buck, M. D., R. T. Sowell, S. M. Kaech, and E. L. Pearce. 2017. 'Metabolic Instruction of Immunity', *Cell*, 169: 570-86.

Carlomagno, M. A., A. E. Alito, D. I. Almiron, and A. Gimeno. 1982. 'T and B lymphocyte function in response to a protein-free diet', *Infect Immun*, 38: 195-200.

Caro-Maldonado, A., R. N. Wang, A. G. Nichols, M. Kuraoka, S. Milasta, L. D. Sun, A. L. Gavin, E. D. Abel, G. Kelsoe, D. R. Green, and J. C. Rathmell. 2014a. 'Metabolic Reprogramming Is Required for Antibody Production That Is Suppressed in Anergic but Exaggerated in Chronically BAFF-Exposed B Cells', *Journal of Immunology*, 192: 3626-36.

Caro-Maldonado, A., R. Wang, A. G. Nichols, M. Kuraoka, S. Milasta, L. D. Sun, A. L. Gavin, E. D. Abel, G. Kelsoe, D. R. Green, and J. C. Rathmell. 2014b. 'Metabolic reprogramming is required for antibody production that is suppressed in anergic but exaggerated in chronically BAFF-exposed B cells', *J Immunol*, 192: 3626-36.

Carroll, B., G. Nelson, Y. Rabanal-Ruiz, O. Kucheryavenko, N. A. Dunhill-Turner, C. C. Chesterman, Q. Zahari, T. Zhang, S. E. Conduit, C. A. Mitchell, O. D. K. Maddocks, P. Lovat, T. von Zglinicki, and V. I. Korolchuk. 2017. 'Persistent mTORC1 signaling in cell senescence results from defects in amino acid and growth factor sensing', *J Cell Biol*, 216: 1949-57.

Caruso, R., M. Ono, M. E. Bunker, G. Nunez, and N. Inohara. 2019. 'Dynamic and Asymmetric Changes of the Microbial Communities after Cohousing in Laboratory Mice', *Cell Rep*, 27: 3401-12 e3.

Casola, S., and K. Rajewsky. 2006. 'B Cell Recruitment and Selection in Mouse GALT Germinal Centers.' in Tasuku Honjo and Fritz Melchers (eds.), *Gut-Associated Lymphoid Tissues* (Springer Berlin Heidelberg: Berlin, Heidelberg).

Chandler, J. D., X. Hu, E. J. Ko, S. Park, Y. T. Lee, M. Orr, J. Fernandes, K. Uppal, S. M. Kang, D. P. Jones, and Y. M. Go. 2016. 'Metabolic pathways of lung inflammation revealed by high-resolution metabolomics (HRM) of H1N1 influenza virus infection in mice', *Am J Physiol Regul Integr Comp Physiol*, 311: R906-R16.

Chantranupong, L., S. M. Scaria, R. A. Saxton, M. P. Gygi, K. Shen, G. A. Wyant, T. Wang, J. W. Harper, S. P. Gygi, and D. M. Sabatini. 2016. 'The CASTOR Proteins Are Arginine Sensors for the mTORC1 Pathway', *Cell*, 165: 153-64.

Chen, C., S. Zhai, L. Zhang, J. Chen, X. Long, J. Qin, J. Li, R. Huo, and X. Wang. 2018. 'Uhrf1 regulates germinal center B cell expansion and affinity maturation to control viral infection', *J Exp Med*, 215: 1437-48.

Chen, J., Y. Ou, Y. Yang, W. Li, Y. Xu, Y. Xie, and Y. Liu. 2018. 'KLHL22 activates amino-acid-dependent mTORC1 signalling to promote tumorigenesis and ageing', *Nature*, 557: 585-89.

Chiu, H., L. V. Jackson, K. I. Oh, A. Mai, Z. A. Ronai, D. Ruggero, and D. A. Fruman. 2019. 'The mTORC1/4E-BP/eIF4E Axis Promotes Antibody Class Switching in B Lymphocytes', *J Immunol*, 202: 579-90.

Cho, S. H., A. K. Ahn, P. Bhargava, C. H. Lee, C. M. Eischen, O. McGuinness, and M. Boothby. 2011. 'Glycolytic rate and lymphomagenesis depend on PARP14, an ADP ribosyltransferase of the B aggressive lymphoma (BAL) family', *Proc Natl Acad Sci U S A*, 108: 15972-7.

Cho, S. H., A. L. Raybuck, K. Stengel, M. Wei, T. C. Beck, E. Volanakis, J. W. Thomas, S. Hiebert, V. H. Haase, and M. R. Boothby. 2016. 'Germinal centre hypoxia and regulation of antibody qualities by a hypoxia response system', *Nature*, 537: 234-38.

Chou, C., D. J. Verbaro, E. Tonc, M. Holmgren, M. Cella, M. Colonna, D. Bhattacharya, and T. Egawa. 2016. 'The Transcription Factor AP4 Mediates Resolution of Chronic Viral Infection through Amplification of Germinal Center B Cell Responses', *Immunity*, 45: 570-82.

Ci, X., M. Kuraoka, H. Wang, Z. Carico, K. Hopper, J. Shin, X. Deng, Y. Qiu, S. Unniraman, G. Kelsoe, and X. P. Zhong. 2015. 'TSC1 Promotes B Cell Maturation but Is Dispensable for Germinal Center Formation', *PLoS One*, 10: e0127527.

Cinamon, G., M. A. Zachariah, O. M. Lam, F. W. Foss, Jr., and J. G. Cyster. 2008. 'Follicular shuttling of marginal zone B cells facilitates antigen transport', *Nat Immunol*, 9: 54-62.

Cobbold, S. P., E. Adams, C. A. Farquhar, K. F. Nolan, D. Howie, K. O. Lui, P. J. Fairchild, A. L. Mellor, D. Ron, and H. Waldmann. 2009. 'Infectious tolerance via the consumption of essential amino acids and mTOR signaling', *Proc Natl Acad Sci U S A*, 106: 12055-60.

Coro, Elizabeth S., W. L. William Chang, and Nicole Baumgarth. 2006. 'Type I IFN Receptor Signals Directly Stimulate Local B Cells Early following Influenza Virus Infection', *The Journal of Immunology*, 176: 4343-51.

Cui, L., D. Zheng, Y. H. Lee, T. K. Chan, Y. Kumar, W. E. Ho, J. Z. Chen, S. R. Tannenbaum, and C. N. Ong. 2016. 'Metabolomics Investigation Reveals Metabolite Mediators Associated with Acute Lung Injury and Repair in a Murine Model of Influenza Pneumonia', *Sci Rep*, 6: 26076.

Dawson, R. E., A. F. Nieto Guil, L. J. Robertson, S. G. Piltz, J. N. Hughes, and P. Q. Thomas. 2019. 'Functional screening of GATOR1 complex variants reveals a role for mTORC1 deregulation in FCD and focal epilepsy', *Neurobiol Dis*, 134: 104640.

de Calbiac, H., A. Dabacan, E. Marsan, H. Tostivint, G. Devienne, S. Ishida, E. Leguern, S. Baulac, R. C. Muresan, E. Kabashi, and S. Ciura. 2018. 'Depdc5 knockdown causes mTOR-dependent motor hyperactivity in zebrafish', *Ann Clin Transl Neurol*, 5: 510-23.

de Jonge, W. J., K. L. Kwikkers, A. A. te Velde, S. J. van Deventer, M. A. Nolte, R. E. Mebius, J. M. Ruijter, M. C. Lamers, and W. H. Lamers. 2002. 'Arginine deficiency affects early B cell maturation and lymphoid organ development in transgenic mice', *J Clin Invest*, 110: 1539-48.

Decker, T., M. Pasca di Magliano, S. McManus, Q. Sun, C. Bonifer, H. Tagoh, and M. Busslinger. 2009. 'Stepwise activation of enhancer and promoter regions of the B cell commitment gene Pax5 in early lymphopoiesis', *Immunity*, 30: 508-20.

DeKoter, R. P., and H. Singh. 2000. 'Regulation of B lymphocyte and macrophage development by graded expression of PU.1', *Science*, 288: 1439-41.

Dennis, P. B., A. Jaeschke, M. Saitoh, B. Fowler, S. C. Kozma, and G. Thomas. 2001. 'Mammalian TOR: a homeostatic ATP sensor', *Science*, 294: 1102-5.

Dent, A. L., A. L. Shaffer, X. Yu, D. Allman, and L. M. Staudt. 1997. 'Control of inflammation, cytokine expression, and germinal center formation by BCL-6', *Science*, 276: 589-92.

Douagi, I., C. Gujer, C. Sundling, W. C. Adams, A. Smed-Sorensen, R. A. Seder, G. B. Karlsson Hedestam, and K. Lore. 2009. 'Human B cell responses to TLR ligands are differentially modulated by myeloid and plasmacytoid dendritic cells', *J Immunol*, 182: 1991-2001.

Doughty, C. A., B. F. Bleiman, D. J. Wagner, F. J. Dufort, J. M. Mataraza, M. F. Roberts, and T. C. Chiles. 2006. 'Antigen receptor-mediated changes in glucose metabolism in B lymphocytes: role of phosphatidylinositol 3-kinase signaling in the glycolytic control of growth', *Blood*, 107: 4458-65.

Dufort, F. J., B. F. Bleiman, M. R. Gumina, D. Blair, D. J. Wagner, M. F. Roberts, Y. Abu-Amer, and T. C. Chiles. 2007. 'Cutting edge: IL-4-mediated protection of primary B lymphocytes from apoptosis via Stat6-dependent regulation of glycolytic metabolism', *J Immunol*, 179: 4953-7.

Dufort, F. J., M. R. Gumina, N. L. Ta, Y. Tao, S. A. Heyse, D. A. Scott, A. D. Richardson, T. N. Seyfried, and T. C. Chiles. 2014. 'Glucose-dependent de novo lipogenesis in B lymphocytes: a requirement for atp-citrate lyase in lipopolysaccharide-induced differentiation', *J Biol Chem*, 289: 7011-24.

Ekim, B., B. Magnuson, H. A. Acosta-Jaquez, J. A. Keller, E. P. Feener, and D. C. Fingar. 2011. 'mTOR kinase domain phosphorylation promotes mTORC1 signaling, cell growth, and cell cycle progression', *Mol Cell Biol*, 31: 2787-801.

Ersching, J., A. Efeyan, L. Mesin, J. T. Jacobsen, G. Pasqual, B. C. Grabiner, D. Dominguez-Sola, D. M. Sabatini, and G. D. Victora. 2017. 'Germinal Center Selection and Affinity Maturation Require Dynamic Regulation of mTORC1 Kinase', *Immunity*, 46: 1045-58 e6.

Fagarasan, S., S. Kawamoto, O. Kanagawa, and K. Suzuki. 2010. 'Adaptive immune regulation in the gut: T cell-dependent and T cell-independent IgA synthesis', *Annu Rev Immunol*, 28: 243-73.

Farmer, J. R., H. Allard-Chamard, N. Sun, M. Ahmad, A. Bertocchi, V. S. Mahajan, T. Aicher, J. Arnold, M. D. Benson, J. Morningstar, S. Barmettler, G. Yuen, S. J. H. Murphy, J. E. Walter, M. Ghebremichael, A. K. Shalek, F. Batista, R. Gerszten, and S. Pillai. 2019. 'Induction of metabolic quiescence defines the transitional to follicular B cell switch', *Sci Signal*, 12.

Fock, R. A., S. L. Blatt, B. Beutler, J. Pereira, M. Tsujita, F. E. de Barros, and P. Borelli. 2010. 'Study of lymphocyte subpopulations in bone marrow in a model of protein-energy malnutrition', *Nutrition*, 26: 1021-8.

Forster, R., A. E. Mattis, E. Kremmer, E. Wolf, G. Brem, and M. Lipp. 1996. 'A putative chemokine receptor, BLR1, directs B cell migration to defined lymphoid organs and specific anatomic compartments of the spleen', *Cell*, 87: 1037-47.

Fukuda, T., T. Yoshida, S. Okada, M. Hatano, T. Miki, K. Ishibashi, S. Okabe, H. Koseki, S. Hirosawa, M. Taniguchi, N. Miyasaka, and T. Tokuhisa. 1997. 'Disruption of the Bcl6 gene results in an impaired germinal center formation', *J Exp Med*, 186: 439-48.

Galbaugh, T., M. G. Cerrito, C. C. Jose, and M. L. Cutler. 2006. 'EGF-induced activation of Akt results in mTOR-dependent p70S6 kinase phosphorylation and inhibition of HC11 cell lactogenic differentiation', *BMC Cell Biol*, 7: 34.

Garcia de Vinuesa, C., P. O'Leary, D. M. Sze, K. M. Toellner, and I. C. MacLennan. 1999. 'T-independent type 2 antigens induce B cell proliferation in multiple splenic sites, but exponential growth is confined to extrafollicular foci', *Eur J Immunol*, 29: 1314-23.

Gatto, D., D. Paus, A. Basten, C. R. Mackay, and R. Brink. 2009. 'Guidance of B cells by the orphan G protein-coupled receptor EBI2 shapes humoral immune responses', *Immunity*, 31: 259-69.

Gitlin, A. D., C. T. Mayer, T. Y. Oliveira, Z. Shulman, M. J. Jones, A. Koren, and M. C. Nussenzweig. 2015. 'HUMORAL IMMUNITY. T cell help controls the speed of the cell cycle in germinal center B cells', *Science*, 349: 643-6.

Gitlin, A. D., Z. Shulman, and M. C. Nussenzweig. 2014. 'Clonal selection in the germinal centre by regulated proliferation and hypermutation', *Nature*, 509: 637-40.

Glatman Zaretsky, A., C. Konradt, F. Depis, J. B. Wing, R. Goenka, D. G. Atria, J. S. Silver, S. Cho, A. I. Wolf, W. J. Quinn, J. B. Engiles, D. C. Brown, D. Beiting, J. Erikson, D. Allman, M. P. Cancro, S. Sakaguchi, L. F. Lu, C. O. Benoist, and C. A. Hunter. 2017. 'T Regulatory Cells Support Plasma Cell Populations in the Bone Marrow', *Cell Rep*, 18: 1906-16.

Goenka, R., A. H. Matthews, B. Zhang, P. J. O'Neill, J. L. Scholz, T. S. Migone, W. J. Leonard, W. Stohl, U. Hershberg, and M. P. Cancro. 2014. 'Local BLyS production by T follicular cells mediates retention of high affinity B cells during affinity maturation', *J Exp Med*, 211: 45-56.

Good-Jacobson, K. L., and M. J. Shlomchik. 2010. 'Plasticity and heterogeneity in the generation of memory B cells and long-lived plasma cells: the influence of germinal center interactions and dynamics', *J Immunol*, 185: 3117-25.

Guertin, D. A., D. M. Stevens, C. C. Thoreen, A. A. Burds, N. Y. Kalaany, J. Moffat, M. Brown, K. J. Fitzgerald, and D. M. Sabatini. 2006. 'Ablation in mice of the mTORC components raptor, rictor, or mLST8 reveals that mTORC2 is required for signaling to Akt-FOXO and PKCalpha, but not S6K1', *Dev Cell*, 11: 859-71.

Gurish, M. F., P. J. Bryce, H. Tao, A. B. Kisselgof, E. M. Thornton, H. R. Miller, D. S. Friend, and H. C. Oettgen. 2004. 'IgE enhances parasite clearance and regulates mast cell responses in mice infected with Trichinella spiralis', *J Immunol*, 172: 1139-45.

Halliley, J. L., C. M. Tipton, J. Liesveld, A. F. Rosenberg, J. Darce, I. V. Gregoretti, L. Popova, D. Kaminiski, C. F. Fucile, I. Albizua, S. Kyu, K. Y. Chiang, K. T. Bradley, R. Burack, M. Slifka, E. Hammarlund, H. Wu, L. Zhao, E. E. Walsh, A. R. Falsey, T. D. Randall, W. C. Cheung, I. Sanz, and F. E. Lee. 2015. 'Long-Lived Plasma Cells Are Contained within the CD19(-)CD38(hi)CD138(+) Subset in Human Bone Marrow', *Immunity*, 43: 132-45.

Hamilton-Easton, A., and M. Eichelberger. 1995. 'Virus-specific antigen presentation by different subsets of cells from lung and mediastinal lymph node tissues of influenza virus-infected mice', *J Virol*, 69: 6359-66.

Han, J., and Y. Wang. 2018. 'mTORC1 signaling in hepatic lipid metabolism', *Protein Cell*, 9: 145-51.

Hardy, R. R., C. E. Carmack, S. A. Shinton, J. D. Kemp, and K. Hayakawa. 1991. 'Resolution and characterization of pro-B and pre-pro-B cell stages in normal mouse bone marrow', *J Exp Med*, 173: 1213-25.

Hay, N., and N. Sonenberg. 2004. 'Upstream and downstream of mTOR', *Genes Dev*, 18: 1926-45.

Hayashi, K., P. Jutabha, H. Endou, H. Sagara, and N. Anzai. 2013. 'LAT1 is a critical transporter of essential amino acids for immune reactions in activated human T cells', *J Immunol*, 191: 4080-5.

Heise, N., N. S. De Silva, K. Silva, A. Carette, G. Simonetti, M. Pasparakis, and U. Klein. 2014. 'Germinal center B cell maintenance and differentiation are controlled by distinct NF-kappaB transcription factor subunits', *J Exp Med*, 211: 2103-18.

Higgins, B. W., L. J. McHeyzer-Williams, and M. G. McHeyzer-Williams. 2019. 'Programming Isotype-Specific Plasma Cell Function', *Trends Immunol*, 40: 345-57.

Hu, Y., I. Semova, X. Sun, H. Kang, S. Chahar, A. N. Hollenberg, D. Masson, M. D. Hirschey, J. Miao, and S. B. Biddinger. 2018. 'Fructose and glucose can regulate mammalian target of rapamycin complex 1 and lipogenic gene expression via distinct pathways', *J Biol Chem*, 293: 2006-14.

Huang, C., D. G. Gonzalez, C. M. Cote, Y. Jiang, K. Hatzi, M. Teater, K. Dai, T. Hla, A. M. Haberman, and A. Melnick. 2014. 'The BCL6 RD2 domain governs commitment of activated B cells to form germinal centers', *Cell Rep*, 8: 1497-508.

Huber, V. C., R. M. McKeon, M. N. Brackin, L. A. Miller, R. Keating, S. A. Brown, N. Makarova, D. R. Perez, G. H. Macdonald, and J. A. McCullers. 2006. 'Distinct contributions of vaccine-induced immunoglobulin G1 (IgG1) and IgG2a antibodies to protective immunity against influenza', *Clin Vaccine Immunol*, 13: 981-90.

Hughes, J., R. Dawson, M. Tea, D. McAninch, S. Piltz, D. Jackson, L. Stewart, M. G. Ricos, L. M. Dibbens, N. L. Harvey, and P. Thomas. 2017. 'Knockout of the epilepsy gene Depdc5 in mice causes severe embryonic dysmorphology with hyperactivity of mTORC1 signalling', *Sci Rep*, 7: 12618.

Iadevaia, V., R. Liu, and C. G. Proud. 2014. 'mTORC1 signaling controls multiple steps in ribosome biogenesis', *Semin Cell Dev Biol*, 36: 113-20.

Ibrahim, M. K., M. Zambruni, C. L. Melby, and P. C. Melby. 2017. 'Impact of Childhood Malnutrition on Host Defense and Infection', *Clin Microbiol Rev*, 30: 919-71.

Inamine, A., Y. Takahashi, N. Baba, K. Miyake, T. Tokuhisa, T. Takemori, and R. Abe. 2005. 'Two waves of memory B-cell generation in the primary immune response', *Int Immunol*, 17: 581-9.

Iwasaki, A., and B. L. Kelsall. 1999. 'Freshly isolated Peyer's patch, but not spleen, dendritic cells produce interleukin 10 and induce the differentiation of T helper type 2 cells', *J Exp Med*, 190: 229-39.

Iwata, T. N., J. A. Ramirez, M. Tsang, H. Park, D. H. Margineantu, D. M. Hockenbery, and B. M. Iritani. 2016. 'Conditional Disruption of Raptor Reveals an Essential Role for mTORC1 in B Cell Development, Survival, and Metabolism', *J Immunol*, 197: 2250-60.

Iwata, T. N., J. A. Ramirez-Komo, H. Park, and B. M. Iritani. 2017. 'Control of B lymphocyte development and functions by the mTOR signaling pathways', *Cytokine Growth Factor Rev*, 35: 47-62.

Jastrzebski, K., K. M. Hannan, E. B. Tchoubrieva, R. D. Hannan, and R. B. Pearson. 2007. 'Coordinate regulation of ribosome biogenesis and function by the ribosomal protein S6 kinase, a key mediator of mTOR function', *Growth Factors*, 25: 209-26.

Jellusova, J., M. H. Cato, J. R. Apgar, P. Ramezani-Rad, C. R. Leung, C. Chen, A. D. Richardson, E. M. Conner, R. J. Benschop, J. R. Woodgett, and R. C. Rickert. 2017. 'Gsk3 is a metabolic checkpoint regulator in B cells', *Nat Immunol*, 18: 303-12.

Jensen, C. T., S. Lang, R. Somasundaram, S. Soneji, and M. Sigvardsson. 2016. 'Identification of Stage-Specific Surface Markers in Early B Cell Development Provides Novel Tools for Identification of Progenitor Populations', *J Immunol*, 197: 1937-44.

Jones, D. D., B. T. Gaudette, J. R. Wilmore, I. Chernova, A. Bortnick, B. M. Weiss, and D. Allman. 2016. 'mTOR has distinct functions in generating versus sustaining humoral immunity', *J Clin Invest*, 126: 4250-61.

Jones, Derek, Irene Chernova, and David Allman. 2014. 'B cell-intrinsic mTOR signaling regulates the generation of germinal center B cells (IRM8P.716)', *The Journal of Immunology*, 192: 127.17-27.17.

Joo, H. M., Y. He, and M. Y. Sangster. 2008. 'Broad dispersion and lung localization of virus-specific memory B cells induced by influenza pneumonia', *Proc Natl Acad Sci U S A*, 105: 3485-90.

Kaidi, A., D. Qualtrough, A. C. Williams, and C. Paraskeva. 2006. 'Direct transcriptional up-regulation of cyclooxygenase-2 by hypoxia-inducible factor (HIF)-1 promotes colorectal tumor cell survival and enhances HIF-1 transcriptional activity during hypoxia', *Cancer Res*, 66: 6683-91.

Kaji, T., A. Ishige, M. Hikida, J. Taka, A. Hijikata, M. Kubo, T. Nagashima, Y. Takahashi, T. Kurosaki, M. Okada, O. Ohara, K. Rajewsky, and T. Takemori. 2012. 'Distinct cellular pathways select germline-encoded and somatically mutated antibodies into immunological memory', *J Exp Med*, 209: 2079-97.

Kakiuchi, Y., T. Yurube, K. Kakutani, T. Takada, M. Ito, Y. Takeoka, Y. Kanda, S. Miyazaki, R. Kuroda, and K. Nishida. 2019. 'Pharmacological inhibition of mTORC1 but not mTORC2 protects against human disc cellular apoptosis, senescence, and extracellular matrix catabolism through Akt and autophagy induction', *Osteoarthritis Cartilage*, 27: 965-76.

Kallies, A., J. Hasbold, D. M. Tarlinton, W. Dietrich, L. M. Corcoran, P. D. Hodgkin, and S. L. Nutt. 2004. 'Plasma cell ontogeny defined by quantitative changes in blimp-1 expression', *J Exp Med*, 200: 967-77.

Kara, E. E., C. R. Bastow, D. R. McKenzie, C. E. Gregor, K. A. Fenix, R. Babb, T. S. Norton, D. Zotos, L. B. Rodda, J. R. Hermes, K. Bourne, D. S. Gilchrist, R. J. Nibbs, M. Alsharifi, C. G. Vinuesa, D. M. Tarlinton, R. Brink, G. R. Hill, J. G. Cyster, I. Comerford, and S. R. McColl. 2018. 'Atypical chemokine receptor 4 shapes activated B cell fate', *J Exp Med*, 215: 801-13.

Katakai, T., H. Suto, M. Sugai, H. Gonda, A. Togawa, S. Suematsu, Y. Ebisuno, K. Katagiri, T. Kinashi, and A. Shimizu. 2008. 'Organizer-like reticular stromal cell layer common to adult secondary lymphoid organs', *J Immunol*, 181: 6189-200.

Keating, Rachael, Tomer Hertz, Marie Wehenkel, Tarsha L. Harris, Benjamin A. Edwards, Jennifer L. McClaren, Scott A. Brown, Sherri Surman, Zachary S. Wilson, Philip Bradley, Julia Hurwitz, Hongbo Chi, Peter C. Doherty, Paul G. Thomas, and Maureen A. McGargill. 2013. 'The kinase mTOR modulates the antibody response to provide cross-protective immunity to lethal infection with influenza virus', *Nature Immunology*, 14: 1266.

Kee, B. L., and C. Murre. 1998. 'Induction of early B cell factor (EBF) and multiple B lineage genes by the basic helix-loop-helix transcription factor E12', *J Exp Med*, 188: 699-713.

Kelly, L. M., J. P. Pereira, T. Yi, Y. Xu, and J. G. Cyster. 2011. 'EBI2 guides serial movements of activated B cells and ligand activity is detectable in lymphoid and nonlymphoid tissues', *J Immunol*, 187: 3026-32.

Kim, H., S. An, S. H. Ro, F. Teixeira, G. J. Park, C. Kim, C. S. Cho, J. S. Kim, U. Jakob, J. H. Lee, and U. S. Cho. 2015. 'Janus-faced Sestrin2 controls ROS and mTOR signalling through two separate functional domains', *Nat Commun*, 6: 10025.

Kim, M. S., H. S. Kuehn, D. D. Metcalfe, and A. M. Gilfillan. 2008. 'Activation and function of the mTORC1 pathway in mast cells', *J Immunol*, 180: 4586-95.

Koike, T., K. Harada, S. Horiuchi, and D. Kitamura. 2019. 'The quantity of CD40 signaling determines the differentiation of B cells into functionally distinct memory cell subsets', *Elife*, 8.

Kunisawa, J., Y. Sugiura, T. Wake, T. Nagatake, H. Suzuki, R. Nagasawa, S. Shikata, K. Honda, E. Hashimoto, Y. Suzuki, M. Setou, M. Suematsu, and H. Kiyono. 2015. 'Mode of Bioenergetic

Metabolism during B Cell Differentiation in the Intestine Determines the Distinct Requirement for Vitamin B1', *Cell Rep*, 13: 122-31.

Kwon, K., C. Hutter, Q. Sun, I. Bilic, C. Cobaleda, S. Malin, and M. Busslinger. 2008. 'Instructive role of the transcription factor E2A in early B lymphopoiesis and germinal center B cell development', *Immunity*, 28: 751-62.

Lalor, P. A., G. J. Nossal, R. D. Sanderson, and M. G. McHeyzer-Williams. 1992. 'Functional and molecular characterization of single, (4-hydroxy-3-nitrophenyl)acetyl (NP)-specific, IgG1+ B cells from antibody-secreting and memory B cell pathways in the C57BL/6 immune response to NP', *Eur J Immunol*, 22: 3001-11.

Lam, J. H., and N. Baumgarth. 2019. 'The Multifaceted B Cell Response to Influenza Virus', *J Immunol*, 202: 351-59.

Landsverk, O. J., O. Snir, R. B. Casado, L. Richter, J. E. Mold, P. Reu, R. Horneland, V. Paulsen, S. Yaqub, E. M. Aandahl, O. M. Oyen, H. S. Thorarensen, M. Salehpour, G. Possnert, J. Frisen, L. M. Sollid, E. S. Baekkevold, and F. L. Jahnsen. 2017. 'Antibody-secreting plasma cells persist for decades in human intestine', *J Exp Med*, 214: 309-17.

Lee, A. Y., S. Y. Chang, J. I. Kim, H. R. Cha, M. H. Jang, M. Yamamoto, and M. N. Kweon. 2008. 'Dendritic cells in colonic patches and iliac lymph nodes are essential in mucosal IgA induction following intrarectal administration via CCR7 interaction', *Eur J Immunol*, 38: 1127-37.

Lee, B. O., J. Moyron-Quiroz, J. Rangel-Moreno, K. L. Kusser, L. Hartson, F. Sprague, F. E. Lund, and T. D. Randall. 2003. 'CD40, but not CD154, expression on B cells is necessary for optimal primary B cell responses', *J Immunol*, 171: 5707-17.

Lee, K., L. Heffington, J. Jellusova, K. T. Nam, A. Raybuck, S. H. Cho, J. W. Thomas, R. C. Rickert, and M. Boothby. 2013. 'Requirement for Rictor in homeostasis and function of mature B lymphoid cells', *Blood*, 122: 2369-79.

Lee, S. K., R. J. Rigby, D. Zotos, L. M. Tsai, S. Kawamoto, J. L. Marshall, R. R. Ramiscal, T. D. Chan, D. Gatto, R. Brink, D. Yu, S. Fagarasan, D. M. Tarlinton, A. F. Cunningham, and C. G. Vinuesa. 2011. 'B cell priming for extrafollicular antibody responses requires Bcl-6 expression by T cells', *J Exp Med*, 208: 1377-88.

Li, B., Z. Li, P. Wang, Q. Huang, L. Xu, R. He, L. Ye, and Q. Bai. 2017. 'Mammalian target of rapamycin complex 1 signalling is essential for germinal centre reaction', *Immunology*, 152: 276-86.

Li, J., W. Yin, Y. Jing, D. Kang, L. Yang, J. Cheng, Z. Yu, Z. Peng, X. Li, Y. Wen, X. Sun, B. Ren, and C. Liu. 2018. 'The Coordination Between B Cell Receptor Signaling and the Actin Cytoskeleton During B Cell Activation', *Front Immunol*, 9: 3096.

Li, Y. S., R. Wasserman, K. Hayakawa, and R. R. Hardy. 1996. 'Identification of the earliest B lineage stage in mouse bone marrow', *Immunity*, 5: 527-35.

Limon, J. J., L. So, S. Jellbauer, H. Chiu, J. Corado, S. M. Sykes, M. Raffatellu, and D. A. Fruman. 2014. 'mTOR kinase inhibitors promote antibody class switching via mTORC2 inhibition', *Proc Natl Acad Sci U S A*, 111: E5076-85.

Lin, Y. C., S. Jhunjhunwala, C. Benner, S. Heinz, E. Welinder, R. Mansson, M. Sigvardsson, J. Hagman, C. A. Espinoza, J. Dutkowski, T. Ideker, C. K. Glass, and C. Murre. 2010. 'A global network of transcription factors, involving E2A, EBF1 and Foxo1, that orchestrates B cell fate', *Nat Immunol*, 11: 635-43.

Liu, D., H. Xu, C. Shih, Z. Wan, X. Ma, W. Ma, D. Luo, and H. Qi. 2015. 'T-B-cell entanglement and ICOSL-driven feed-forward regulation of germinal centre reaction', *Nature*, 517: 214-8.

Liu, Y., H. Xu, and M. An. 2017. 'mTORC1 regulates apoptosis and cell proliferation in pterygium via targeting autophagy and FGFR3', *Sci Rep*, 7: 7339.

Lopez, P., B. de Paz, J. Rodriguez-Carrio, A. Hevia, B. Sanchez, A. Margolles, and A. Suarez. 2016. 'Th17 responses and natural IgM antibodies are related to gut microbiota composition in systemic lupus erythematosus patients', *Sci Rep*, 6: 24072.

Lui, S. L., R. Tsang, K. W. Chan, F. Zhang, S. Tam, S. Yung, and T. M. Chan. 2008. 'Rapamycin attenuates the severity of established nephritis in lupus-prone NZB/W F-1 mice', *Nephrology Dialysis Transplantation*, 23: 2768-76.

Ma, T., N. Tzavaras, P. Tsokas, E. M. Landau, and R. D. Blitzer. 2011. 'Synaptic stimulation of mTOR is mediated by Wnt signaling and regulation of glycogen synthetase kinase-3', *J Neurosci*, 31: 17537-46.

MacLennan, I. C. 1994. 'Germinal centers', *Annu Rev Immunol*, 12: 117-39.

Magnuson, B., B. Ekim, and D. C. Fingar. 2012. 'Regulation and function of ribosomal protein S6 kinase (S6K) within mTOR signalling networks', *Biochem J*, 441: 1-21.

Manz, R. A., S. Arce, G. Cassese, A. E. Hauser, F. Hiepe, and A. Radbruch. 2002. 'Humoral immunity and long-lived plasma cells', *Curr Opin Immunol*, 14: 517-21.

Martin, S. K., S. Fitter, A. K. Dutta, M. P. Matthews, C. R. Walkley, M. N. Hall, M. A. Ruegg, S. Gronthos, and A. C. Zannettino. 2015. 'Brief report: the differential roles of mTORC1 and mTORC2 in mesenchymal stem cell differentiation', *Stem Cells*, 33: 1359-65.

Martin, V. G., Y. B. Wu, C. L. Townsend, G. H. Lu, J. S. O'Hare, A. Mozeika, A. C. Coolen, D. Kipling, F. Fraternali, and D. K. Dunn-Walters. 2016. 'Transitional B Cells in Early Human B Cell Development - Time to Revisit the Paradigm?', *Front Immunol*, 7: 546.

Matsumoto, M., S. F. Lo, C. J. Carruthers, J. Min, S. Mariathasan, G. Huang, D. R. Plas, S. M. Martin, R. S. Geha, M. H. Nahm, and D. D. Chaplin. 1996. 'Affinity maturation without germinal centres in lymphotoxin-alpha-deficient mice', *Nature*, 382: 462-6.

McIlwain, D. R., T. Berger, and T. W. Mak. 2013. 'Caspase functions in cell death and disease', *Cold Spring Harb Perspect Biol*, 5: a008656.

McMurray, D. N., R. R. Watson, and M. A. Reyes. 1981. 'Effect of renutrition on humoral and cell-mediated immunity in severely malnourished children', *Am J Clin Nutr*, 34: 2117-26.

Meena, N. K., S. P. Pattanayak, Y. Ben-Nun, S. Benhamron, S. Kumar, E. Merquiol, N. Hovelmeyer, G. Blum, and B. Tirosh. 2018. 'mTORC1 activation in B cells confers impairment of marginal zone microarchitecture by exaggerating cathepsin activity', *Immunology*, 155: 505-18.

Mendoza, P., N. Martinez-Martin, E. R. Bovolenta, D. Reyes-Garau, P. Hernansanz-Agustin, P. Delgado, M. D. Diaz-Munoz, C. L. Oeste, I. Fernandez-Pisonero, E. Castellano, A. Martinez-Ruiz, D. Alonso-Lopez, E. Santos, X. R. Bustelo, T. Kurosaki, and B. Alarcon. 2018. 'R-Ras2 is required for germinal center formation to aid B cells during energetically demanding processes', *Sci Signal*, 11.

Menon, S., C. C. Dibble, G. Talbott, G. Hoxhaj, A. J. Valvezan, H. Takahashi, L. C. Cantley, and B. D. Manning. 2014. 'Spatial control of the TSC complex integrates insulin and nutrient regulation of mTORC1 at the lysosome', *Cell*, 156: 771-85.

Mesin, L., J. Ersching, and G. D. Victora. 2016. 'Germinal Center B Cell Dynamics', *Immunity*, 45: 471-82.

Miragaia, R. J., T. Gomes, A. Chomka, L. Jardine, A. Riedel, A. N. Hegazy, N. Whibley, A. Tucci, X. Chen, I. Lindeman, G. Emerton, T. Krausgruber, J. Shields, M. Haniffa, F. Powrie, and S. A. Teichmann. 2019. 'Single-Cell Transcriptomics of Regulatory T Cells Reveals Trajectories of Tissue Adaptation', *Immunity*, 50: 493-504 e7.

Miyashita, T., M. J. McIlraith, A. C. Grammer, Y. Miura, J. F. Attrep, Y. Shimaoka, and P. E. Lipsky. 1997. 'Bidirectional regulation of human B cell responses by CD40-CD40 ligand interactions', *J Immunol*, 158: 4620-33.

Mizuno, Y., S. Shimada, Y. Akiyama, S. Watanabe, T. Aida, K. Ogawa, H. Ono, Y. Mitsunori, D. Ban, A. Kudo, S. Arii, S. Yamaoka, M. Tanabe, and S. Tanaka. 2018. 'DEPDC5 deficiency

contributes to resistance to leucine starvation via p62 accumulation in hepatocellular carcinoma', *Sci Rep*, 8: 106.

Mond, J. J., A. Lees, and C. M. Snapper. 1995. 'T cell-independent antigens type 2', *Annu Rev Immunol*, 13: 655-92.

Mond, J. J., Q. Vos, A. Lees, and C. M. Snapper. 1995. 'T cell independent antigens', *Curr Opin Immunol*, 7: 349-54.

Moyron-Quiroz, J. E., J. Rangel-Moreno, K. Kusser, L. Hartson, F. Sprague, S. Goodrich, D. L. Woodland, F. E. Lund, and T. D. Randall. 2004. 'Role of inducible bronchus associated lymphoid tissue (iBALT) in respiratory immunity', *Nat Med*, 10: 927-34.

Mueller, J., M. Matloubian, and J. Zikherman. 2015. 'Cutting edge: An in vivo reporter reveals active B cell receptor signaling in the germinal center', *J Immunol*, 194: 2993-7.

Murakami, M., T. Ichisaka, M. Maeda, N. Oshiro, K. Hara, F. Edenhofer, H. Kiyama, K. Yonezawa, and S. Yamanaka. 2004. 'mTOR is essential for growth and proliferation in early mouse embryos and embryonic stem cells', *Mol Cell Biol*, 24: 6710-8.

Muramatsu, M., K. Kinoshita, S. Fagarasan, S. Yamada, Y. Shinkai, and T. Honjo. 2000. 'Class switch recombination and hypermutation require activation-induced cytidine deaminase (AID), a potential RNA editing enzyme', *Cell*, 102: 553-63.

Nagai, M., R. Noguchi, D. Takahashi, T. Morikawa, K. Koshida, S. Komiyama, N. Ishihara, T. Yamada, Y. I. Kawamura, K. Muroi, K. Hattori, N. Kobayashi, Y. Fujimura, M. Hirota, R. Matsumoto, R. Aoki, M. Tamura-Nakano, M. Sugiyama, T. Katakai, S. Sato, K. Takubo, T. Dohi, and K. Hase. 2019. 'Fasting-Refeeding Impacts Immune Cell Dynamics and Mucosal Immune Responses', *Cell*, 178: 1072-87 e14.

Nakaya, M., Y. Xiao, X. Zhou, J. H. Chang, M. Chang, X. Cheng, M. Blonska, X. Lin, and S. C. Sun. 2014. 'Inflammatory T cell responses rely on amino acid transporter ASCT2 facilitation of glutamine uptake and mTORC1 kinase activation', *Immunity*, 40: 692-705.

Nascimento, F. A., F. Borlot, P. Cossette, B. A. Minassian, and D. M. Andrade. 2015. 'Two definite cases of sudden unexpected death in epilepsy in a family with a DEPDC5 mutation', *Neurol Genet*, 1: e28.

Nohr, C. W., J. I. Tchervenkov, J. L. Meakins, and N. V. Christou. 1986. 'Malnutrition and humoral immunity: long-term protein deprivation', *J Surg Res*, 40: 432-7.

Nunez, S., C. Moore, B. Gao, K. Rogers, Y. Hidalgo, P. J. Del Nido, S. Restaino, Y. Naka, G. Bhagat, J. C. Madsen, M. R. Bono, and E. Zorn. 2016. 'The human thymus perivascular space is a functional niche for viral-specific plasma cells', *Sci Immunol*, 1.

Nutt, S. L., and B. L. Kee. 2007. 'The transcriptional regulation of B cell lineage commitment', *Immunity*, 26: 715-25.

O'Sullivan, D., and E. L. Pearce. 2015. 'Targeting T cell metabolism for therapy', *Trends Immunol*, 36: 71-80.

Obukhanych, T. V., and M. C. Nussenzweig. 2006. 'T-independent type II immune responses generate memory B cells', *J Exp Med*, 203: 305-10.

Okada, T., M. J. Miller, I. Parker, M. F. Krummel, M. Neighbors, S. B. Hartley, A. O'Garra, M. D. Cahalan, and J. G. Cyster. 2005. 'Antigen-engaged B cells undergo chemotaxis toward the T zone and form motile conjugates with helper T cells', *PLoS Biol*, 3: e150.

Okada, T., T. Otsubo, T. Hagiwara, F. Inazuka, E. Kobayashi, S. Fukuda, T. Inoue, K. Higuchi, Y. I. Kawamura, and T. Dohi. 2017. 'Intermittent fasting prompted recovery from dextran sulfate sodium-induced colitis in mice', *J Clin Biochem Nutr*, 61: 100-07.

Olson, T. S., G. Bamias, M. Naganuma, J. Rivera-Nieves, T. L. Burcin, W. Ross, M. A. Morris, T. T. Pizarro, P. B. Ernst, F. Cominelli, and K. Ley. 2004. 'Expanded B cell population blocks regulatory T cells and exacerbates ileitis in a murine model of Crohn disease', *J Clin Invest*, 114: 389-98.

Omori, S. A., M. H. Cato, A. Anzelon-Mills, K. D. Puri, M. Shapiro-Shelef, K. Calame, and R. C. Rickert. 2006. 'Regulation of class-switch recombination and plasma cell differentiation by phosphatidylinositol 3-kinase signaling', *Immunity*, 25: 545-57.

Onodera, T., Y. Takahashi, Y. Yokoi, M. Ato, Y. Kodama, S. Hachimura, T. Kurosaki, and K. Kobayashi. 2012. 'Memory B cells in the lung participate in protective humoral immune responses to pulmonary influenza virus reinfection', *Proc Natl Acad Sci U S A*, 109: 2485-90.

Ouchida, R., H. Mori, K. Hase, H. Takatsu, T. Kurosaki, T. Tokuhisa, H. Ohno, and J. Y. Wang. 2012. 'Critical role of the IgM Fc receptor in IgM homeostasis, B-cell survival, and humoral immune responses', *Proc Natl Acad Sci U S A*, 109: E2699-706.

Owen, O. E., S. C. Kalhan, and R. W. Hanson. 2002. 'The key role of anaplerosis and cataplerosis for citric acid cycle function', *J Biol Chem*, 277: 30409-12.

Palm, A. E., and C. Henry. 2019. 'Remembrance of Things Past: Long-Term B Cell Memory After Infection and Vaccination', *Front Immunol*, 10: 1787.

Pape, K. A., D. M. Catron, A. A. Itano, and M. K. Jenkins. 2007. 'The humoral immune response is initiated in lymph nodes by B cells that acquire soluble antigen directly in the follicles', *Immunity*, 26: 491-502.

Paus, D., T. G. Phan, T. D. Chan, S. Gardam, A. Basten, and R. Brink. 2006. 'Antigen recognition strength regulates the choice between extrafollicular plasma cell and germinal center B cell differentiation', *J Exp Med*, 203: 1081-91.

Pearson, C., A. Silva, and B. Seddon. 2012. 'Exogenous amino acids are essential for interleukin-7 induced CD8 T cell growth. [corrected]', *PLoS One*, 7: e33998.

Peng, T., T. R. Golub, and D. M. Sabatini. 2002. 'The immunosuppressant rapamycin mimics a starvation-like signal distinct from amino acid and glucose deprivation', *Mol Cell Biol*, 22: 5575-84.

Perlmutter, R. M., D. Hansburg, D. E. Briles, R. A. Nicolotti, and J. M. Davie. 1978. 'Subclass restriction of murine anti-carbohydrate antibodies', *J Immunol*, 121: 566-72.

Peruchon, S., N. Chaoul, C. Burelout, B. Delache, P. Brochard, P. Laurent, F. Cognasse, S. Prevot, O. Garraud, R. Le Grand, and Y. Richard. 2009. 'Tissue-specific B-cell dysfunction and generalized memory B-cell loss during acute SIV infection', *PLoS One*, 4: e5966.

Petro, J. B., R. M. Gerstein, J. Lowe, R. S. Carter, N. Shinners, and W. N. Khan. 2002. 'Transitional type 1 and 2 B lymphocyte subsets are differentially responsive to antigen receptor signaling', *J Biol Chem*, 277: 48009-19.

Phan, T. G., J. A. Green, E. E. Gray, Y. Xu, and J. G. Cyster. 2009. 'Immune complex relay by subcapsular sinus macrophages and noncognate B cells drives antibody affinity maturation', *Nat Immunol*, 10: 786-93.

Phan, T. G., D. Paus, T. D. Chan, M. L. Turner, S. L. Nutt, A. Basten, and R. Brink. 2006. 'High affinity germinal center B cells are actively selected into the plasma cell compartment', *J Exp Med*, 203: 2419-24.

Ramirez, J., K. Lukin, and J. Hagman. 2010. 'From hematopoietic progenitors to B cells: mechanisms of lineage restriction and commitment', *Curr Opin Immunol*, 22: 177-84.

Rangan, P., I. Choi, M. Wei, G. Navarrete, E. Guen, S. Brandhorst, N. Enyati, G. Pasia, D. Maesincee, V. Ocon, M. Abdulridha, and V. D. Longo. 2019. 'Fasting-Mimicking Diet Modulates Microbiota and Promotes Intestinal Regeneration to Reduce Inflammatory Bowel Disease Pathology', *Cell Rep*, 26: 2704-19 e6.

Rangel-Moreno, J., D. M. Carragher, R. S. Misra, K. Kusser, L. Hartson, A. Moquin, F. E. Lund, and T. D. Randall. 2008. 'B cells promote resistance to heterosubtypic strains of influenza via multiple mechanisms', *J Immunol*, 180: 454-63.

Rangel-Moreno, J., J. E. Moyron-Quiroz, L. Hartson, K. Kusser, and T. D. Randall. 2007. 'Pulmonary expression of CXC chemokine ligand 13, CC chemokine ligand 19, and CC chemokine ligand 21 is essential for local immunity to influenza', *Proc Natl Acad Sci U S A*, 104: 10577-82.

Ravindran, Rajesh, Jens Loebbermann, Helder I. Nakaya, Nooruddin Khan, Hualing Ma, Leonardo Gama, Deepa K. Machiah, Benton Lawson, Paul Hakimpour, Yi-chong Wang, Shuzhao Li, Prachi Sharma, Randal J. Kaufman, Jennifer Martinez, and Bali Pulendran. 2016. 'The amino acid sensor GCN2 controls gut inflammation by inhibiting inflammasome activation', *Nature*, 531: 523-27.

Rawlings, D. J., M. A. Schwartz, S. W. Jackson, and A. Meyer-Bahlburg. 2012. 'Integration of B cell responses through Toll-like receptors and antigen receptors', *Nat Rev Immunol*, 12: 282-94.

Raybuck, A. L., S. H. Cho, J. Li, M. C. Rogers, K. Lee, C. L. Williams, M. Shlomchik, J. W. Thomas, J. Chen, J. V. Williams, and M. R. Boothby. 2018. 'B Cell-Intrinsic mTORC1 Promotes Germinal Center-Defining Transcription Factor Gene Expression, Somatic Hypermutation, and Memory B Cell Generation in Humoral Immunity', *J Immunol*, 200: 2627-39.

Reboldi, A., and J. G. Cyster. 2016. 'Peyer's patches: organizing B-cell responses at the intestinal frontier', *Immunol Rev*, 271: 230-45.

Ren, W., G. Liu, J. Yin, B. Tan, G. Wu, F. W. Bazer, Y. Peng, and Y. Yin. 2017. 'Amino-acid transporters in T-cell activation and differentiation', *Cell Death Dis*, 8: e2757.

Rhoads, J. M., X. Niu, J. Odle, and L. M. Graves. 2006. 'Role of mTOR signaling in intestinal cell migration', *Am J Physiol Gastrointest Liver Physiol*, 291: G510-7.

Ribierre, T., C. Deleuze, A. Bacq, S. Baldassari, E. Marsan, M. Chipaux, G. Muraca, D. Roussel, V. Navarro, E. Leguern, R. Miles, and S. Baulac. 2018. 'Second-hit mosaic mutation in mTORC1 repressor DEPDC5 causes focal cortical dysplasia-associated epilepsy', *J Clin Invest*, 128: 2452-58.

Ricci, Jean-Ehrland, and Johanna Chiche. 2018. 'Metabolic Reprogramming of Non-Hodgkin's B-Cell Lymphomas and Potential Therapeutic Strategies', *Frontiers in Oncology*, 8.

Ricos, M. G., B. L. Hodgson, T. Pippucci, A. Saidin, Y. S. Ong, S. E. Heron, L. Licchetta, F. Bisulli, M. A. Bayly, J. Hughes, S. Baldassari, F. Palombo, Group Epilepsy Electroclinical Study, M. Santucci, S. Meletti, S. F. Berkovic, G. Rubboli, P. Q. Thomas, I. E. Scheffer, P. Tinuper, J. Geoghegan, A. W. Schreiber, and L. M. Dibbens. 2016. 'Mutations in the mammalian target of rapamycin pathway regulators NPRL2 and NPRL3 cause focal epilepsy', *Ann Neurol*, 79: 120-31.

Ritz, B. W., I. Aktan, S. Nogusa, and E. M. Gardner. 2008. 'Energy restriction impairs natural killer cell function and increases the severity of influenza infection in young adult male C57BL/6 mice', *J Nutr*, 138: 2269-75.

Roco, J. A., L. Mesin, S. C. Binder, C. Nefzger, P. Gonzalez-Figueroa, P. F. Canete, J. Ellyard, Q. Shen, P. A. Robert, J. Cappello, H. Vohra, Y. Zhang, C. R. Nowosad, A. Schiepers, L. M. Corcoran, K. M. Toellner, J. M. Polo, M. Meyer-Hermann, G. D. Victora, and C. G. Vinuesa. 2019. 'Class-Switch Recombination Occurs Infrequently in Germinal Centers', *Immunity*, 51: 337-50 e7.

Rodriguez, P. C., M. S. Ernstoff, C. Hernandez, M. Atkins, J. Zabaleta, R. Sierra, and A. C. Ochoa. 2009. 'Arginase I-producing myeloid-derived suppressor cells in renal cell carcinoma are a subpopulation of activated granulocytes', *Cancer Res*, 69: 1553-60.

Rodriguez, P. C., C. P. Hernandez, D. Quiceno, S. M. Dubinett, J. Zabaleta, J. B. Ochoa, J. Gilbert, and A. C. Ochoa. 2005. 'Arginase I in myeloid suppressor cells is induced by COX-2 in lung carcinoma', *J Exp Med*, 202: 931-9.

Ruprecht, C. R., and A. Lanzavecchia. 2006. 'Toll-like receptor stimulation as a third signal required for activation of human naive B cells', *Eur J Immunol*, 36: 810-6.

Ruth, M. R., and C. J. Field. 2013. 'The immune modifying effects of amino acids on gut-associated lymphoid tissue', *J Anim Sci Biotechnol*, 4: 27.

Saric, A., V. E. Hipolito, J. G. Kay, J. Canton, C. N. Antonescu, and R. J. Botelho. 2016. 'mTOR controls lysosome tubulation and antigen presentation in macrophages and dendritic cells', *Mol Biol Cell*, 27: 321-33.

Saxton, R. A., K. E. Knockenhauer, R. L. Wolfson, L. Chantranupong, M. E. Pacold, T. Wang, T. U. Schwartz, and D. M. Sabatini. 2016. 'Structural basis for leucine sensing by the Sestrin2-mTORC1 pathway', *Science*, 351: 53-8.

Schaerli, P., K. Willimann, A. B. Lang, M. Lipp, P. Loetscher, and B. Moser. 2000. 'CXC chemokine receptor 5 expression defines follicular homing T cells with B cell helper function', *J Exp Med*, 192: 1553-62.

Schwickert, T. A., H. Tagoh, S. Gultekin, A. Dakic, E. Axelsson, M. Minnich, A. Ebert, B. Werner, M. Roth, L. Cimmino, R. A. Dickins, J. Zuber, M. Jaritz, and M. Busslinger. 2014. 'Stage-specific control of early B cell development by the transcription factor Ikaros', *Nat Immunol*, 15: 283-93.

Schwickert, T. A., G. D. Victora, D. R. Fooksman, A. O. Kamphorst, M. R. Mugnier, A. D. Gitlin, M. L. Dustin, and M. C. Nussenzweig. 2011. 'A dynamic T cell-limited checkpoint regulates affinity-dependent B cell entry into the germinal center', *J Exp Med*, 208: 1243-52.

Shapiro-Shelef, M., K. I. Lin, L. J. McHeyzer-Williams, J. Liao, M. G. McHeyzer-Williams, and K. Calame. 2003. 'Blimp-1 is required for the formation of immunoglobulin secreting plasma cells and pre-plasma memory B cells', *Immunity*, 19: 607-20.

Sharonov, G. V., E. O. Serebrovskaya, D. V. Yuzhakova, O. V. Britanova, and D. M. Chudakov. 2020. 'B cells, plasma cells and antibody repertoires in the tumour microenvironment', *Nat Rev Immunol*.

Shen, K., R. K. Huang, E. J. Brignole, K. J. Condon, M. L. Valenstein, L. Chantranupong, A. Bomaliyamu, A. Choe, C. Hong, Z. Yu, and D. M. Sabatini. 2018. 'Architecture of the human GATOR1 and GATOR1-Rag GTPases complexes', *Nature*, 556: 64-69.

Shi, J., S. Hou, Q. Fang, X. Liu, X. Liu, and H. Qi. 2018. 'PD-1 Controls Follicular T Helper Cell Positioning and Function', *Immunity*, 49: 264-74 e4.

Shinnakasu, R., T. Inoue, K. Kometani, S. Moriyama, Y. Adachi, M. Nakayama, Y. Takahashi, H. Fukuyama, T. Okada, and T. Kurosaki. 2016. 'Regulated selection of germinal-center cells into the memory B cell compartment', *Nat Immunol*, 17: 861-9.

Shroff, K. E., K. Meslin, and J. J. Cebra. 1995. 'Commensal enteric bacteria engender a self-limiting humoral mucosal immune response while permanently colonizing the gut', *Infect Immun*, 63: 3904-13.

Shulman, Z., A. D. Gitlin, J. S. Weinstein, B. Lainez, E. Esplugues, R. A. Flavell, J. E. Craft, and M. C. Nussenzweig. 2014. 'Dynamic signaling by T follicular helper cells during germinal center B cell selection', *Science*, 345: 1058-62.

Silver, R. J., M. K. Paczosa, A. L. McCabe, J. M. Balada-Llasat, J. D. Baleja, and J. Mecsas. 2019. 'Amino Acid Biosynthetic Pathways Are Required for Klebsiella pneumoniae Growth in Immunocompromised Lungs and Are Druggable Targets during Infection', *Antimicrob Agents Chemother*, 63.

Sinclair, L. V., J. Rolf, E. Emslie, Y. B. Shi, P. M. Taylor, and D. A. Cantrell. 2013. 'Control of amino-acid transport by antigen receptors coordinates the metabolic reprogramming essential for T cell differentiation', *Nat Immunol*, 14: 500-8.

Sintes, J., M. Gentile, S. Zhang, Y. Garcia-Carmona, G. Magri, L. Cassis, D. Segura-Garzon, A. Ciociola, E. K. Grasset, S. Bascones, L. Comerma, M. Pybus, D. Llige, I. Puga, C. Gutzeit, B. He, W. DuBois, M. Crespo, J. Pascual, A. Mensa, J. I. Arostegui, M. Juan, J. Yague, S. Serrano, J. Lloreta, E. Meffre, M. Hahne, C. Cunningham-Rundles, B. A. Mock, and A.

Cerutti. 2017. 'mTOR intersects antibody-inducing signals from TACI in marginal zone B cells', *Nat Commun*, 8: 1462.

Smith, K. G., T. D. Hewitson, G. J. Nossal, and D. M. Tarlinton. 1996. 'The phenotype and fate of the antibody-forming cells of the splenic foci', *Eur J Immunol*, 26: 444-8.

Subashchandrabose, S., R. M. LeVeque, T. K. Wagner, R. N. Kirkwood, M. Kiupel, and M. H. Mulks. 2009. 'Branched-chain amino acids are required for the survival and virulence of Actinobacillus pleuropneumoniae in swine', *Infect Immun*, 77: 4925-33.

Suzuki, A., T. Kaisho, M. Ohishi, M. Tsukio-Yamaguchi, T. Tsubata, P. A. Koni, T. Sasaki, T. W. Mak, and T. Nakano. 2003. 'Critical roles of Pten in B cell homeostasis and immunoglobulin class switch recombination', *J Exp Med*, 197: 657-67.

Suzuki, K., I. Grigorova, T. G. Phan, L. M. Kelly, and J. G. Cyster. 2009. 'Visualizing B cell capture of cognate antigen from follicular dendritic cells', *J Exp Med*, 206: 1485-93.

Swaminathan, A., R. Hassan-Abdi, S. Renault, A. Siekierska, R. Riche, M. Liao, P. A. M. de Witte, C. Yanicostas, N. Soussi-Yanicostas, P. Drapeau, and E. Samarut. 2018. 'Non-canonical mTOR-Independent Role of DEPDC5 in Regulating GABAergic Network Development', *Curr Biol*, 28: 1924-37 e5.

Taketani, M., A. Naitoh, N. Motoyama, and T. Azuma. 1995. 'Role of conserved amino acid residues in the complementarity determining regions on hapten-antibody interaction of anti-(4-hydroxy-3-nitrophenyl) acetyl antibodies', *Mol Immunol*, 32: 983-90.

Tan, H. X., R. Esterbauer, H. A. Vanderven, J. A. Juno, S. J. Kent, and A. K. Wheatley. 2019. 'Inducible Bronchus-Associated Lymphoid Tissues (iBALT) Serve as Sites of B Cell Selection and Maturation Following Influenza Infection in Mice', *Front Immunol*, 10: 611.

Taylor, A. K., W. Cao, K. P. Vora, J. De La Cruz, W. J. Shieh, S. R. Zaki, J. M. Katz, S. Sambhara, and S. Gangappa. 2013. 'Protein energy malnutrition decreases immunity and increases susceptibility to influenza infection in mice', *J Infect Dis*, 207: 501-10.

Taylor, J. J., K. A. Pape, and M. K. Jenkins. 2012. 'A germinal center-independent pathway generates unswitched memory B cells early in the primary response', *J Exp Med*, 209: 597-606.

Teague, B. N., Y. Pan, P. A. Mudd, B. Nakken, Q. Zhang, P. Szodoray, X. Kim-Howard, P. C. Wilson, and A. D. Farris. 2007. 'Cutting edge: Transitional T3 B cells do not give rise to mature B cells, have undergone selection, and are reduced in murine lupus', *J Immunol*, 178: 7511-5.

Tellier, J., W. Shi, M. Minnich, Y. Liao, S. Crawford, G. K. Smyth, A. Kallies, M. Busslinger, and S. L. Nutt. 2016. 'Blimp-1 controls plasma cell function through the regulation of immunoglobulin secretion and the unfolded protein response', *Nat Immunol*, 17: 323-30.

Timmermans, W. M., J. A. van Laar, T. B. van der Houwen, L. S. Kamphuis, S. J. Bartol, K. H. Lam, R. J. Ouwendijk, M. P. Sparrow, P. R. Gibson, P. M. van Hagen, and M. C. van Zelm. 2016. 'B-Cell Dysregulation in Crohn's Disease Is Partially Restored with Infliximab Therapy', *PLoS One*, 11: e0160103.

Tohma, S., S. Hirohata, and P. E. Lipsky. 1991. 'The role of CD11a/CD18-CD54 interactions in human T cell-dependent B cell activation', *J Immunol*, 146: 492-9.

Toyama, H., S. Okada, M. Hatano, Y. Takahashi, N. Takeda, H. Ichii, T. Takemori, Y. Kuroda, and T. Tokuhisa. 2002. 'Memory B cells without somatic hypermutation are generated from Bcl6-deficient B cells', *Immunity*, 17: 329-39.

Turner, J. S., Z. L. Benet, and I. Grigorova. 2017. 'Transiently antigen primed B cells can generate multiple subsets of memory cells', *PLoS One*, 12: e0183877.

Tze, L. E., B. R. Schram, K. P. Lam, K. A. Hogquist, K. L. Hippen, J. Liu, S. A. Shinton, K. L. Otipoby, P. R. Rodine, A. L. Vegoe, M. Kraus, R. R. Hardy, M. S. Schlissel, K. Rajewsky, and T. W. Behrens. 2005. 'Basal immunoglobulin signaling actively maintains developmental stage in immature B cells', *PLoS Biol*, 3: e82.

Uchimura, Y., T. Fuhrer, H. Li, M. A. Lawson, M. Zimmermann, B. Yilmaz, J. Zindel, F. Ronchi, M. Sorribas, S. Hapfelmeier, S. C. Ganal-Vonarburg, M. Gomez de Aguero, K. D. McCoy, U. Sauer, and A. J. Macpherson. 2018. 'Antibodies Set Boundaries Limiting Microbial Metabolite Penetration and the Resultant Mammalian Host Response', *Immunity*, 49: 545-59 e5.

van Zelm, M. C., S. J. Bartol, G. J. Driessen, F. Mascart, I. Reisli, J. L. Franco, B. Wolska-Kusnierz, H. Kanegane, L. Boon, J. J. van Dongen, and M. van der Burg. 2014. 'Human CD19 and CD40L deficiencies impair antibody selection and differentially affect somatic hypermutation', *J Allergy Clin Immunol*, 134: 135-44.

van Zelm, M. C., T. Szczepanski, M. van der Burg, and J. J. van Dongen. 2007. 'Replication history of B lymphocytes reveals homeostatic proliferation and extensive antigen-induced B cell expansion', *J Exp Med*, 204: 645-55.

Vander Haar, E., S. I. Lee, S. Bandhakavi, T. J. Griffin, and D. H. Kim. 2007. 'Insulin signalling to mTOR mediated by the Akt/PKB substrate PRAS40', *Nat Cell Biol*, 9: 316-23.

Victora, G. D., T. A. Schwickert, D. R. Fooksman, A. O. Kamphorst, M. Meyer-Hermann, M. L. Dustin, and M. C. Nussenzweig. 2010. 'Germinal center dynamics revealed by multiphoton microscopy with a photoactivatable fluorescent reporter', *Cell*, 143: 592-605.

Vikstrom, I., S. Carotta, K. Luthje, V. Peperzak, P. J. Jost, S. Glaser, M. Busslinger, P. Bouillet, A. Strasser, S. L. Nutt, and D. M. Tarlinton. 2010. 'Mcl-1 is essential for germinal center formation and B cell memory', *Science*, 330: 1095-9.

Vilagos, B., M. Hoffmann, A. Souabni, Q. Sun, B. Werner, J. Medvedovic, I. Bilic, M. Minnich, E. Axelsson, M. Jaritz, and M. Busslinger. 2012. 'Essential role of EBF1 in the generation and function of distinct mature B cell types', *J Exp Med*, 209: 775-92.

Vinuesa, C. G., M. A. Linterman, D. Yu, and I. C. MacLennan. 2016. 'Follicular Helper T Cells', *Annu Rev Immunol*, 34: 335-68.

Vogelzang, A., H. M. McGuire, D. Yu, J. Sprent, C. R. Mackay, and C. King. 2008. 'A fundamental role for interleukin-21 in the generation of T follicular helper cells', *Immunity*, 29: 127-37.

Vossenkamper, A., and J. Spencer. 2011. 'Transitional B cells: how well are the checkpoints for specificity understood?', *Arch Immunol Ther Exp (Warsz)*, 59: 379-84.

Wang, Y., G. Huang, J. Wang, H. Molina, D. D. Chaplin, and Y. X. Fu. 2000. 'Antigen persistence is required for somatic mutation and affinity maturation of immunoglobulin', *Eur J Immunol*, 30: 2226-34.

Waters, L. R., F. M. Ahsan, D. M. Wolf, O. Shirihai, and M. A. Teitell. 2018. 'Initial B Cell Activation Induces Metabolic Reprogramming and Mitochondrial Remodeling', *iScience*, 5: 99-109.

Weisel, F. J., G. V. Zuccarino-Catania, M. Chikina, and M. J. Shlomchik. 2016. 'A Temporal Switch in the Germinal Center Determines Differential Output of Memory B and Plasma Cells', *Immunity*, 44: 116-30.

Welinder, E., R. Mansson, E. M. Mercer, D. Bryder, M. Sigvardsson, and C. Murre. 2011. 'The transcription factors E2A and HEB act in concert to induce the expression of FOXO1 in the common lymphoid progenitor', *Proc Natl Acad Sci U S A*, 108: 17402-7.

Wennhold, K., A. Shimabukuro-Vornhagen, and M. von Bergwelt-Baildon. 2019. 'B Cell-Based Cancer Immunotherapy', *Transfus Med Hemother*, 46: 36-46.

Wensveen, F. M., E. Slinger, M. H. van Attekum, R. Brink, and E. Eldering. 2016. 'Antigen-affinity controls pre-germinal center B cell selection by promoting Mcl-1 induction through BAFF receptor signaling', *Sci Rep*, 6: 35673.

Wolfson, R. L., L. Chantranupong, R. A. Saxton, K. Shen, S. M. Scaria, J. R. Cantor, and D. M. Sabatini. 2016. 'Sestrin2 is a leucine sensor for the mTORC1 pathway', *Science*, 351: 43-8.

Wong, M. H., A. Xue, R. C. Baxter, N. Pavlakis, and R. C. Smith. 2016. 'Upstream and Downstream Co-inhibition of Mitogen-Activated Protein Kinase and PI3K/Akt/mTOR Pathways in Pancreatic Ductal Adenocarcinoma', *Neoplasia*, 18: 425-35.

Wray-Dutra, M. N., R. Chawla, K. R. Thomas, B. J. Seymour, T. Arkatkar, K. M. Sommer, S. Khim, C. Trapnell, R. G. James, and D. J. Rawlings. 2018. 'Activated CARD11 accelerates germinal center kinetics, promoting mTORC1 and terminal differentiation', *J Exp Med*, 215: 2445-61.

Yang, C., B. Ko, C. T. Hensley, L. Jiang, A. T. Wasti, J. Kim, J. Sudderth, M. A. Calvaruso, L. Lumata, M. Mitsche, J. Rutter, M. E. Merritt, and R. J. DeBerardinis. 2014. 'Glutamine oxidation maintains the TCA cycle and cell survival during impaired mitochondrial pyruvate transport', *Mol Cell*, 56: 414-24.

Ye, L., J. Lee, L. Xu, A. U. Mohammed, W. Li, J. S. Hale, W. G. Tan, T. Wu, C. W. Davis, R. Ahmed, and K. Araki. 2017. 'mTOR Promotes Antiviral Humoral Immunity by Differentially Regulating CD4 Helper T Cell and B Cell Responses', *J Virol*, 91.

Yoshida, T., S. Y. Ng, J. C. Zuniga-Pflucker, and K. Georgopoulos. 2006. 'Early hematopoietic lineage restrictions directed by Ikaros', *Nat Immunol*, 7: 382-91.

Yuskaitis, C. J., B. M. Jones, R. L. Wolfson, C. E. Super, S. C. Dhamne, A. Rotenberg, D. M. Sabatini, M. Sahin, and A. Poduri. 2018. 'A mouse model of DEPDC5-related epilepsy: Neuronal loss of Depdc5 causes dysplastic and ectopic neurons, increased mTOR signaling, and seizure susceptibility', *Neurobiol Dis*, 111: 91-101.

Yuskaitis, C. J., L. A. Rossitto, S. Gurnani, E. Bainbridge, A. Poduri, and M. Sahin. 2019. 'Chronic mTORC1 inhibition rescues behavioral and biochemical deficits resulting from neuronal Depdc5 loss in mice', *Hum Mol Genet*.

Zeng, H., S. Cohen, C. Guy, S. Shrestha, G. Neale, S. A. Brown, C. Cloer, R. J. Kishton, X. Gao, B. Youngblood, M. Do, M. O. Li, J. W. Locasale, J. C. Rathmell, and H. Chi. 2016. 'mTORC1 and mTORC2 Kinase Signaling and Glucose Metabolism Drive Follicular Helper T Cell Differentiation', *Immunity*, 45: 540-54.

Zhang, C. S., B. Jiang, M. Li, M. Zhu, Y. Peng, Y. L. Zhang, Y. Q. Wu, T. Y. Li, Y. Liang, Z. Lu, G. Lian, Q. Liu, H. Guo, Z. Yin, Z. Ye, J. Han, J. W. Wu, H. Yin, S. Y. Lin, and S. C. Lin. 2014. 'The lysosomal v-ATPase-Ragulator complex is a common activator for AMPK and mTORC1, acting as a switch between catabolism and anabolism', *Cell Metab*, 20: 526-40.

Zhang, S., M. Pruitt, D. Tran, W. Du Bois, K. Zhang, R. Patel, S. Hoover, R. M. Simpson, J. Simmons, J. Gary, C. M. Snapper, R. Casellas, and B. A. Mock. 2013. 'B cell-specific deficiencies in mTOR limit humoral immune responses', *J Immunol*, 191: 1692-703.

Zhang, S., J. A. Readinger, W. DuBois, M. Janka-Junttila, R. Robinson, M. Pruitt, V. Bliskovsky, J. Z. Wu, K. Sakakibara, J. Patel, C. A. Parent, L. Tessarollo, P. L. Schwartzberg, and B. A. Mock. 2011. 'Constitutive reductions in mTOR alter cell size, immune cell development, and antibody production', *Blood*, 117: 1228-38.

Zhang, Y. L., H. Guo, C. S. Zhang, S. Y. Lin, Z. Yin, Y. Peng, H. Luo, Y. Shi, G. Lian, C. Zhang, M. Li, Z. Ye, J. Ye, J. Han, P. Li, J. W. Wu, and S. C. Lin. 2013. 'AMP as a low-energy charge signal autonomously initiates assembly of AXIN-AMPK-LKB1 complex for AMPK activation', *Cell Metab*, 18: 546-55.

Ziegler, T. R., M. E. Evans, C. Fernandez-Estivariz, and D. P. Jones. 2003. 'Trophic and cytoprotective nutrition for intestinal adaptation, mucosal repair, and barrier function', *Annu Rev Nutr*, 23: 229-61.

Zotos, D., J. M. Coquet, Y. Zhang, A. Light, K. D'Costa, A. Kallies, L. M. Corcoran, D. I. Godfrey, K. M. Toellner, M. J. Smyth, S. L. Nutt, and D. M. Tarlinton. 2010. 'IL-21 regulates germinal center B cell differentiation and proliferation through a B cell-intrinsic mechanism', *J Exp Med*, 207: 365-78.

Chapter 6